

AD651103

AD

**USAAVLABS TECHNICAL REPORT 66-88**

**SMALL GAS TURBINE ENGINE COMPONENT TECHNOLOGY,  
HIGH-TEMPERATURE TURBINE MATERIALS RESEARCH**

By

F. H. Simpson

L. J. Fiedler

J. Acurio

December 1966



**U. S. ARMY AVIATION MATERIEL LABORATORIES  
FORT EUSTIS, VIRGINIA**

**CONTRACT DA 44-177-AMC-173(T)  
THE BOEING COMPANY  
SEATTLE, WASHINGTON**

*Distribution of this  
document is unlimited*



**ARCHIVE COPY**

168

Disclaimers

The findings in this report are not to be construed as an official Department of the Army position unless so designated by other authorized documents.

When Government drawings, specifications, or other data are used for any purpose other than in connection with a definitely related Government procurement operation, the United States Government thereby incurs no responsibility nor any obligation whatsoever; and the fact that the Government may have formulated, furnished, or in any way supplied the said drawings, specifications, or other data is not to be regarded by implication or otherwise as in any manner licensing the holder or any other person or corporation, or conveying any rights or permission, to manufacture, use, or sell any patented invention that may in any way be related thereto.

Trade names cited in this report do not constitute an official endorsement or approval of the use of such commercial hardware or software.

Disposition Instructions

Destroy this report when no longer needed. Do not return it to originator.

ACCESSION FOR		
CFSTI	WHITE SECTION	<input checked="" type="checkbox"/>
DDC	BUFF SECTION	<input type="checkbox"/>
UNANNOUNCED		<input type="checkbox"/>
JUSTIFICATION .....		
BY .....		
DISTRIBUTION/AVAILABILITY CODE		
DIST.	AVAIL. and/or	SPECIAL
/		



**DEPARTMENT OF THE ARMY**  
**U. S. ARMY AVIATION MATERIEL LABORATORIES**  
**FORT EUSTIS, VIRGINIA 23604**

Appropriate technical personnel have reviewed this report and concur with the conclusions contained herein.

The findings and recommendations as outlined in this report will be used in planning future research programs for high-temperature uncooled turbines.

Task 1M121401D14413  
Contract DA 44-177-AMC-173(T)  
USAAVLABS Technical Report 66-88  
December 1966

**SMALL GAS TURBINE ENGINE COMPONENT TECHNOLOGY,  
HIGH-TEMPERATURE TURBINE MATERIALS RESEARCH**

**Final Report  
Boeing Document D4-3298**

by

**F. H. Simpson  
L. J. Fiedler  
J. Acurio**

Prepared by

**THE BOEING COMPANY  
TURBINE DIVISION  
SEATTLE, WASHINGTON**

for

**U.S. ARMY AVIATION MATERIEL LABORATORIES  
FORT EUSTIS, VIRGINIA**

Distribution of this  
document is unlimited

## SUMMARY

Research and development work was conducted on two new material systems to determine their potential for future use, without special cooling, in the turbine section of an advanced small (2-pound-per-second airflow) gas turbine engine operating at a turbine inlet temperature of 2300°F. The two new systems are macrolaminate metal-ceramic composites and dispersion-strengthened nickel-base alloys. From preliminary studies, conducted prior to initiating work on this contract, these materials showed promise for allowing large gains in turbine inlet temperature. Based on initial estimates and an understanding of the risks involved, it was believed that the research was both a desirable and necessary attempt to develop the potential of the materials because of their advantages in increasing specific power of future gas turbines. Although the research showed that the targeted high-temperature material properties could not be achieved with the macrolaminate composites or the dispersion-strengthened nickel, it was felt that these types of materials could be developed to increase turbine operational temperatures to a level of about 2100°F. However, it was recognized that this gain would not be sufficient in view of improvements being made with other new material systems.

Macrolaminate composites were evaluated for possible nozzle vane application, and the dispersion-strengthened alloys were evaluated for possible turbine blade and shroud application. The investigations included macrolaminate composites of molybdenum-hafnia (Mo-HfO<sub>2</sub>), nickel-magnesia (Ni-MgO), and nickel-alumina (Ni-Al<sub>2</sub>O<sub>3</sub>) and dispersion-strengthened alloys of nickel-chromium-thoria (Ni-Cr-ThO<sub>2</sub>) and nickel-chromium-molybdenum-thoria (Ni-Cr-Mo-ThO<sub>2</sub>). The program involved studies of compositional variables, studies to improve processing techniques, and laboratory tests to determine properties.

Of the macrolaminate composites evaluated, the Ni-Al<sub>2</sub>O<sub>3</sub> composite showed the most promise for nozzle vane applications. The oxidation resistance of the Ni-Al<sub>2</sub>O<sub>3</sub> composites was better than that for any of the other composites studied. Ni-Al<sub>2</sub>O<sub>3</sub> also showed approximately double the elevated temperature strength of Ni-MgO. However, both strength and oxidation resistance were below the target. When chromium was added to Ni-Al<sub>2</sub>O<sub>3</sub> composites to improve the oxidation resistance, reductions in elevated temperature strength occurred. The reduced properties were attributed to the presence of excessive chromium oxide and diffusion reactions that apparently occurred between the metal and ceramic phases. While significantly higher properties are potentially available in the Ni-Al<sub>2</sub>O<sub>3</sub> composite system, the melting point and reactivity of the constituents at elevated temperatures would probably

limit this material to a maximum average turbine inlet temperature of 2100°F in a nozzle vane application. However, the application of the material was not attempted in the course of this program.

Test results indicated that the Mo-HfO<sub>2</sub> and Ni-MgO macrolaminate composite systems were not suited for the intended high-temperature nozzle vane application because of insufficient oxidation resistance and low strength characteristics. The oxidation resistance of the basic Mo-HfO<sub>2</sub> composite was significantly improved by modifying the HfO<sub>2</sub> ceramic phase and by applying protective coatings over the composite; however, the modified composite studied did not indicate potential for long-time oxidation resistance. As a result, it was not possible to capitalize on the high-temperature strength of the metal phase. The Ni-MgO composite exhibited significantly better oxidation resistance than Mo-HfO<sub>2</sub>; however, oxidation resistance, tensile properties and resistance to thermal fatigue were considered inadequate for further investigation in this program.

The work on dispersion-strengthened alloys was aimed primarily at improving high-temperature strength by developing and evaluating improved processing techniques to minimize or eliminate oxygen contamination. An evaluation of thermal decomposition techniques showed that neither modified decomposition cycles nor the use of thorium organic compounds as a source of thoria was effective in eliminating oxygen contamination. Selective reduction treatments were subsequently evaluated, and a vacuum-carbon reduction cycle was found to be capable of reducing the oxygen contamination level to about one-third of its original value. Properties of material produced with the modified processing techniques were, however, lower than anticipated. The low properties were attributed to a relatively coarse dispersoid, typically in the 0.1-to-1.0-micron range.

## FOREWORD

This program was authorized by Task 1M121401D14413.

Work conducted by The Boeing Company under this task included component development on the compressor, turbine, and regenerator of a small high-temperature gas turbine engine. This final report describes only work related to the turbine portion of the contract. This work involved development and evaluation of selected new material systems for application in an uncooled turbine operating at a turbine inlet temperature of 2300° F.

Acknowledgement is given to the New England Materials Laboratory (NEMLAB), Melford, Massachusetts, and to Dr. Allan S. Bufferd, project metallurgist at NEMLAB, for conducting the development work on the dispersion-strengthened alloys covered by this program.

This report covers activities on this research program from May 1, 1964, to August 31, 1965.

## C O N T E N T S

	<u>Page</u>
SUMMARY . . . . .	iii
FOREWORD . . . . .	v
LIST OF ILLUSTRATIONS . . . . .	ix
LIST OF TABLES . . . . .	xiii
LIST OF SYMBOLS . . . . .	xvii
1.0 INTRODUCTION . . . . .	1
1.1 CYCLE ANALYSIS . . . . .	1
1.2 APPROACH TO TURBINE MATERIALS . . . . .	4
1.3 MATERIAL GOALS . . . . .	11
2.0 PROGRAM APPROACH . . . . .	14
2.1 MACROLAMINATE COMPOSITE MATERIALS DEVELOPMENT . . . . .	14
2.2 DISPERSION-STRENGTHENED ALLOY DEVELOPMENT . . . . .	22
2.3 TEST PROCEDURES . . . . .	23
2.4 TEST MATERIALS . . . . .	30
3.0 DEVELOPMENT PROGRAM . . . . .	35
3.1 Mo-HfO <sub>2</sub> MACROLAMINATE COMPOSITES . . . . .	35
3.2 Ni-MgO MACROLAMINATE COMPOSITES . . . . .	58
3.3 Ni-Al <sub>2</sub> O <sub>3</sub> MACROLAMINATE COMPOSITES . . . . .	94
3.4 DISPERSION-STRENGTHENED NICKEL-BASE ALLOYS . . . . .	122

CONTENTS (Continued)

	<u>Page</u>
4.0 CONCLUSIONS . . . . .	143
4.1 Ni-Al <sub>2</sub> O <sub>3</sub> MACROLAMINATE COMPOSITES . . . . .	143
4.2 Ni-MgO MACROLAMINATE COMPOSITES . . . . .	143
4.3 Mo-HfO <sub>2</sub> MACROLAMINATE COMPOSITES . . . . .	144
4.4 DISPERSION-STRENGTHENED ALLOYS . . . . .	144
4.5 COMPARATIVE PROPERTIES . . . . .	145
BIBLIOGRAPHY . . . . .	147
DISTRIBUTION . . . . .	149

## ILLUSTRATIONS

<u>Figure</u>		<u>Page</u>
1	Effect of Compressor Performance on Simple-Cycle Engine Performance . . . . .	2
2	Effect of Gas Temperature on Simple-Cycle Engine Performance . . . . .	3
3	Effect of Gas Temperature on Regenerative Engine Cycle Performance . . . . .	4
4	Effect of Cycle Temperature and Pressure on Part-Load Specific Fuel Consumption . . . . .	5
5	Estimated First-Stage Turbine Component Temperature . . . . .	6
6	Macrolaminate Metal-Ceramic Composite Schematic . . . . .	7
7	Oxidation Tests - Macrolaminate Metal-Metal Oxide Composites . . . . .	9
8	Predicted Stress-Rupture Strength Improvements in Dispersion-Strengthened Nickel-Base Alloys . . . . .	12
9	Process for Preparing Macrolaminate Composites . . . . .	17
10	Hot-Press Facility . . . . .	20
11	Sketch of Oxidation Test Setup . . . . .	25
12	Macrolaminate Composite Tensile Test Specimen . . . . .	27
13	Tensile Test Fixture Assembly for Macrolaminate Composites . . . . .	27
14	Tensile Test Setup for Macrolaminate Composites . . . . .	28
15	Thermal-Fatigue Test Specimen for Macrolaminate Composites . . . . .	29
16	Thermal-Fatigue Test Machine . . . . .	30
17	Combined Organic Binder Decomposition and Sintering Cycle . . . . .	36

ILLUSTRATIONS (Continued)

<u>Figure</u>		<u>Page</u>
18	Separate Organic Binder Decomposition and Sintering Cycles . . . . .	40
19	Hot-Press Cycle for Mo-HfO <sub>2</sub> Composites . . . . .	42
20	Modified Vacuum-Sintering Cycle . . . . .	45
21	Hot-Press Cycles for Nickel Specimens . . . . .	65
22	Post-Treat Cycle . . . . .	66
23	Modified Post-Treat Cycle . . . . .	67
24	Hot-Press Cycles for Ni-MgO Composites . . . . .	70
25	Hot-Press Cycles for Ni-MgO Composites . . . . .	72
26	Fracture in a Ni-MgO Specimen . . . . .	74
27	Fracture in Macrolaminate Composites . . . . .	76
28	Draw-Knife Apparatus . . . . .	78
29	Hot-Press Cycle for Ni-MgO Composites . . . . .	80
30	Modified Method of Assembling Hot-Press Die . . . . .	82
31	Post-Treat Cycle . . . . .	84
32	Flexural Strength Versus Metal Content for (Ni · 2ThO <sub>2</sub> ) · 2TiN-(MgO · 5HfO <sub>2</sub> ) Composites . . . . .	84
33	Oxidation Resistance at 2300° F Versus Metal Content for (Ni · 2ThO <sub>2</sub> ) · 2TiN-(MgO · 5HfO <sub>2</sub> ) Composites . . . . .	85
34	Oxidation in a 50:50 Metal-Ceramic Ratio Specimen of (Ni · 2ThO <sub>2</sub> ) · 2TiN-(MgO · 5HfO <sub>2</sub> ) . . . . .	86
35	Thermal Strains in Test Specimen . . . . .	88
36	Thermal-Fatigue Test Specimens of (Ni · 2ThO <sub>2</sub> ) · 2TiN-(MgO · 5HfO <sub>2</sub> ) Composites . . . . .	88

ILLUSTRATIONS (Continued)

<u>Figure</u>		<u>Page</u>
37	Tensile Strength Versus Metal Content for (Ni · 2ThO <sub>2</sub> ) · 2TiN-(MgO · 5HfO <sub>2</sub> ) Composites . . . . .	89
38	Effect of Temperature on Tensile Fracture of (Ni · 2ThO <sub>2</sub> ) · TiN-(MgO · 5HfO <sub>2</sub> ) Specimens With 50:50 Metal-Ceramic Ratio . . . . .	90
39	Hot-Press Cycle for Ni-Al <sub>2</sub> O <sub>3</sub> Composites . . . . .	96
40	Surface Oxidation in Metal Phase . . . . .	100
41	Nonmetallic Inclusions in Metal Phase . . . . .	103
42	Metal Infiltration in a Ni · 17Cr · 2ThO <sub>2</sub> - Al <sub>2</sub> O <sub>3</sub> Composite . . . . .	106
43	Flexural Strength Versus Metal Content for Ni · 17Cr-Al <sub>2</sub> O <sub>3</sub> · 1/4 TiO <sub>2</sub> Composites . . . . .	111
44	Oxidation Resistance at 2300° F Versus Metal Content for Ni · 17Cr-Al <sub>2</sub> O <sub>3</sub> · 1/4 TiO <sub>2</sub> Composites . . . . .	112
45	Variations in Porosity in Ni · 17Cr-Al <sub>2</sub> O <sub>3</sub> · 1/4 TiO <sub>2</sub> Composites . . . . .	112
46	Microstructure of a (Ni · 2ThO <sub>2</sub> ) - Al <sub>2</sub> O <sub>3</sub> · 1/4 TiO <sub>2</sub> Composite . . . . .	113
47	Oxidation in a 70-Volume-Percent Metal Composite After 100 Hours at 2300° F . . . . .	114
48	Subsurface Oxidation in a 50-Volume-Percent Metal Composite After 100 Hours at 2300° F . . . . .	115
49	Tensile Strength Versus Metal Content for Ni · 17Cr-Al <sub>2</sub> O <sub>3</sub> · 1/4 TiO <sub>2</sub> Composites . . . . .	117
50	Process Diagram and Results for Thermal Decomposition Studies . . . . .	125

ILLUSTRATIONS (Continued)

<u>Figure</u>		<u>Page</u>
51	Process Diagram and Results for Selective Reduction Studies . . . . .	129
52	Process Diagram and Analysis Data for Extruded Alloys . . . . .	131
53	Process Diagram and Analysis Data for Extruded Alloys . . . . .	132
54	As-Extruded Longitudinal Microstructures of Ni-Cr-ThO <sub>2</sub> Alloys . . . . .	133
55	Electron Micrograph of Ni-Cr-ThO <sub>2</sub> Alloy (Alloy Number 5) After Extrusion . . . . .	139
56	Effect of Cold-Work and Anneal Cycles on Hardness . .	140

## TABLES

<u>Table</u>		<u>Page</u>
I	Performance Comparisons . . . . .	2
II	Material Target Properties . . . . .	13
III	Macrolaminate Paint Formulation . . . . .	15
IV	Analysis of Molybdenum Powder . . . . .	31
V	Analysis of Hafnia Powder . . . . .	31
VI	Analysis of Nickel Powder . . . . .	32
VII	Analysis of Carbonyl-Nickel Powder . . . . .	32
VIII	Analysis of Nickel-Chromium Alloy Powder . . . . .	33
IX	Analysis of Hafnium Chloride . . . . .	34
X	Impurity Range for Linde-A . . . . .	34
XI	Flexural Strength of Mo-(HfO <sub>2</sub> · 5CeO <sub>2</sub> ) and Separate Phases . . . . .	36
XII	Results of X-Ray Diffraction Analysis . . . . .	38
XIII	Effects of Varying CeO <sub>2</sub> Concentration on Flexural Strength . . . . .	41
XIV	Flexural Strength of Hot-Pressed Mo-(HfO <sub>2</sub> · 5CeO <sub>2</sub> ) Composites . . . . .	43
XV	Effect of Sintering Atmosphere on Flexural Properties of Mo-(HfO <sub>2</sub> · 5CeO <sub>2</sub> ) Composites . . . . .	44
XVI	Effect of Various Sintering Parameters on Flexural Properties . . . . .	46
XVII	Mullite · Alumina Formulations . . . . .	47
XVIII	Flexural Properties of Mo-MAT Composites . . . . .	49

TABLES (Continued)

<u>Table</u>		<u>Page</u>
XXIX	Oxidation Resistance of First Composition Level . . . . .	51
XX	Oxidation Resistance of Second and Third Composition Levels . . . . .	52
XXI	Flexural Properties of Ni-MgO and Separate Phases . . .	59
XXII	Effect of Additives on Flexural Strength of MgO. . . . .	61
XXIII	Effect of Additions on Flexural Strength of Ni-MgO . . . .	62
XXIV	Effect of Oxide Additions on Flexural Strength of Metal Phase. . . . .	64
XXV	Flexural Properties of Ni-MgO Composites With Metal Phase Oxide Additions. . . . .	69
XXVI	Flexural Properties of Ni-MgO Composites With Additions to Both Phases . . . . .	71
XXVII	Flexural Properties of (Ni · 0.72CaO)-(MgO · 5HfO <sub>2</sub> ) Composites . . . . .	73
XXVIII	Thickness Data for Knife-Coated Laminate Sheets . . . . .	79
XXIX	Carbon Contamination Resulting From Various Organic Burnout Cycles . . . . .	79
XXX	Effect of Organic Burnout Cycles on Flexural Properties	81
XXXI	Thermal-Fatigue Test Results for (Ni · 2ThO <sub>2</sub> ) · 2TiN- (MgO · 5HfO <sub>2</sub> ) Composites . . . . .	87
XXXII	Summary of (Ni · 2ThO <sub>2</sub> ) · 2TiN-(MgO · 5HfO <sub>2</sub> ) Composite Test Data for Various Metal-Ceramic Ratios	91
XXXIII	Flexural Properties of Preliminary Ni-Al <sub>2</sub> O <sub>3</sub> Composites	95
XXXIV	Flexural Properties of Ni · 13Cr · 0.7ThO <sub>2</sub> - Al <sub>2</sub> O <sub>3</sub> Composites . . . . .	97

TABLE (Continued)

<u>Table</u>		<u>Page</u>
XXXV	Flexural Properties of Ni-Al <sub>2</sub> O <sub>3</sub> · 1/4 TiO <sub>2</sub> Composites.	98
XXXVI	Flexural Properties of Ni · 20W-Al <sub>2</sub> O <sub>3</sub> · 1/4 TiO <sub>2</sub> Composites . . . . .	99
XXXVII	Oxidation Resistance of Ni-Al <sub>2</sub> O <sub>3</sub> Composites . . . . .	100
XXXVIII	Flexural Properties of Ni · 17Cr-Al <sub>2</sub> O <sub>3</sub> Composites . . .	102
XXXIX	Elevated Temperature Properties of Macrolaminate Composites With Chromium Additions . . . . .	105
XL	Effect of Sintering Aids on Flexural Properties . . . . .	107
XLI	Elevated Temperature Properties of (Ni · 2ThO <sub>2</sub> )-Al <sub>2</sub> O <sub>3</sub> 1/4 TiO <sub>2</sub> Composites . . . . .	109
XLII	Thermal-Fatigue Results of Ni · 17Cr-Al <sub>2</sub> O <sub>3</sub> · 1/4 TiO <sub>2</sub> Composites . . . . .	116
XLIII	Summary of Ni · 17Cr-Al <sub>2</sub> O <sub>3</sub> · 1/4 TiO <sub>2</sub> Composite Test Data for Various Metal-Ceramic Ratios . . . . .	118
XLIV	Oxygen Content of Ground Powder . . . . .	123
XLV	Effect of Temperature and Atmosphere on ThO <sub>2</sub> Particle Size . . . . .	126
XLVI	Contamination Levels in 80Ni-20Cr-5ThO <sub>2</sub> Processed Powder . . . . .	127
XLVII	Preliminary Extruded Alloys . . . . .	128
XLVIII	Tensile Properties of Extruded Alloys . . . . .	134
XLIX	Results of Vacuum-Carbon Reduction Cycles . . . . .	135
L	Composition of Extruded Alloys . . . . .	135
LI	Oxygen and Carbon Analysis of Extruded Alloys . . . . .	137

TABLE (Continued)

<u>Table</u>		<u>Page</u>
LII	Properties of Extruded Alloys . . . . .	138
LIII	Tensile Properties at 1800° F on Cold-Worked Alloys . . .	141
LIV	Comparison of Target and Best Test Properties . . . . .	145

SYMBOLS

<b>FYS</b>	<b>Flexural Yield Strength</b>
<b>UFS</b>	<b>Ultimate Flexural Stress</b>
<b>YS</b>	<b>Yield Strength (Tensile)</b>
<b>UTS</b>	<b>Ultimate Tensile Strength</b>
<b>ksi</b>	<b>1000 psi</b>
<b>hp</b>	<b>Horsepower</b>
<b>lb</b>	<b>Pound</b>
<b>sec</b>	<b>Second</b>

**BLANK PAGE**

## SECTION 1.0 - INTRODUCTION

Advancement of small-gas-turbine component technology to provide future engines with double the power-to-weight ratio, reduced full- and part-load specific fuel consumption, and reduced cost per horsepower compared to current engines is necessary to meet the requirements of future Army aviation and ground equipment. Prior Boeing preliminary design studies have shown the high-temperature turbine, high-pressure-ratio compressor concept to be the best approach to these goals for Army engines, with and without regeneration.

The objective of this research program was the advancement of small-axial-turbine technology to permit operation of a future turbine stage at an inlet-gas temperature of 2300° F without requiring special blade cooling. This turbine technology, combined with high-pressure compressor technology, will provide a potential for increasing specific power to 190 hp/lb-airflow/sec for nonregenerative engines and 182 hp/lb-airflow/sec for regenerative engines. These increases would permit achievement of power-to-weight ratios (hp/lb) of 4.0:1 without regeneration or 2.5:1 with regeneration.

### 1.1 CYCLE ANALYSIS

Boeing's approach to achieve the above-stated goals has been to initiate development on new materials capable of operating without special turbine-blade cooling in a high-pressure ratio cycle (10:1 to 16:1) at turbine-inlet-gas temperatures of 2300° F. Table I compares such a future engine with a current LOH-type engine. Potentially, this future engine can be designed with a minimum of additional complexity and a minimum of component stages.

High-pressure-ratio and high-efficiency components would provide much of the needed reduction in specific fuel consumption. However, as illustrated in Figure 1, increases in specific power by this means are only moderate. For a significant increase in specific power, the cycle temperature must be increased. Figures 2 and 3 show the effects of pressure ratio and turbine-inlet-gas temperature on the overall performance of regenerative and non-regenerative engines. Power output per pound of airflow is doubled for both engine types when the turbine inlet temperature is increased from 1650° F to 2300° F.

**TABLE I  
PERFORMANCE COMPARISONS**

	Current Engine	Future Engine Nonregenerative	Future Engine Regenerative
Specific power (hp/lb-airflow/sec)	93	190	182
Specific fuel consumption (lb/hp-hr)	0.68	0.49	0.38
Turbine inlet temperature (°F)	1650	2300	2300
Compressor pressure ratio	6:1	10:1	10:1

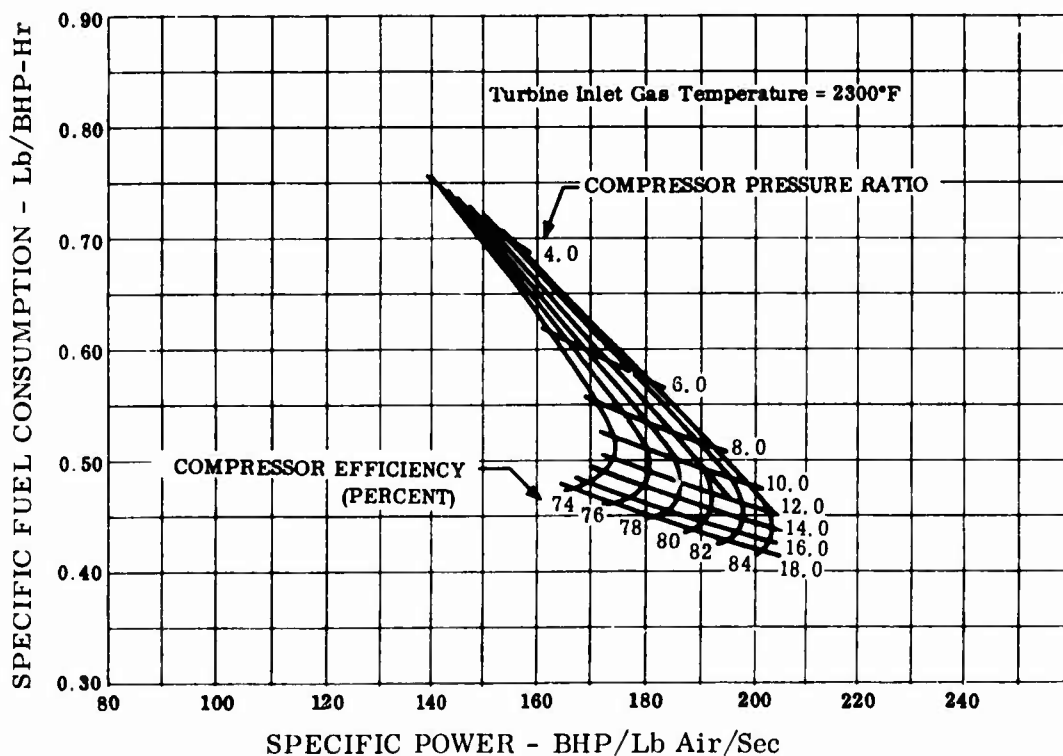


Figure 1. Effect of Compressor Performance on Simple-Cycle Engine Performance.

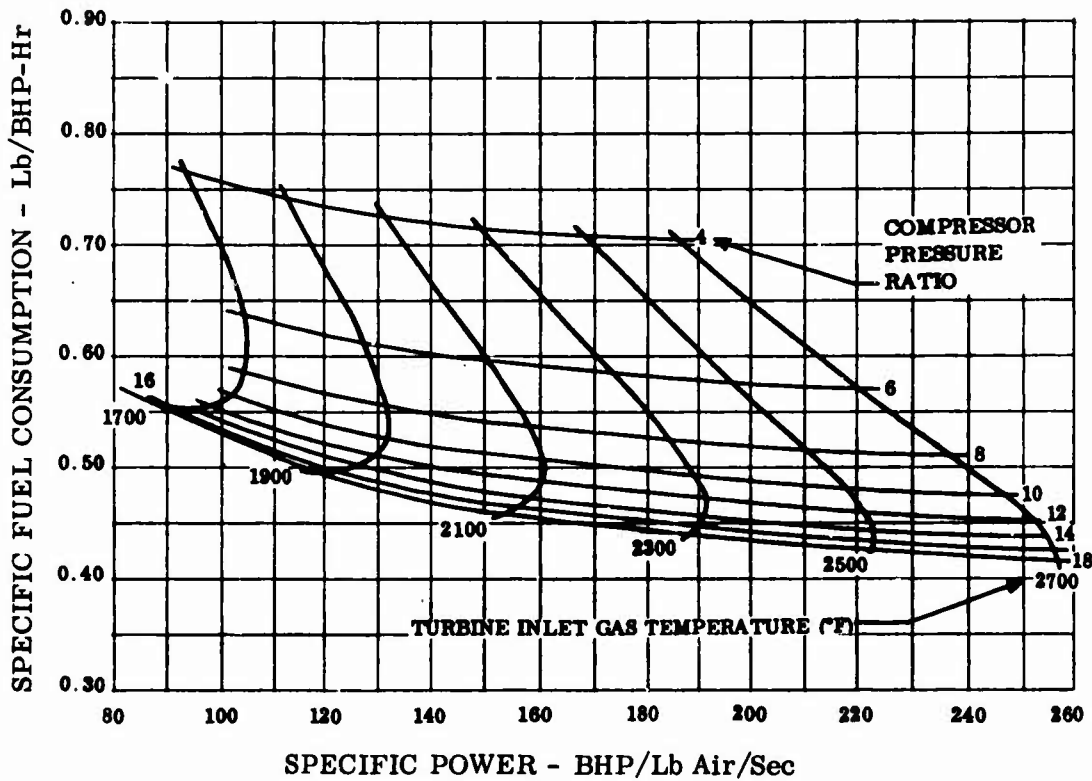


Figure 2. Effect of Gas Temperature on Simple-Cycle Engine Performance.

An itemized breakdown of design-point cycle parameters used to prepare Figures 1 through 3 is as follows:

Compressor Total-to-Static Efficiency (percent)	80
Gas-Producer-Turbine Total-to-Total Efficiency (percent)	86
Power-Turbine Total-to-Static Efficiency (percent)	83
Burner Pressure Drop (percent)	4
Burner Efficiency (percent)	98

The gas producer and power turbine efficiencies selected for the cycle studies are compatible with current Boeing turbine performance, and achieving this performance would not require an advancement in turbine technology. Burner performance values are based on parallel research studies conducted by Boeing. The mean turbine inlet temperature of 2300° F selected for this program allows for a reasonable peak-to-mean gas temperature spread of 200° F.

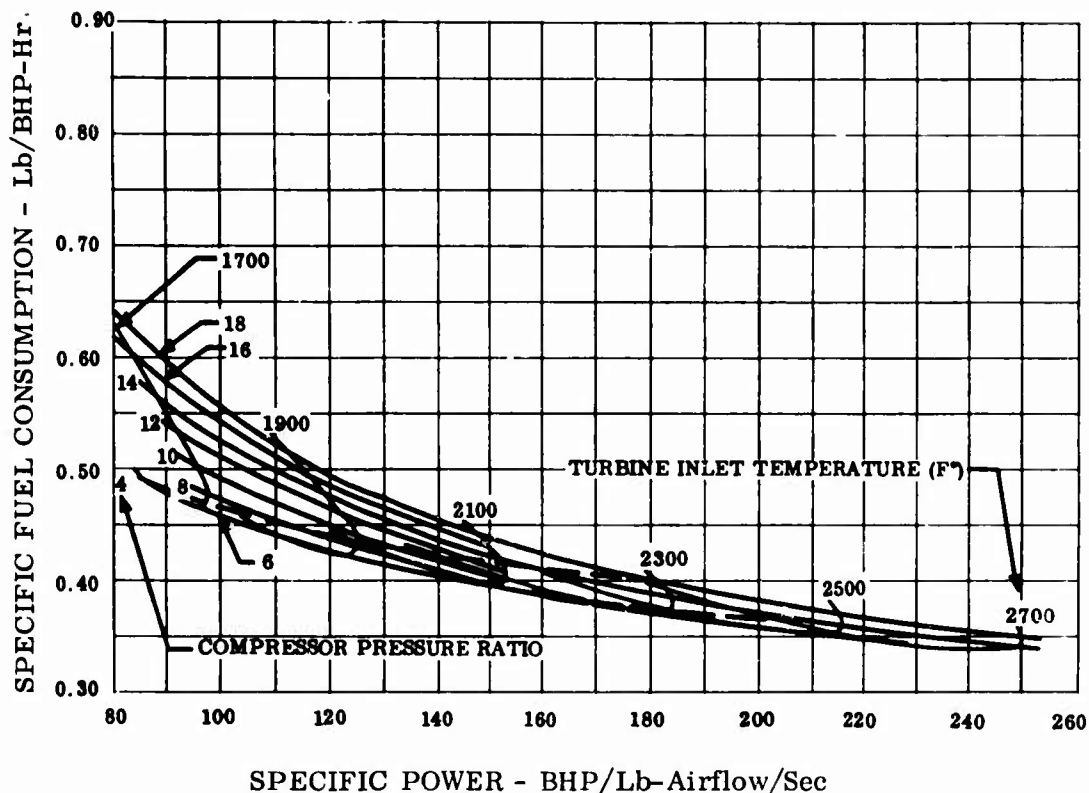


Figure 3. Effect of Gas Temperature on Regenerative Engine Cycle Performance.

Engine characteristics discussed above are for full load. The effect of high-cycle pressure ratio and high-cycle temperature on the part-load performance is shown in Figure 4. Here, the part-load performance of both the regenerative and nonregenerative engines is compared with the performance of a current LOH-type aircraft gas-turbine engine. As shown, the fuel consumption of the future high-pressure, high-temperature engine increase advantages as load decreases. At 40-percent load, the nonregenerative engine shows a 34-percent reduction in part-load specific fuel consumption relative to current engines. At 40-percent load, the regenerative engine shows a 50-percent reduction in part-load specific fuel consumption relative to current engines.

## 1.2 APPROACH TO TURBINE MATERIALS

Materials for the stator-ring assembly, shrouds, and rotor of the high-temperature turbine section are of primary interest for operation at the 2300°F inlet gas temperature. As shown in Figure 5, metal temperatures for these components are expected to range

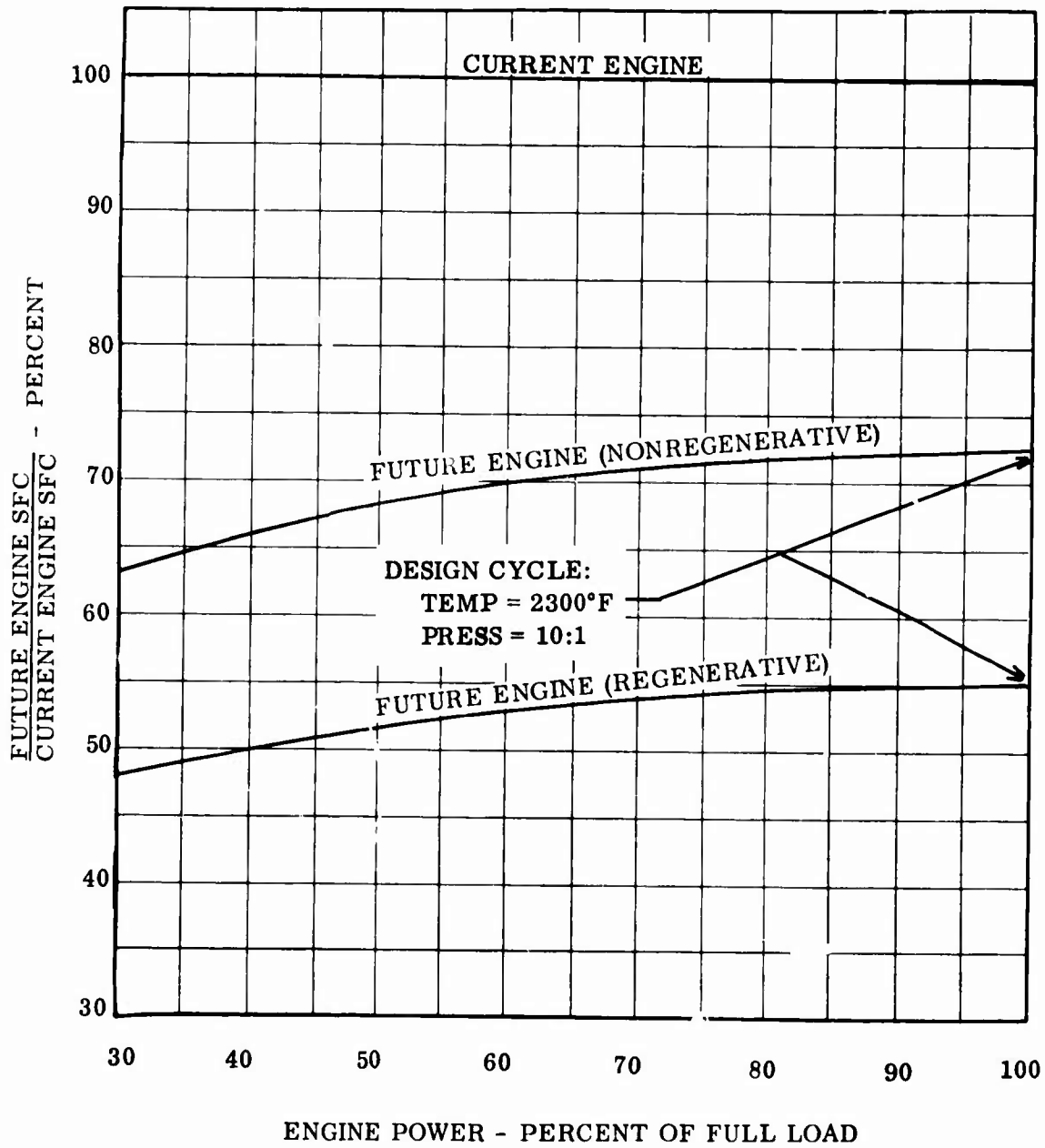
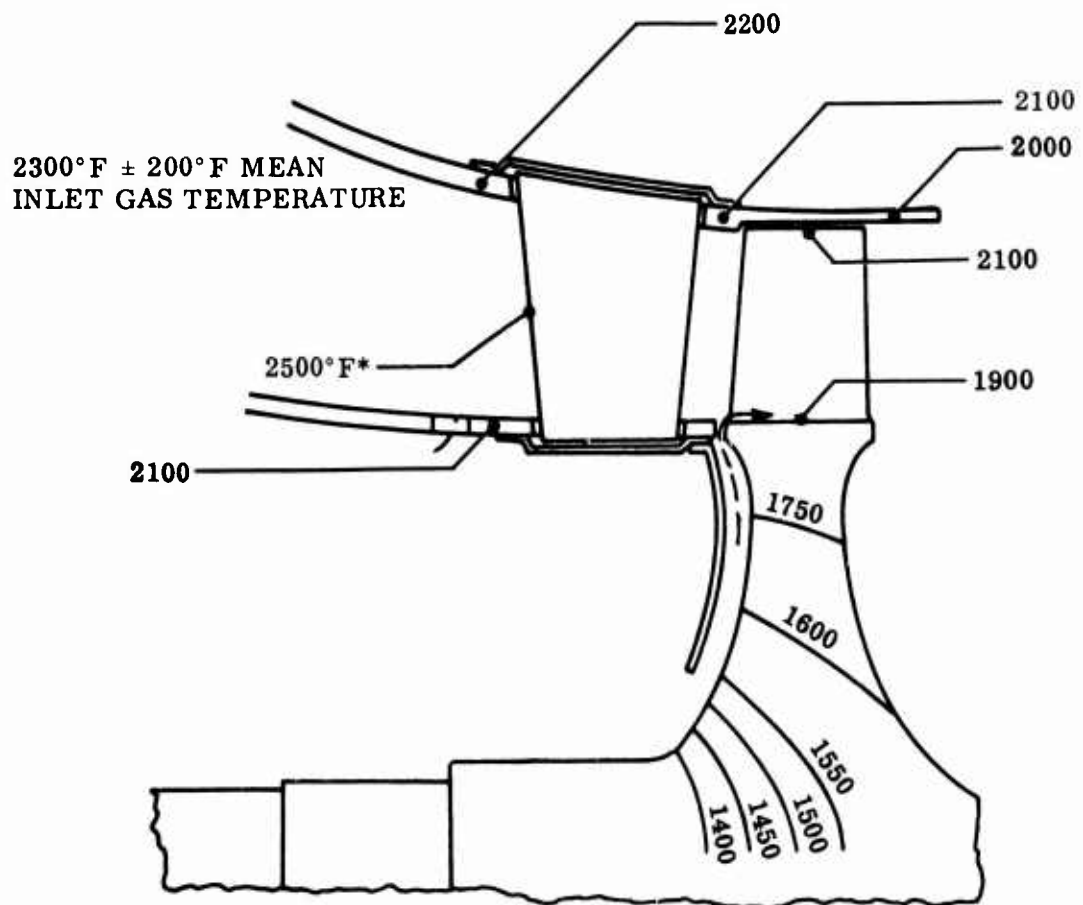


Figure 4. Effect of Cycle Temperature and Pressure on Part-Load Specific Fuel Consumption.



\* ALLOWANCE FOR INLET GAS TEMPERATURE PROFILE

Figure 5. Estimated First-Stage Turbine Component Temperature.

from 1400° to 2500°F at rated power, depending on location in the gas stream and on the inlet temperature profile. Materials with physical and mechanical properties superior to those of current alloys will be required. These properties must include resistance to thermal shock, oxidation, and erosion, consistent with good operating life. The properties must also be maintained over the part-load operating temperature range of the components.

This program was conducted to determine the potential of two new material systems for these high-temperature gas turbine applications. The systems investigated were macrolaminate metal-ceramic composites and dispersion-strengthened nickel-base alloys. The scope of the program specifically involved the

development and evaluation of three macrolaminate composites, i. e., Mo-HfO<sub>2</sub>, Ni-MgO and Ni-Al<sub>2</sub>O<sub>3</sub>, and dispersion-strengthened alloys of Ni-Cr-ThO<sub>2</sub> and Ni-Cr-Mo-ThO<sub>2</sub>. Preliminary analysis of these material systems indicated that the macrolaminate composites might be suitable for turbine stator vane application, and the dispersion-strengthened nickel-base alloys for turbine blade and turbine shroud applications.

### 1.2.1 Macrolaminate Composites

A macrolaminate metal-ceramic composite consists of macroscopic particles or grains, with each grain being composed of alternate layers of a ductile metal and ceramic as shown in Figure 6. The processes for producing composite systems of this type have been described by Knapp and Shanley (U. S. Patent 3,089,196). These material systems have been under development by The Boeing Company for possible space vehicle reentry applications at operating temperatures of 3000° to 4000° F.

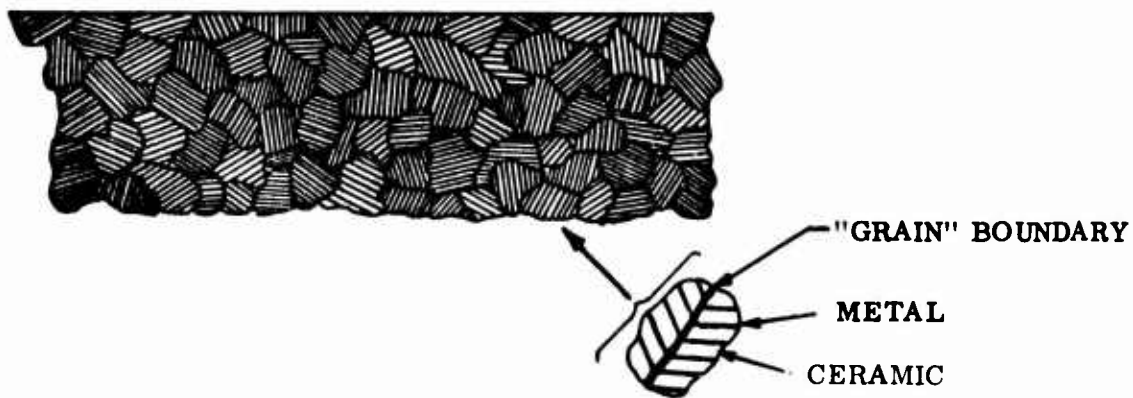


Figure 6. Macrolaminate Metal-Ceramic Composite Schematic.

A macrolaminate metal-ceramic composite material is prepared by suspending powdered ceramics and powdered metals in separate liquid organic vehicles to form paints, which are then applied in alternate layers on a backing plate. The resulting laminated sheet of metal and ceramic is stripped from the backing plate and broken into particles. These particles, which maintain the laminar structure, are compacted in dies to form parts, either by press and sinter techniques or by hot-pressing at the sintering temperature. The sintering or hot-pressing temperatures are below the melting point of the metal phase so as to preserve the laminate structure.

In the case of the Mo-HfO<sub>2</sub> composite, the primary purpose of the metal phase is to provide strength and ductility to the composite system, while the primary purpose of the ceramic phase is to provide oxidation resistance. A feature of the system is its self-healing characteristic, which is attributed to the ability of the exposed ceramic to form a glassy deposit over the composite surface at the operating temperature. If the protective coating on the composite is damaged locally, the alternating layers of ceramic act as barriers and also reform the glassy deposits to seal off the exposed metal layers.

Modulus-of-rupture tests, conducted prior to initiation of this program, indicated that the strength of the Mo-HfO<sub>2</sub> composite at 3000°F was improved over that of recrystallized molybdenum. On this basis, macrolaminate Mo-HfO<sub>2</sub> composites indicated a potential strength level at 2500°F that was comparable to the 1925°F strength of the best cast nickel-base superalloy available.

Thermal shock resistance of the macrolaminate composite system also showed promise. A Mo-HfO<sub>2</sub> specimen was torch-heated to a hot-face temperature near 4000°F in less than 1 minute, maintained at heat for 30 minutes with a gradient of more than 1500°F through the 0.3-inch thickness, and rapidly cooled by shutting off the torch. No cracking or spalling was observed. Other tests were conducted in which specimens were rapidly heated to 2000°F in an air atmosphere, held at temperature for 10 minutes, and air quenched. These specimens maintained their room-temperature flexural strength. For comparison, similar tests on high-strength alumina ceramic caused surface cracks and resulted in a loss of 62 percent of room-temperature strength.

Because the original compositions of the Mo-HfO<sub>2</sub> composites were formulated for relatively short-time service in the range of 3000° to 4000°F, further evaluation was considered essential to assess the suitability of this composite for turbine vane application. In this program, research work on the Mo-HfO<sub>2</sub> composite was concerned with improving its oxidation resistance in the 1200° to 2500°F temperature range.

Preliminary tests showed that SiO<sub>2</sub> and CeO<sub>2</sub> additions provided substantial improvements in stabilizing oxidation resistance at 2500°F. The oxidation resistance of these modifications compared to a basic Mo-HfO<sub>2</sub> composite and pure molybdenum is shown in Figure 7.



strength levels at elevated temperatures. For example, mean flexural strengths of 19,000 psi and 47,000 psi have been reported at 2300° F for fine grain polycrystalline MgO and Al<sub>2</sub>O<sub>3</sub>, respectively (References 1 and 2). The metal phase (nickel) primarily is intended to provide ductility to the composite system. As nickel is inherently oxidation resistant and has a melting point of 2655° F, it should be suitable for extended service in the temperature region of 2300° F. Both the MgO and Al<sub>2</sub>O<sub>3</sub> ceramic phase should be able to supplement the oxidation resistance of nickel. A comparison of the oxidation resistance of a Ni-MgO composite to that of several Mo-HfO<sub>2</sub> composites is shown in Figure 7.

In this program, the primary emphasis on the Ni-MgO and Ni-Al<sub>2</sub>O<sub>3</sub> composites was placed on improving their strength. Studies were conducted to evaluate the effect of additives to the metal and ceramic phases separately, and finally to evaluate their combined effect in a macrolaminate composite. Subsequent elevated temperature tensile, oxidation, and thermal-fatigue tests were conducted to assess the suitability of these composites for turbine vane applications.

### 1.2.2 Dispersion-Strengthened Alloys

Dispersion strengthening is considered to be the most effective strengthening mechanism above temperatures equal to 50 percent of the absolute melting temperature of the metal. Dispersion-strengthened aluminum alloys, commonly known as SAP alloys, were the first to become commercially available. Through continued development, this technique has been employed to strengthen many pure metals. The most recent commercial alloy to be produced is dispersion-strengthened nickel, introduced in 1963 by duPont as TD Nickel.

Dispersion-strengthened alloys are generally produced by powder metallurgical techniques. They normally contain a small volume fraction (less than 10 volume percent) of inert submicron sized particles (less than 0.1 micron) dispersed in the matrix. To be effective, the dispersoid must be uniformly distributed in the matrix and have an interparticle spacing of about 1 micron. The alloy derives its mechanical properties, not from bulk strength of the second phase, as does the macrolaminate composite, but primarily from the fine grain size and substructure that is introduced and retained in the matrix. The dispersoid serves to stabilize microstructure, and thereby to prevent loss of strength at elevated temperatures.

Dispersion-strengthened nickel-base alloys suitable for use in turbine components at metal temperatures up to 2200° F need to have inherent oxidation resistance and at least twice the strength of TD Nickel. These requirements appeared to be attainable by dispersion strengthening a solid-solution nickel-base matrix. As indicated previously, dispersion strengthening has been successfully accomplished with a number of pure metals, but has been attempted only to a limited extent with solid-solution alloys. The approach used in this program to obtain dispersion-strengthened solid-solution alloys was to start with nickel-chromium and nickel-chromium-molybdenum alloy powders and to add ThO<sub>2</sub> as the dispersoid. This procedure involved coating the matrix metal powder with a thorium salt, and then thermally decomposing the salt to ThO<sub>2</sub>. This technique showed evidence of producing a more uniform distribution of the dispersoid than methods involving straight mechanical mixing. Following thermal decomposition, the alloy powder-ThO<sub>2</sub> mixture is consolidated by hot extrusion and is subsequently cold-worked.

Figure 8 illustrates the predicted combined strengthening effects of solid-solution strengthening for a nickel-chromium-molybdenum dispersion-strengthened alloy in comparison with pure nickel, a nickel-chromium alloy, and dispersion-strengthened nickel. On this basis, dispersion-strengthened nickel-base alloys indicated strength levels at 2200° F equivalent to the 1900° F strength level of the best cast nickel-base superalloy.

The program on dispersion-strengthened nickel-base alloys included an initial research effort to develop techniques for preparing alloy powder-ThO<sub>2</sub> mixtures with low levels of contamination, and finally an evaluation of laboratory quantities of dispersion-strengthened alloys to assess their suitability for turbine applications.

### 1.3 MATERIAL GOALS

Initial target properties for the materials were established on the basis of their strength potential and on the predicted requirements for the intended gas turbine applications. The material goals are given in Table II.

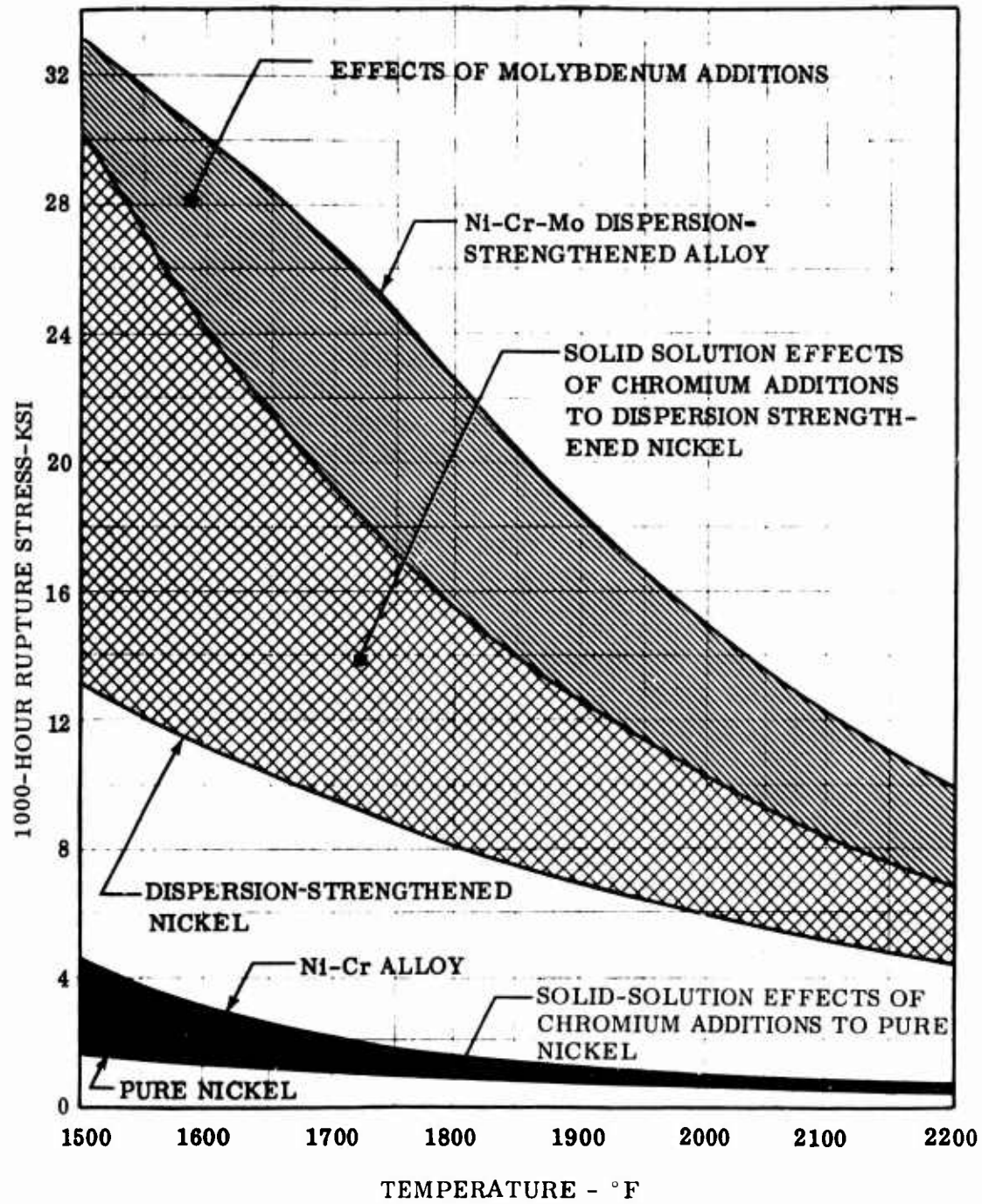


Figure 8. Predicted Stress-Rupture Strength Improvements in Dispersion-Strengthened Nickel-Base Alloys.

**TABLE II**  
**MATERIAL TARGET PROPERTIES**

a) Short-Time Tensile Strength

Material	Temperature °F	Ultimate Tensile Strength psi	0.2% Yield Strength psi
Mo-HfO <sub>2</sub>	70	45,000	40,000
	2500	28,000	22,400
Ni-MgO and Ni-Al <sub>2</sub> O <sub>3</sub>	70	40,000	36,000
	1800	27,500	23,500
	2200	18,000	14,000
Dispersion- Strengthened Alloy	70	120,000	95,000
	1800	45,000	40,000
	2200	30,000	28,000

b) Oxidation Resistance

Material	Exposure	Weight Change After Exposure mg/cm <sup>2</sup>
Mo-HfO <sub>2</sub>	24 Hours at 1200°F	2.0
	24 Hours at 1800°F	2.0
	24 Hours at 2500°F	2.0
Ni-MgO	100 Hours at 2300°F	2.0
Ni-Al <sub>2</sub> O <sub>3</sub>	100 Hours at 2300°F	2.0
Dispersion-Strengthened Alloys	100 Hours at 2200°F	(.0008 inch max.) oxide penetration

c) Thermal-Fatigue Resistance

Material	Temperature Range	Number Cycles Without Failure
Ni-MgO	300°F - 2300°F	500
Ni-Al <sub>2</sub> O <sub>3</sub>	300°F - 2300°F	500
Mo-HfO <sub>2</sub>	300°F - 2500°F	500

1 ▷ Cycle to consist of a 30-second heat cycle and a 20-second cool cycle

## SECTION 2.0 - PROGRAM APPROACH

The object of this program was to assess the suitability of macrolaminate composites and dispersion-strengthened alloys for high-temperature turbine application. The general technical approach taken was to (1) conduct studies to determine the related effects of composition and process variables, (2) define compositions and/or processes based on these studies, and (3) conduct tests on laboratory quantities of material prepared to evaluate capability for gas turbine applications. Details of the program approach and general procedures used in conducting the program are given in the following paragraphs.

### 2.1 MACROLAMINATE COMPOSITE MATERIALS DEVELOPMENT

Three macrolaminate composite systems, Mo-HfO<sub>2</sub>, Ni-MgO, and Ni-Al<sub>2</sub>O<sub>3</sub>, were selected for evaluation in this program. While emphasis was placed on the ceramic phase of each system, the nature of the studies conducted for each was significantly different so that the overall program conducted on each system will be described in separate sections. Certain general procedures which were common to preparing all of the macrolaminate composite materials will be initially described in the following section.

#### 2.1.1 General Fabrication Procedures for Macrolaminate Composites

Unless otherwise specified, composites were prepared with a 50:50 metal-ceramic ratio. The fabrication procedure followed for these composites is outlined in the following steps and is further described in subsequent paragraphs.

- 1) Prepare ceramic and/or metal powders.
- 2) Prepare separate paints pigmented with the above powders.
- 3) Paint laminate sheet with alternate metal and ceramic layers.
- 4) Cut laminate sheet to form particles.
- 5) Size particles by screening.
- 6) Warm-press particles to form composite blanks.

- 7) Preheat at a low temperature to remove organic binder, and sinter at a temperature below the melting point of the metal to consolidate the composites. These operations were normally combined in a single thermal cycle.
- 8) As an alternate to Steps 6 and 7, preheat particles at a low temperature to remove organic binder, and hot-press in graphite dies at a temperature below the melting point of the metal to consolidate the composites.
- 9) Grind or machine to final shape.

The ceramic alloy powders were prepared by making a wet slurry from -325 mesh oxide powders, drying the slurry at 250° F, and pelletizing it by passing the material through a 12-mesh screen. The blended materials were then calcined in air by heating to elevated temperatures between 2500° to 2700° F and allowing reaction by solid-state diffusion. This material was then broken up in a jaw crusher and washed with hydrochloric acid to remove iron contaminants introduced during crushing. After drying, the crushed material was passed through a fluid energy Trost Jet mill to reduce it to 5-micron powder by collision with particles in opposing airstreams.

The metal powder was normally used in the as-purchased condition. When the starting material was too coarse, it was passed through a sluice to separate large particles (larger than 4 microns) so as to maintain the material in a paint suspension.

Paints were prepared for each of the metal and ceramic phases by blending the pigment powder with acrylic resin binders and solvents. Separate resin solvent systems were used for the metal and ceramic phases to prevent re-resolution and lifting of the underlying layer. Table III gives a typical paint formulation.

**TABLE III**  
**MACROLAMINATE PAINT FORMULATION**

<u>Material-Metal Phase</u>	<u>Source</u>	<u>Parts by Weight</u>
Metal Powder	-	100
Ethyl Cellosolve	Scientific Supply	44
Butyl Cellosolve	Scientific Supply	8
Acryloid B66	Rohm and Haas	9

TABLE III (Continued)

Material-Metal Phase	Source	Parts by Weight
Acryloid F10	Rohm and Haas	5
Material-Ceramic Phase	Source	Parts by Weight
Ceramic Powder	-	100
Acryloid F10	Rohm and Haas	14
Solvent No. 350	Standard Oil Co.	24

The laminate sheets were dried overnight at 150°F and cut into particles in a Wiley mill. The particles were screened to pass through a 24-mesh sieve. The particles were pressed to shape in tool steel dies at a temperature of 150°F and a pressure of 12.5 ksi. Various organic burnout and sintering cycles or hot-press cycles were used during this program and are described in detail in other sections as applicable.

A flow diagram of the above described process is shown in Figure 9.

### 2.1.2 Mo-HfO<sub>2</sub> Macrolaminate Composites

The Mo-HfO<sub>2</sub> system provides a refractory metal (melting point 4742°F) and an oxide (melting point 5000°F) which are chemically compatible and have nearly identical thermal expansion of approximately  $5.0 \times 10^{-6}$  inches/inch/°C. Early Boeing development (Reference 4) showed that this system, of all the refractory metal-oxide systems evaluated, had the best potential for atmospheric reentry at temperatures of from 3000° to 4000°F. This has been attributed to the ability of HfO<sub>2</sub> to react with the volatile MoO<sub>3</sub> at elevated temperatures and produce a self-protecting coating. Preliminary attempts to improve oxidation resistance by modifying the ceramic were encouraging; weight loss resulting from oxidation at 2500°F was reduced from 0.33 gm/cm<sup>2</sup> per hour to 0.016 gm/cm<sup>2</sup> per hour. To evaluate the potential of the Mo-HfO<sub>2</sub> composite for turbine application, this program was oriented primarily

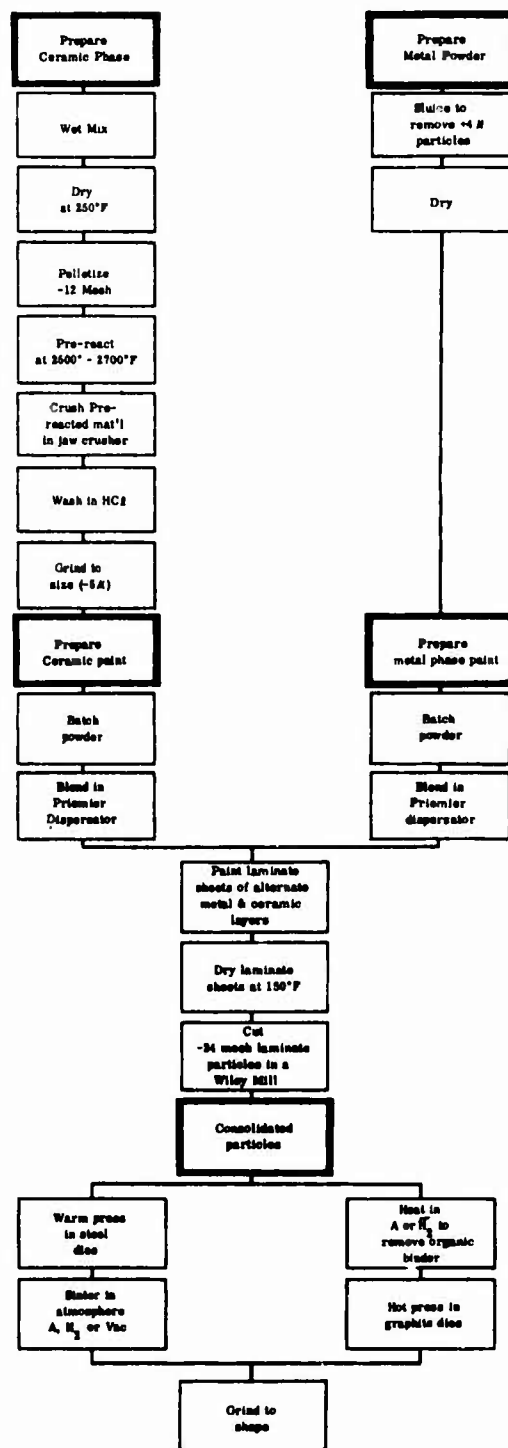


Figure 9. Process for Preparing Macrolaminate Composites.

toward further improving the oxidation resistance of the composite while retaining the elevated temperature properties associated with the metal phase.

Prior work indicated that  $\text{CeO}_2$  - modified  $\text{HfO}_2$  (monoclinic crystallographic structure) is the most compatible with molybdenum for strength and oxidation considerations. Monoclinic  $\text{HfO}_2$  does, however, undergo a phase transformation which could have an effect on the strength. Parallel studies were conducted to determine the nature of the transformation reaction in the  $\text{HfO}_2$  ceramic phase and the effectiveness of other oxide additives in improving the oxidation resistance of the composite. The oxide additives used in the oxidation improvement study included  $\text{MgO}$ ,  $\text{Cr}_2\text{O}_3$ ,  $\text{BaO}$ ,  $\text{SrO}$ , and  $\text{HfSiO}_4$ .

A study was also conducted to evaluate the effectiveness of four types of protective coatings applied to a  $\text{Mo}-(\text{HfO}_2 \cdot 5\text{CeO}_2)^*$  composite. The coatings evaluated included a disilicide coating, solution-sprayed zirconia and chromia coatings, ceramic glazes, and slurry-applied  $\text{TiB}_2$  -  $\text{MoSi}_2$  coatings.

General procedures for preparing the  $\text{Mo}-\text{HfO}_2$  composites are described in Section 2.1.1. Various organic binder burnout and sintering cycles were used during this program and are described in Section 3.1 as applicable.

### 2.1.3 Ni-MgO Macrolaminate Composites

The properties of nickel and magnesia make them ideal in many respects for the development of macrolaminate particle composites. Nickel is ductile and has relatively good resistance to oxidation. Magnesia, which has a melting point close to  $5000^\circ\text{F}$ , has been fabricated to theoretical densities by hot-pressing at temperatures between  $2100^\circ$  and  $2300^\circ\text{F}$ . Its coefficient of expansion,  $14 \times 10^{-6}$  inches/inch/ $^\circ\text{C}$ , matches that of nickel and  $\text{NiO}$ .  $\text{NiO}$  is always present to some degree and forms a continuous solid solution with  $\text{MgO}$ . The low density of magnesia,  $3.6 \text{ gm/cm}^2$ , is also desirable to produce a lightweight structure.

---

\*Note: For describing either the metal or the ceramic phase of a composite, numerals will be used to indicate weight percentages of additives; no numeral will be used for the major component. Parentheses are used to indicate a thermal cycle, as calcining, on the enclosed constituents.

The primary aim of the studies conducted with the Ni-MgO macrolaminate composites was to define compositions and fabricating techniques which could produce composites with low porosity and high strength. Initially, tests were conducted to evaluate the effects of additives and process variables on the strengths of the metal and ceramic phases separately. Subsequently, similar tests were conducted on selected macrolaminate compositions. The additives consisted of inert oxide particles dispersed in the metal and ceramic phases, solid-solution oxide additions to the ceramic phase, and additions of titanium compounds to improve the metal-ceramic bond. The purpose of the dispersed oxide particles was to maintain a fine grain size in the matrix phases. Because of the progressive sequence in which the studies were conducted, specific details on composition and process procedures will be discussed and results will be given in Section 3.2.

Metal-ceramic ratio studies were conducted using a basic macrolaminate composition corresponding to  $(\text{Ni} \cdot 2\text{ThO}_2) \cdot 2\text{TiN} - (\text{MgO} \cdot 5\text{HfO}_2)$ . Metal-ceramic ratios (volume basis of 70:30, 50:50, and 30:70) were evaluated by means of tensile tests at room temperature, 1800°F, and 2200°F; by oxidation tests at 2300°F; and by thermal-fatigue tests with temperature cycle of 300° to 2300°F. Procedures for these tests are given in Section 2.3.

With the exception of the composites prepared for the metal-ceramic ratio study, all composite specimens were prepared with a metal-ceramic ratio (volume basis) of approximately 50:50. The fabrication procedures for preparing the Ni-MgO laminate sheets and macroscopic particles were described previously in Section 2.1.1. To preserve the macrolaminate structure during consolidation of the particles, temperatures below the melting point of the metal phase had to be used. For the Ni-MgO system, hot-pressing at temperatures of 2100° to 2400°F was found to be preferable to warm-pressing and sinter techniques, because higher composite densities were produced.

To prepare the laminate particles for hot-pressing, it was first necessary to remove the organic binder to prevent the rapid evolution of decomposition products which would otherwise occur during the relatively short hot-press cycle. This was accomplished by heating the particles to temperatures of 900° to 1100°F for 3 hours in a controlled atmosphere. Hot-pressing was carried out in graphite dies under an argon cover atmosphere. The dies were heated inside an inductively heated graphite furnace, and pressure was applied to graphite rams by a hydraulic pump. The hot-press facility is shown in Figure 10.

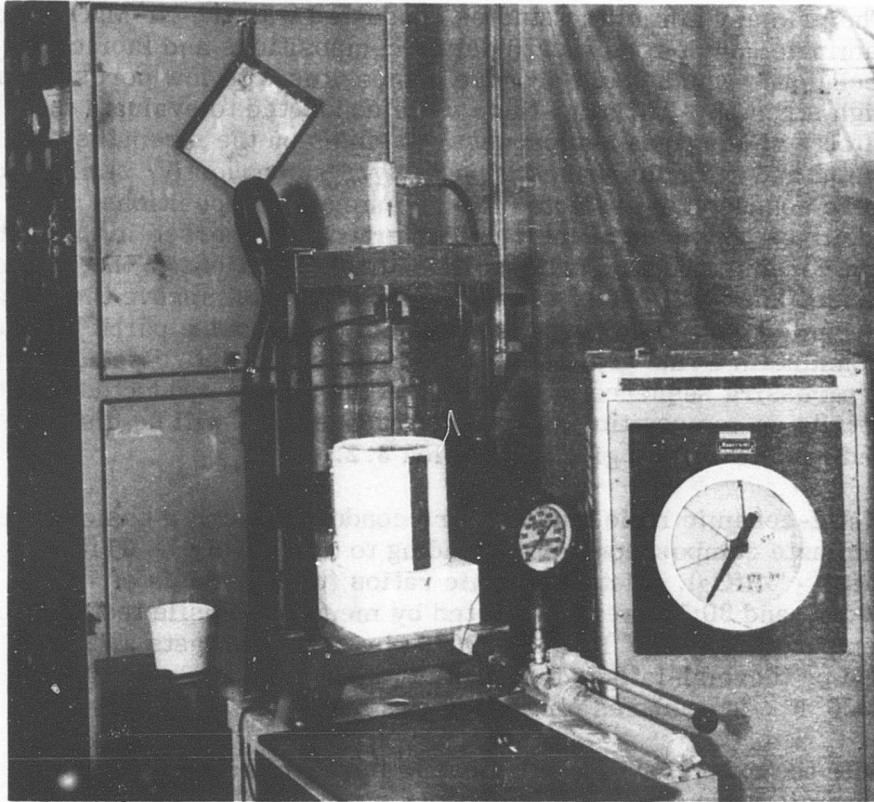


Figure 10. Hot-Press Facility.

Hot-pressing temperatures between 2100° and 2400°F, times at temperature from 1 to 120 minutes, and pressures from 2 to 5 ksi were used, depending on the particular study being conducted. To prevent sticking of the composite part to the die, the dies were initially painted with acrylic-bonded alumina paint, which was used because it provided slightly better parting characteristics.

Following hot-pressing, a majority of specimens were given post-heat-treatment to allow entrapped gasses to diffuse out of the specimens and to effect further consolidation. Specific details of the processing procedures used and the results obtained are described in Section 3.2.

#### 2.1.4 Ni-Al<sub>2</sub>O<sub>3</sub> Macrolaminate Composites

The Ni-Al<sub>2</sub>O<sub>3</sub> macrolaminate composite was considered in this program because of the higher potential strength of Al<sub>2</sub>O<sub>3</sub> compared to MgO. Vasilos (References 2 and 3) reported achieving flexure strengths in excess of 100 ksi from hot-pressed Al<sub>2</sub>O<sub>3</sub> at room temperature and nearly 50 ksi at 2200°F, which made it appear very attractive for use in a macrolaminate composite. It was not known, however, whether hot-pressing conditions compatible to both nickel and Al<sub>2</sub>O<sub>3</sub> could be obtained to achieve high ceramic density in a composite. Also, the coefficient of thermal expansion for Al<sub>2</sub>O<sub>3</sub> is considerably lower than that for nickel ( $9 \times 10^{-6}$  compared to  $14 \times 10^{-6}$  inches/inch/°C) and could result in a high internal stress in the composite.

To assess the potential of the Ni-Al<sub>2</sub>O<sub>3</sub> macrolaminate composite, it was first necessary that time-temperature-pressure parameters for hot-pressing be evaluated and a procedure be established. Because Al<sub>2</sub>O<sub>3</sub> is normally hot-pressed at temperatures in excess of 2500°F, the studies included an attempt to achieve densification at lower temperatures by the introduction of a second component. Jones (Reference 5) showed that minor additions of components like titanium and manganese oxides which form solid solutions were effective in promoting sintering of Al<sub>2</sub>O<sub>3</sub>. Major additions of chromium (up to 17 percent) to the metal phase were also evaluated to determine their effect on the strength and oxidation resistance of the composite.

Following the above studies, a Ni · 1%Cr - Al<sub>2</sub>O<sub>3</sub> · 1/4 TiO<sub>2</sub> macrolaminate composite was selected for metal-ceramic ratio studies. The metal-ceramic ratios evaluated and the tests conducted were the same as those previously described for the Ni-MgO composite in Section 2.1.3.

All of the Ni-Al<sub>2</sub>O<sub>3</sub> macrolaminate composites prepared in this program used the basic hot-pressing procedure previously described for the Ni-MgO system. With the exception of specimens prepared for the metal-ceramic ratio study, all of the Ni-Al<sub>2</sub>O<sub>3</sub> composites were prepared with a metal-ceramic ratio of approximately 50:50. Specific conditions of the processing procedures used are described in Section 3.3.

## 2.2 DISPERSION-STRENGTHENED ALLOY DEVELOPMENT

The preparation of dispersion-strengthened pure nickel by powder metallurgical techniques has been reported by a number of investigators (References 6, 7, 8). Thoria has been used most successfully as the dispersoid because of its ability to be prepared in fine submicron particles and its chemical inertness in a nickel matrix. It is generally accepted that both oxidation resistance and strength can be significantly improved by the addition of chromium and other refractory metals to the dispersion-strengthened pure nickel alloy.

The development of processing techniques to allow the addition of alloying elements, principally chromium, was the area of primary interest. For dispersion-strengthened pure nickel, the possible formation of NiO during processing was considered to be only a minor problem because of the relative ease with which NiO can be reduced. However, additions of chromium and the subsequent formation of chromium oxide during processing presented a more difficult problem. The high heat of formation of  $\text{Cr}_2\text{O}_3$  (267.39 K-cal/mol compared to 57.83 K-cal/mol for NiO) is indicative of the high affinity of chromium for oxygen. Any excess oxygen that is introduced into the alloy, i. e., oxygen not tied up as  $\text{ThO}_2$ , will exist predominantly as  $\text{Cr}_2\text{O}_3$ . The presence of  $\text{Cr}_2\text{O}_3$  in a Ni-Cr- $\text{ThO}_2$  alloy is believed to have an undesirable effect on the dispersoid and to result in low mechanical properties; however, no information is available on the tolerance limit of  $\text{Cr}_2\text{O}_3$  in such an alloy.

This program was concerned with the development of processing techniques which will reduce the level of oxygen contamination in Ni-Cr- $\text{ThO}_2$  alloys. The approach used was to identify the sources of oxygen contamination and then to develop processes to reduce the level of oxygen contamination. To determine the sources of oxygen, studies were conducted on the comminution of alloy powder and on the thermal decomposition of thorium nitrate. In an effort to reduce the level of oxygen contamination, work was conducted to improve the decomposition cycle, to substitute thorium organic salts for thorium nitrate, and to develop a selective reduction process. The selective reduction treatment would be performed on the alloy powder after the thermal decomposition cycle, and its purpose would be to reduce  $\text{Cr}_2\text{O}_3$  selectively without affecting the more thermally stable  $\text{ThO}_2$ .

To evaluate the effectiveness of these procedures, quantities of bar stock were prepared and evaluated by metallographic analysis and tensile test at room temperature and 1800°F. Preliminary cold-work studies were also conducted on extruded bar stock by subjecting the material to repetitive cold swaging and annealing cycles. Hardness tests and tensile tests at 1800°F were conducted on the bar stock after various numbers of cold swaging and annealing cycles.

Specific details on the studies conducted are described and the results are given in Section 3.4.

#### 2.2.1 General Fabrication Procedures for Dispersion-Strengthened Materials

As indicated previously, powder metallurgical techniques were employed to produce the materials. Because the interparticle spacing of the dispersoid in the final alloy is dependent on the powder size, the as-received powders were ground in an attrition mill.

Thermal decomposition of thorium nitrate was used as the basic method of introducing the dispersoid. This method has been found to provide a more uniform distribution of the dispersoid than was possible by mechanical mixing. Selective reduction treatments were employed to reduce the excess oxygen of the powders. Consolidation of the material was accomplished by canning the powders in a mild steel container and extruding at 1800°F with a reduction ratio of approximately 22:1.

Specific details on the studies conducted for the dispersion-strengthened materials are described and the results are given in Section 3.4.

### 2.3 TEST PROCEDURES

Procedures for general tests used in the course of the program are described in this section of the report.

#### 2.3.1 Flexural Test

Flexural testing was used extensively on the macrolaminate composite development programs. The specimens prepared by hot-pressing were nominally 0.1 x 0.5 x 2.5 inches, while the specimens prepared by warm-press and sinter techniques were generally slightly narrower and shorter because of the shrinkage

of specimens during sintering. The amount of shrinkage averaged about 13 percent; however, it was dependent on the specific composition being sintered.

Flexural test specimens were finished by surface grinding with a diamond wheel and hand polishing on 600-grit silicon carbide paper. Inspection of specimens prior to testing was accomplished by visual inspection. The use of penetrant inspection techniques to determine flaws was generally unsatisfactory; penetrant adhered to the surface of the ceramic platelets and thereby produced a background which interfered with the detection of possible flaws. The detection of flaws by X-ray inspection was unsatisfactory due to the difference in X-ray density between the metal and ceramic phases.

All flexural testing was conducted at room temperature on 1- or 2-inch centers by using center point loading. When flexural strength was evaluated in both the as-pressed and post-treated conditions, the as-pressed specimens were tested on 2-inch centers and the broken halves were tested on 1-inch centers after post-treating. A Tinius-Olsen test machine, with load ranges from 120 to 12,000 pounds, was used to conduct the tests. Head travel was held constant at 0.05 inch per minute. Load-deformation curves were obtained using a Tinius-Olsen Model D-2 deflector to measure head travel. Strength values were calculated as follows:

$$\text{Flexural strength in psi} = \frac{3 Pl}{2bd^2}$$

where

- P = load in pounds
- l = span in inches
- b = specimen width in inches
- d = specimen thickness in inches

Flexural yield loads were measured from the load-deflection diagrams. The yield load was defined as the load which caused plastic deformation, i. e., departure from the slope of the load-deflection line.

### 2.3.2 Oxidation Tests

Oxidation tests on the Mo-HfO<sub>2</sub> composite system were conducted on cylindrical specimens 0.5 inch in diameter by 0.5 inch in height. All of these specimens were prepared by warm-press and sinter

techniques to approximately 0.060 inch oversize and were finished by grinding. Centerless and surface grinding operations were conducted using silicon carbide wheels. Cooling was with a water-base solution. Tests of a 24-hour duration were conducted at temperatures of 1200°, 1800°, and 2500° F.

The test at 2500° F was conducted by suspending a specimen in a vertical tube furnace from a weight balance by means of a platinum wire basket. Weight change data as a function of time could be obtained directly from the balance. Initial and final weights were recorded on a separate balance to enable compensation for possible buildup of MoO<sub>3</sub> on the platinum suspension wire. Air was allowed to pass through the tube furnace by natural convection. Specimen temperatures were measured using an optical pyrometer, which provided an accuracy of ±10° F.

Oxidation tests at 1200° and 1800° F were conducted in a box furnace, with weight change measurements made after 1, 3, and 24 hours of exposure. Specimens were supported on the zirconia rods lying in alumina boats, so as to allow air circulation around the specimens.

Oxidation tests on Ni-MgO and Ni-Al<sub>2</sub>O<sub>3</sub> composite systems used rectangular specimens measuring approximately 0.1 x 0.5 x 1.0 inch. The oxidation specimens were prepared from fractured flexural test specimens. The tests were conducted in box furnaces at temperatures of 2200° and 2300° F, with weight change data recorded at 24- and 100-hour intervals. The specimens were held in slotted alumina trays to allow air circulation on all sides of the specimen, as shown in Figure 11.

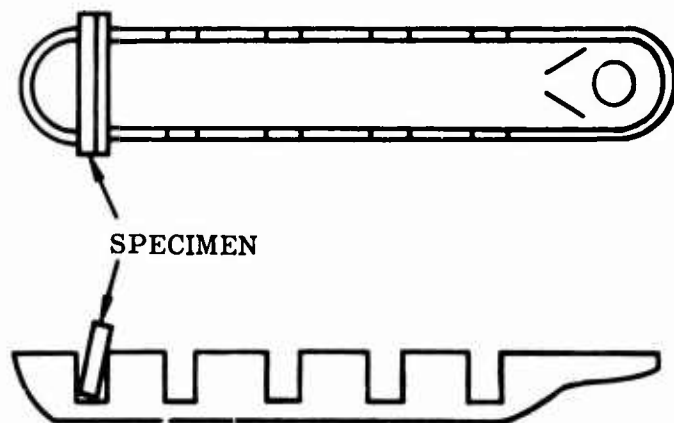


Figure 11. Sketch of Oxidation Test Setup.

### 2.3.3 Density Measurements

Bulk density measurements on macrolaminate composites were made by using immersion techniques. Specimens to be checked were saturated with the immersion liquid, either kerosene or water, by boiling for 2 hours. The saturated specimens were then weighed in air and in the immersion liquid. Bulk density was calculated as follows:

$$\text{Bulk density (gm/cc)} = \frac{W}{W_x - W_y} K$$

where

W = weight of specimen

W<sub>x</sub> = weight of specimen saturated with liquid

W<sub>y</sub> = weight of saturated specimen suspended in liquid

K = specific gravity of liquid

Apparent porosity is the porosity that is open to the surface, and is sometimes referred to as open porosity. Apparent porosity was based on the amount of liquid absorbed while determining bulk density as described above, and was calculated as follows:

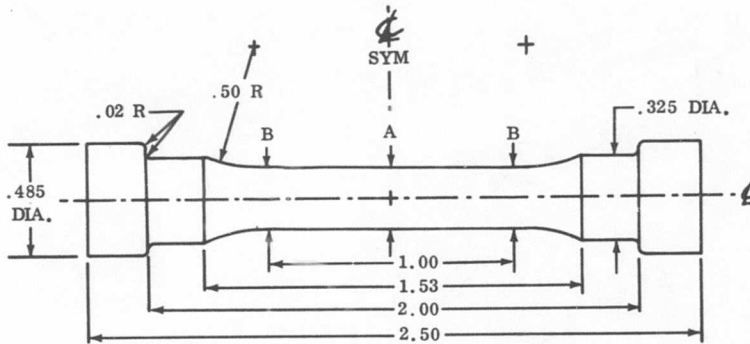
$$\text{Apparent porosity (\%)} = \frac{W_x - W}{W_x - W_y} \times 100$$

### 2.3.4 Tensile Tests

Tensile tests on macrolaminate composites were conducted at room temperature, 1800°, and 2200°F on button-head specimens shown in Figure 12. The specimens were machined from 4-1/2 x 1/2 x 2-1/2-inch blanks by center grinding using a fine-grain (220-240 grit) silicon carbide grinding wheel and standard center grinding techniques.

Following center grinding, the reduced section of the test bars was polished using 600-grit paper.

A photograph of the grip assembly is shown in Figure 13. The split collets were fabricated from cast 713C alloy, and the extension rods were fabricated from Udimet 500 alloy bar stock. A quartz lamp radiant heating furnace was used for the elevated temperature tensile tests. Temperatures were monitored with chromel-alumel thermocouples attached on each end of the specimen reduced section with nichrome wire. The tests were conducted on a 12,000-pound-capacity Baldwin test machine, and a Baldwin



B DIA. TO BLEND UNIFORMLY INTO A DIA.

A	.250 MAX	.247 MIN
B	A + .003 TO + .005	

Figure 12. Macrolaminate Composite Tensile Test Specimen.

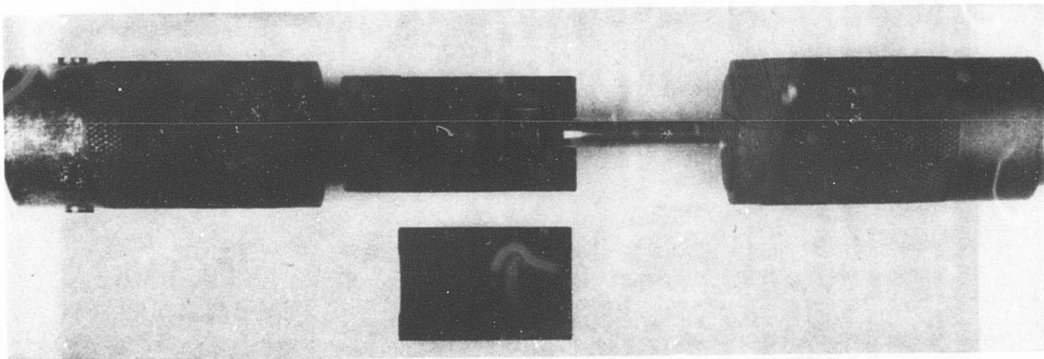


Figure 13. Tensile Test Fixture Assembly for Macrolaminate Composites.

TSMD dual-range extensometer was used to measure strain. A strain rate of 0.005 inch/inch/minute was maintained throughout the test. The test setup is shown in Figure 14.

Room temperature and elevated temperature tensile tests on the dispersion-strengthened alloys were conducted in accordance with ASTM E8-61T and ASTM E21-58T, respectively. Due to the limited quantity and size of material available, substandard test specimens were utilized. The gage section was machined to a

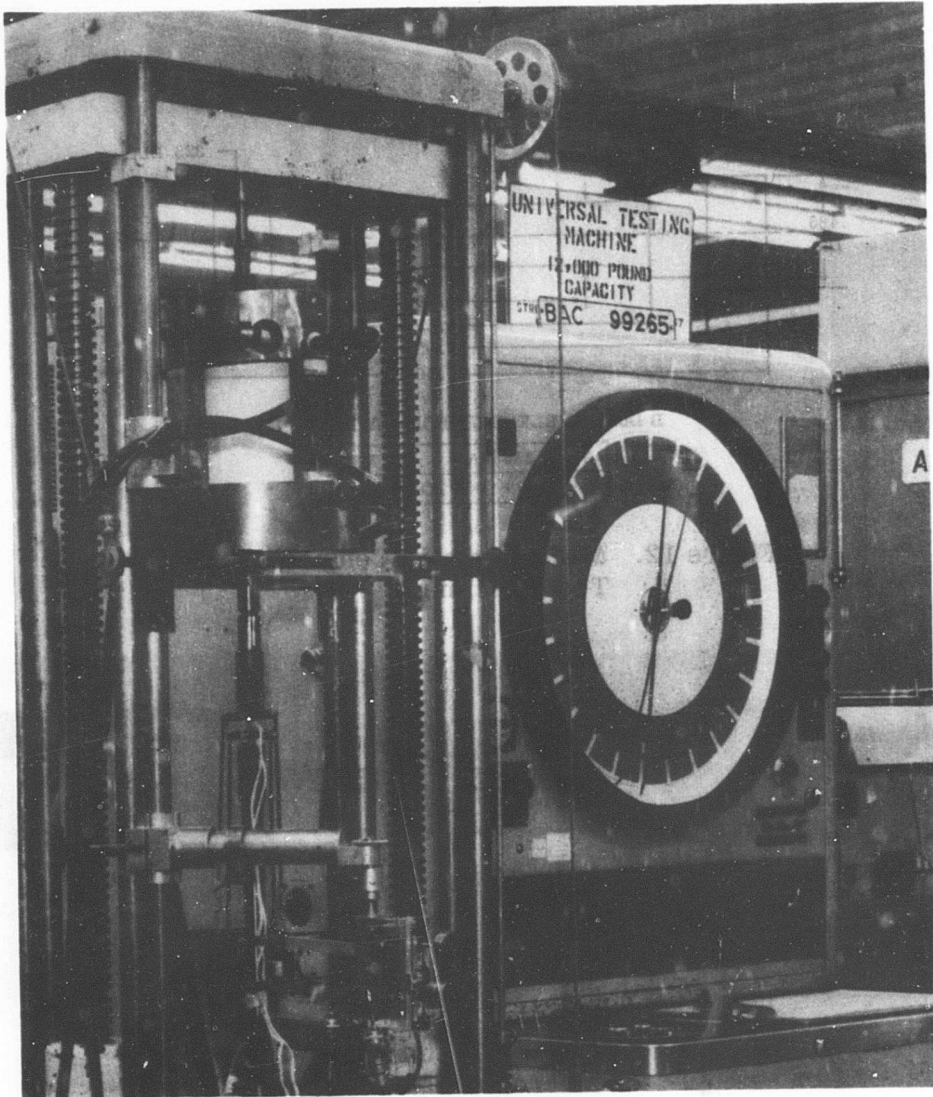


Figure 14. Tensile Test Setup for  
Macrolaminate Composites.

0.160-inch diameter, with other dimensions proportional to those described in Figure 8 of ASTM E8-61T. A strain rate of 0.005 inch/inch/minute was maintained up to the yield point, and then increased to 0.05 inch/inch/minute to fracture.

### 2.3.5 Thermal-Fatigue Tests

Prior work with superalloys has shown that thermal-fatigue testing is an effective laboratory method of evaluating turbine nozzle vane materials. The thermal-fatigue tests conducted on the macrolaminate composites consisted of subjecting wedge-shaped test specimens to alternate flame heating and air-blast cooling cycles. The specimen configuration used is shown in Figure 15.

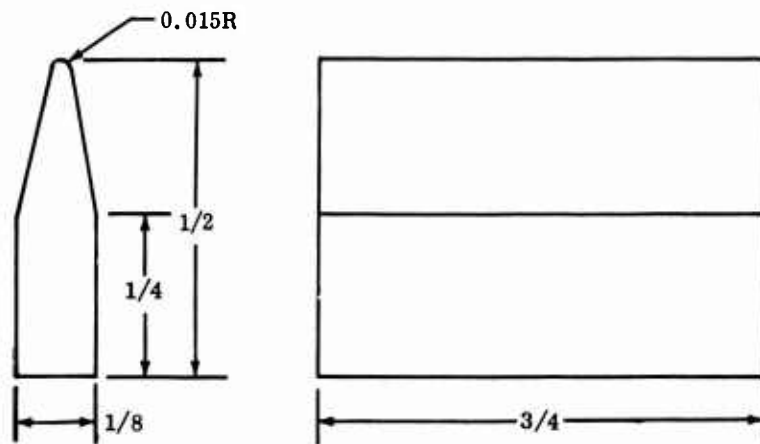


Figure 15. Thermal-Fatigue Test Specimen for Macrolaminate Composites.

The thermal-fatigue test machine, shown in Figure 16, contained multiple flame-heating and air-blast cooling stations mounted on a movable platform. Burners were equipped with static pressure taps to aid in balancing the gas flow between burners.

The thermal cycle consisted of a 30-second heat cycle to  $2300^{\circ}\text{F} \pm 25^{\circ}$  and a 20-second cool cycle to  $300^{\circ}\text{F}$ . Temperatures at specimen leading edges were measured with a total radiation pyrometer and monitored with an optical pyrometer. The upper temperature of the thermal cycle was controlled by the radiation pyrometer and a recording controller. The cooling cycle was timer-controlled, and was established with the use of temperature-indicating crayons, which have an accuracy of approximately  $\pm 25^{\circ}\text{F}$ .

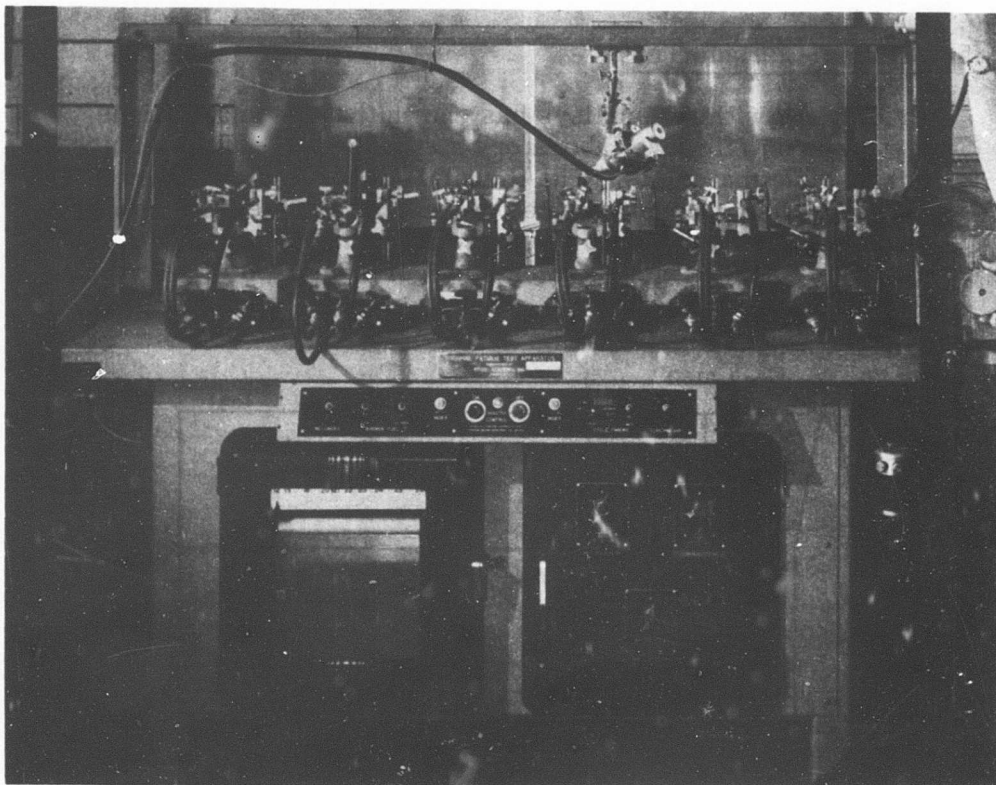


Figure 16. Thermal-Fatigue Test Machine.

#### 2.4 TEST MATERIALS

Analyses of powdered materials used for the preparation of Mo-HfO<sub>2</sub> composites are given in Tables IV and V.

For the oxidation study, MgO, SrO, BaO, Cr<sub>2</sub>O<sub>3</sub> and HfSiO<sub>4</sub> were added to the HfO<sub>2</sub> ceramic phase, as described in Section 3.1.5. MgO, SrO and BaO were added as carbonates. HfSiO<sub>4</sub> was prepared from HfO<sub>2</sub> and SiO<sub>2</sub>. All of the materials used, except the HfO<sub>2</sub> which was described in Table V, were Baker's Reagent Grade Chemicals.

Additions of CeO<sub>2</sub> to the HfO<sub>2</sub> ceramic were made using - 325 mesh Frederick Smith Chemical Co. Reagent Grade CeO<sub>2</sub> powder.

The analysis of Sherritt-Gordon nickel powder used for preparing the Ni-MgO and Ni-Al<sub>2</sub>O<sub>3</sub> composites is given in Table VI.

**TABLE IV**  
**ANALYSIS OF MOLYBDENUM POWDER**

Source: Wah Chang Corporation  
 Grade: Hydrogen Reduced (-325 Mesh).  
 Lot No: Mo = 221 (Analysis Certified by Vendor)

Composition (Weight Percent):	W	Al	C	Co	Cr	Cu
	.04	.003	.0041	<.001	.0015	.001
	Fe	Mg	Mn	NVM	O <sub>2</sub>	Pb
	.008	<.001	<.001	.02	.086	<.001
	Si	Sn	Ni	Mo		
	.015	.006	.0015	99.8		

Fisher Sub Sieve: 1.50 microns

**TABLE V**  
**ANALYSIS OF HAFNIA POWDER**

Source: Wah Chang Corporation  
 Grade: Reactor Grade II (-325 Mesh)  
 Lot No: 90 (Analysis Certified by Vendor)

Composition (Weight Percent):	Fe	Si	Ti	Zr	Ta	Cb
	.42	.25	.27	.55	.02	.01
	Al	B	Cd	Co	Cu	Mg
	.024	.003	<.0001	<.0005	<.004	.01
	Mn	Mo	Ni	Pb	Sn	V
	.005	<.001	.0025	.005	<.001	<.005
	W	HfO <sub>2</sub>				
	<.002	Bal.				

Median Particle  
 Diameter: 5.35 microns

TABLE VI  
ANALYSIS OF NICKEL POWDER

---



---

Source: Sherritt-Gordon Mines Limited  
 Grade: NF-IM  
 Lot No: P-445 (Analysis Certified by Vendor)

Composition  
 (Weight Percent):

	C	S	Fe	Cu	Co	Ni
	.029	.022	.042	.004	.043	Bal.

Fisher Sub Sieve: 0.94 micron

Density: 1.12 grams/cc

---



---

Analyses of Mond carbonyl-nickel powder used for preparing the Ni-MgO and Ni-Al<sub>2</sub>O<sub>3</sub> composites are given in Table VII.

TABLE VII  
ANALYSIS OF CARBONYL-NICKEL POWDER

---



---

Source: The International Nickel Company, Inc.  
 Grade: Type 122 Carbonyl Powder  
 (Analyses Certified by Vendor)

Composition  
 (Weight Percent):

	Fe	C	S
	.002	.074	.0004

Particle Size: 4.67 microns

Density: 2.16 grams/cc

---

Grade: Type 255 Carbonyl Powder

Composition  
 (Weight Percent):

	Fe	C	O <sub>2</sub>	S
	.004	.13	.7	.0004

Particle Size: 2.83 microns

Density: .48 gram/cc

---



---

The analysis of the nickel-chromium powder used to prepare the Ni · Cr-Al<sub>2</sub>O<sub>3</sub> composites is given in Table VIII. This is the same material used for the dispersion-strengthened alloy program conducted by NEMLAB.

TABLE VIII  
ANALYSIS OF NICKEL-CHROMIUM ALLOY POWDER

---

Source: New England Materials Laboratory; Manufactured by  
Acieries de Gennevilliers, Paris, France

Grade: 80 Ni-20 Cr (Analysis Performed by Boeing)

Composition (Weight Percent):	C	Cr	Mg	Si	Fe	Al
	.12	20.48	.5	.2	.2	.1
	Mn	Ti	Co	Cu	Ni	
	.1	.05	.01	.01	Bal.	

Particle Size: 9.0 Microns

---

Mallinckrodt Reagent Grade MgO (average particle size approximately 0.1 micron) and Baker's Analyzed Reagent Grades of Mg(NO<sub>3</sub>)<sub>2</sub> and MgCO<sub>3</sub> were used to prepare the ceramic phase for the Ni-MgO composites. The analysis of the HfCl<sub>4</sub> used in preparing the (MgO · 5HfO<sub>2</sub>) ceramic phase is given in Table IX.

Linde A 0.3 micron Al<sub>2</sub>O<sub>3</sub> was used to prepare the ceramic phase for the Ni-Al<sub>2</sub>O<sub>3</sub> composites. This material is furnished by the manufacturer to meet the impurity range specified in Table X.

TABLE IX  
ANALYSIS OF HAFNIUM CHLORIDE

---



---

Source: Wah Chang Corporation  
 Grade: Reactor Grade  
 Lot No.: H-157 (Analysis Certified by Vendor)

Composition	Al	Cb	Cd	Co	Cr	Cu
(Weight Percent):	.0175	<.01	<.0001	<.0005	<.001	<.004
	Fe	Mg	Mn	Mo	Ni	Pb
	<.005	<.001	<.001	<.001	<.001	<.005
	Si	Sn	Ta	Ti	V	W
	.0065	<.001	<.02	.005	<.005	<.005
	Zr	HfCl <sub>4</sub>				
	3.0	Bal.				

---



---

TABLE X  
IMPURITY RANGE FOR LINDE-A

---



---

Source: Union Carbide Corporation, Linde Division  
 Grade: Linde-A Al<sub>2</sub>O<sub>3</sub> (Impurity Range Specified by Manufacturer)

Impurity Range:  
 (Parts per Million):

	Mg	Si	Ca	Fe
	<.2	30-60	10-20	2-5
	Pb	Ga	Cu	Ag
	50-100	<10	<1	<1
	Cr	Ni		
	Trace	Trace		

---



---

## SECTION 3.0 - DEVELOPMENT PROGRAM

This section of the report will describe the studies conducted and the test results obtained for each of the material systems considered in this program.

### 3.1 Mo-HfO<sub>2</sub> MACROLAMINATE COMPOSITES

Prior Boeing work showed that a 5-percent addition of CeO<sub>2</sub> to an HfO<sub>2</sub>-base ceramic was instrumental in improving both the strength and oxidation resistance of the composite. The CeO<sub>2</sub> additions were believed to aid in the sintering of the ceramic phase and to improve the metal-ceramic bond. Ceria produces no change in normally monoclinic hafnia. The CeO<sub>2</sub>-modified monoclinic phase provides an excellent thermal expansion match with molybdenum, but does undergo a reversible phase transformation to the tetragonal phase at elevated temperatures.

The research and development effort conducted on Mo-(HfO<sub>2</sub> · 5 CeO<sub>2</sub>) composites consisted of

- Base-Line Property Evaluation
- Phase Transformation Studies
- Process Evaluation Studies
- Molybdenum-Mullite · Alumina Composites
- Oxidation Studies
- Protective Coating Study

These studies are described in the following paragraphs.

#### 3.1.1 Preliminary Flexural Tests

Some preliminary room temperature flexural tests were conducted on Mo-(HfO<sub>2</sub> · 5CeO<sub>2</sub>) macrolaminate composites and the separate metal and ceramic components. A combined organic burnout and sintering cycle, shown in Figure 17, was used to prepare the flexural test specimens. The test results are shown in Table XI.

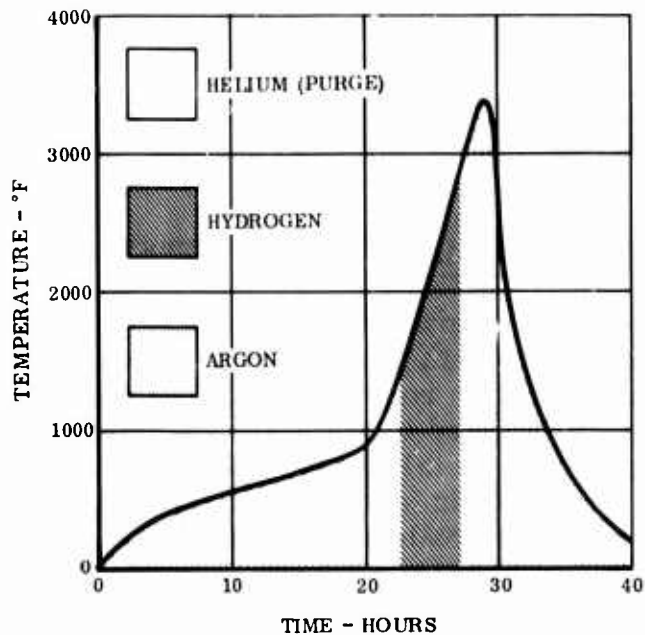


Figure 17. Combined Organic Binder Decomposition and Sintering Cycle.

TABLE XI  
FLEXURAL STRENGTH OF Mo-(HfO<sub>2</sub> · 5CeO<sub>2</sub>)  
AND SEPARATE PHASES

Specimen	FYS, psi	UFS, psi	Deformation, in.
Mo	86,300	94,200	0.015
(HfO <sub>2</sub> · 5CeO <sub>2</sub> )	*	8,300	-
Mo-(HfO <sub>2</sub> · 5CeO <sub>2</sub> )	*	33,300	-

\* No yield point reached

The ceramic phase showed a high (6.4 percent) apparent porosity, and also showed evidence of microcracking on metallographic evaluation. The low ceramic strength indicated that effort should be concentrated on improving these low ceramic properties. Phase transformation studies were conducted as a part of this effort.

### 3.1.2 Phase Transformation Studies

Hafnia is isomorphous with  $ZrO_2$  and goes through a monoclinic-to-tetragonal phase transformation which entails a rapid volume contraction on heating and a volume expansion on cooling. In  $ZrO_2$ , the transformation occurs near  $1800^\circ F$ . Relatively little data are reported on the phase transformation of  $HfO_2$ , and available data are not always in agreement. Curtis (Reference 9) reported that the transformation in  $HfO_2$  occurred near  $3100^\circ F$ . Ohnystry, Basil, and Rose (Reference 10) measured the thermal expansion of reactor Grade II  $HfO_2$ , the same type used in this program. They report a rapid volume contraction, indicative of a phase transformation, starting near  $2800^\circ F$  on heating. Impurities or additives to a pure material tend to shift the transformation temperature and may also increase or decrease the magnitude of the change. To be suitable for repeated cycling to temperatures of  $2500^\circ F$  in a gas turbine engine, the transformation temperature of the  $HfO_2$  ceramic phase would have to be above  $2500^\circ F$ . The transformation temperature should also be above the fabrication temperature in order to avoid damage during consolidation. In order to evaluate further the suitability of the Mo- $HfO_2$  system and plan subsequent work, additional data on the nature of the phase transformation were required.

Initial transformation studies were made using differential thermal analysis (DTA) on  $(HfO_2 \cdot 5CeO_2)$  specimens. The specimens,  $5/16$  inch in diameter by 1 inch in length, were prepared by bisque-firing prereacted  $(HfO_2 \cdot 5CeO_2)$  powder at  $2500^\circ F$ . The specimen was heated in an induction furnace using a graphite susceptor. Thermocouples of tungsten-5 rhenium/tungsten were used to measure the temperatures, and an argon atmosphere was utilized to prevent oxidation of the test setup.

On heating the specimens for thermal analysis, temperatures above  $2200^\circ F$  could not be accurately measured due to an induced signal in the thermocouples from the power supply. However, with the power supply shut off, a DTA curve was obtained on cooling from  $3400^\circ F$ . The transformation was indicated to start at  $2830^\circ F$  and to reach a peak at approximately  $2760^\circ F$ .

A repeat analysis was conducted in an air environment using a resistance heated furnace and platinum-rhodium/platinum thermocouples. No evidence of a transformation was observed on heating to  $2900^\circ F$ , which was the limiting temperature of the furnace used.

To obtain more definitive information, small specimens of ( $\text{HfO}_2 \cdot 5\text{CeO}_2$ ), fabricated as above, were heated in air at temperatures from  $2400^\circ$  to  $3000^\circ\text{F}$  for different lengths of time, were water-quenched to retain the structure, and were analyzed by X-ray diffraction techniques. Test conditions and results are shown in Table XII.

TABLE XII  
RESULTS OF X-RAY DIFFRACTION ANALYSIS

Temperature, °F	Time at Temperature, hr.	X-ray Diffraction Results
2400	6	Monoclinic Strong
2500	6	Monoclinic Strong, Tetragonal Weak
2650	6	Monoclinic Strong, Tetragonal Moderate
2700	0.5	Monoclinic Strong, Tetragonal Weak
2750	0.5	Monoclinic Strong, Tetragonal Moderate
2750	6	Monoclinic Strong, Tetragonal Moderate
2800	0.5	Monoclinic Strong, Tetragonal Moderate
3000	0.5	Monoclinic Strong, Tetragonal Moderate

This study showed that the phase transformation was sluggish and that the structure was stable up to  $2700^\circ\text{F}$  for short intervals of time and up to  $2400^\circ\text{F}$  for longer periods of time. The data indicate that a phase transformation was occurring at temperatures lower than initially anticipated and could be contributing to the

low properties of the ceramic phase. Subsequent work was conducted to evaluate the effect of reduced  $\text{CeO}_2$  content and to evaluate modified fabrication processes that would avoid or minimize the effects of the transformation.

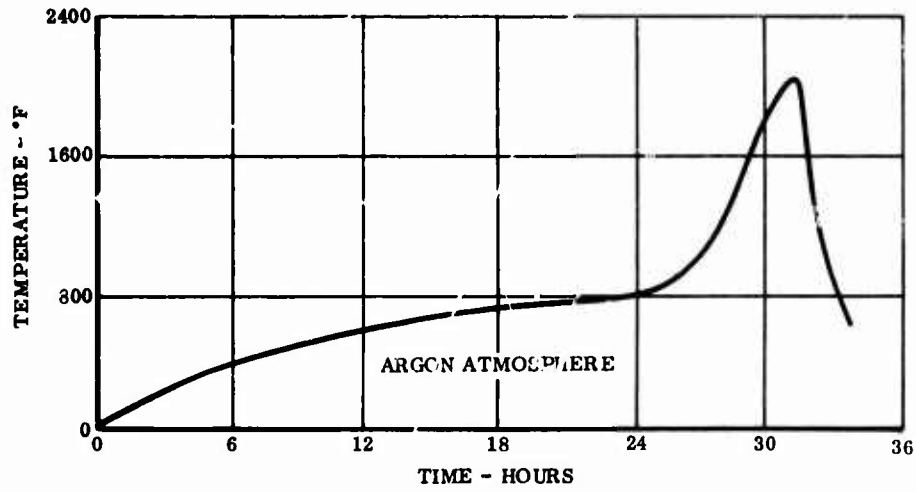
Reduced  $\text{CeO}_2$  Content - To determine the effect of  $\text{CeO}_2$  content on the phase transformation, specimens of  $(\text{HfO}_2 \cdot 3\text{CeO}_2)$  and  $(\text{HfO}_2 \cdot 1\text{CeO}_2)$  were fabricated and evaluated for stability. X-ray analysis of specimens water-quenched after heating in air at  $2700^\circ\text{F}$  for 6 hours showed no trace of the high-temperature tetragonal phase.

These results showed that the phase transformation could be moved well beyond the use temperature by reducing the  $\text{CeO}_2$  content. Mo- $\text{HfO}_2$  flexure test specimens with 1-, 3-, and 5-percent  $\text{CeO}_2$  additions to the ceramic phase were prepared to evaluate the effect of  $\text{CeO}_2$  content on the strength of the composite. Based on some preliminary results of process studies being conducted concurrently (see Section 3.1.3), these specimens were vacuum-sintered ( $1 \times 10^{-4}$  Torr) using separate organic binder decomposition and sintering cycles as shown in Figure 18. Separate cycles were necessary because removal of the organic binder during vacuum-sintering would have contaminated the vacuum system. The organic binder decomposition cycle also incorporated a short heating period to  $2000^\circ\text{F}$ . The purpose was to effect a partial sinter so that the composite specimens would have adequate "green" strength to permit handling when transferring to the vacuum-sintering furnace.

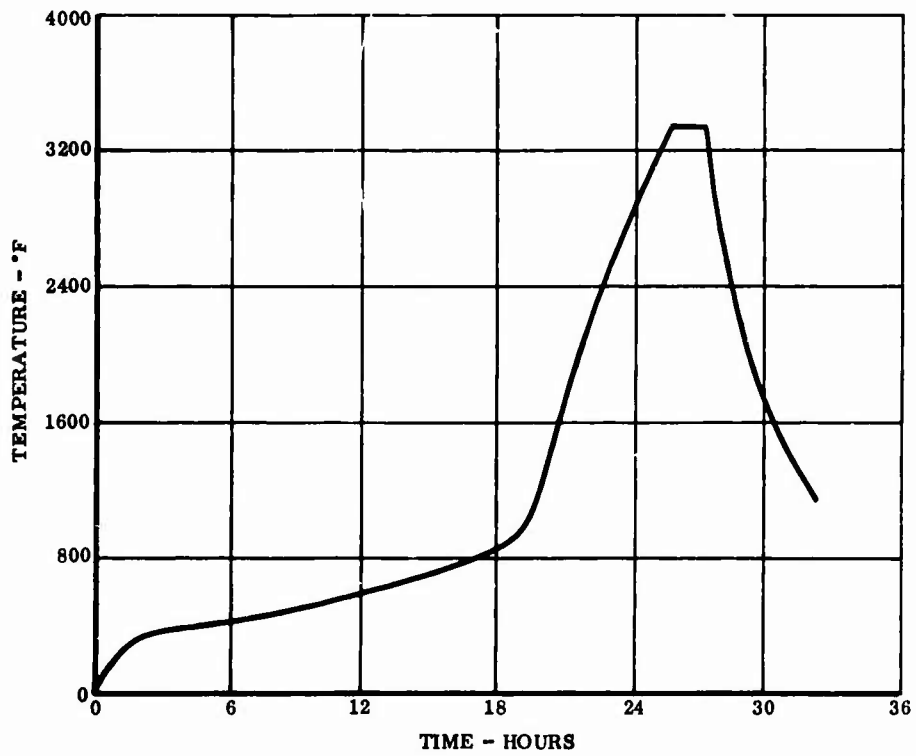
The composites with lower  $\text{CeO}_2$  content had higher porosity and lower flexural strengths than the composite with 5-percent  $\text{CeO}_2$ , as shown in Table XIII. All subsequent work was conducted using a base ceramic composition of  $(\text{HfO}_2 \cdot 5\text{CeO}_2)$ .

### 3.1.3 Process Evaluation Studies

Studies were conducted to determine whether fabrication processes could be developed for Mo- $(\text{HfO}_2 \cdot 5\text{CeO}_2)$  composites which would avoid or minimize the effects of the phase transformation. The work involved an evaluation of hot-pressing and of various sintering parameters.



(a) BINDER DECOMPOSITION CYCLE



(b) SINTERING CYCLE

Figure 18. Separate Organic Binder Decomposition and Sintering Cycles.

TABLE XIII  
EFFECTS OF VARYING CeO<sub>2</sub> CONCENTRATION ON  
FLEXURAL STRENGTH

Composition	Apparent Porosity, %	UFS, psi*
Mo-(HfO <sub>2</sub> · 1CeO <sub>2</sub> )	9.5	26,100
Mo-(HfO <sub>2</sub> · 1CeO <sub>2</sub> )	8.6	31,000
Mo-(HfO <sub>2</sub> · 3CeO <sub>2</sub> )	5.2	30,900
Mo-(HfO <sub>2</sub> · 3CeO <sub>2</sub> )	6.8	32,900
Mo-(HfO <sub>2</sub> · 5CeO <sub>2</sub> )	0.0	53,400
Mo-(HfO <sub>2</sub> · 5CeO <sub>2</sub> )	0.0	52,100

\* No yield point reached

Hot-Pressing - A hot-pressing study was made with Mo-(HfO<sub>2</sub> · 5CeO<sub>2</sub>) macrolaminate composites in an attempt to fabricate parts at temperatures below the transformation range, or in the transformation range for periods of time short enough to avoid the phase change in the ceramic. Laminate particles used for hot-pressing were prepared in the normal manner and then heated in an argon or H<sub>2</sub> atmosphere to remove the acrylic binder. Hot-pressing was accomplished in a graphite die under an argon cover atmosphere or in vacuum. The material was allowed to outgas in the die to a temperature of 1500°F, after which pressure was applied. Heating under pressure was continued until the desired temperature was reached. Pressure was held constant during a soak period at temperature but was released prior to cool-down, as shown in Figure 19.

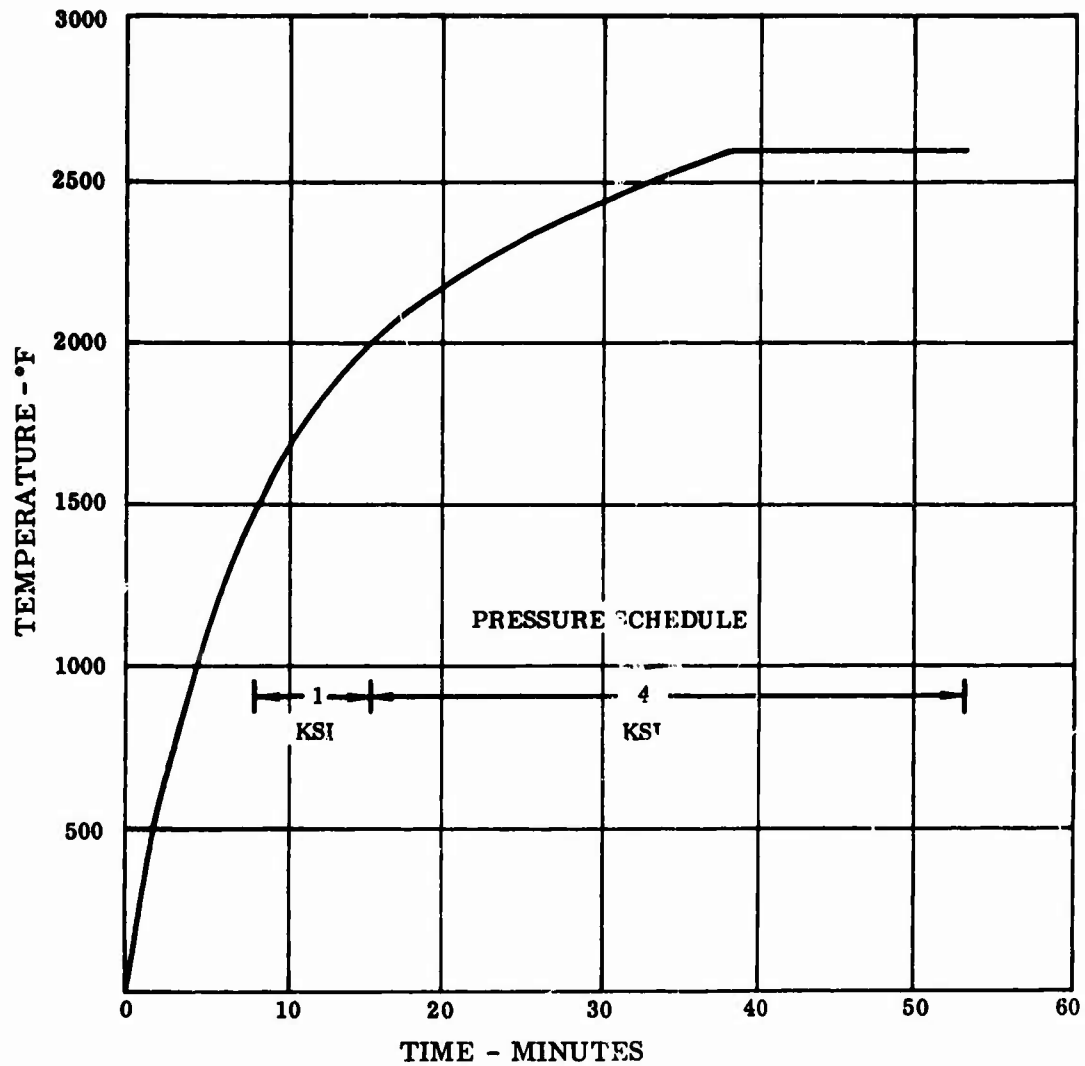


Figure 19. Hot-Press Cycle for Mo-HfO<sub>2</sub> Composites.

Initial hot-pressed specimens were found to be cracked in the middle, and there was evidence that the specimens had adhered to the graphite rams. The cracking was attributed to differential expansion between the part and the graphite rams. To avoid adherence of the part, the graphite rams were painted with the acrylic HfO<sub>2</sub> paint used in making the laminate sheet. This oxide film provided a satisfactory parting agent for the remainder of the hot-press trials. Test results of parts pressed with varying conditions of temperature and time are shown in Table XIV.

TABLE XIV  
 FLEXURAL STRENGTH OF HOT-PRESSED  
 Mo-(HfO<sub>2</sub> · 5CeO<sub>2</sub>) COMPOSITES

Hot-Press Temperature, °F	Time at Temp, min	UFS, psi*
2600 (Argon Cover)	15	22,960
2700     "	5	40,750
2700     "	4	36,500
2700     "	20	26,000
2400     "	30	38,600
2400     "	5	34,500
2400 (Vacuum)	30	42,500

\* No yield point reached.

The results of the hot-pressed specimens showed some improvement in strength over the initial sintered specimens (Table XI); however, the data show no general trend with respect to hot-press parameters. Metallographic analysis showed that the ceramic phase was relatively transparent when pressed at 2700°F and was generally more opaque and more porous when pressed at lower temperatures. These facts indicate that better properties should have been produced at the higher hot-pressing temperatures. The surface appearance of hot-pressed parts did suggest, however, that some contamination from the graphite dies was occurring, and could be contributing to the scatter in data.

Simultaneous sintering studies on Mo-(HfO<sub>2</sub> · 5CeO<sub>2</sub>) composites were showing more promising results than the work on hot-pressing. In view of the better sintering data and the contamination problem described above, no further hot-press work was conducted on the Mo-HfO<sub>2</sub> system.

**Sintering** - The sluggish nature of the phase transformation in  $(\text{HfO}_2 \cdot 5\text{CeO}_2)$  suggested that a modified sintering cycle could be developed to minimize the effects of the transformation. A study was conducted to evaluate the effect of various factors, such as atmosphere, heating rate, maximum firing temperature, time at temperature, and cooling rates. Data obtained from room temperature flexural tests were used for the comparative evaluation.

Sintering atmospheres evaluated were argon, tank hydrogen, hydrogen dried and purified by passing it through a liquid nitrogen cold trap, and a vacuum of  $1 \times 10^{-4}$  Torr. The organic binder was decomposed in an argon atmosphere at  $1000^\circ\text{F}$  except as noted in Table XV. The thermal cycle for sintering was the same as that described in Figure 18(b). The results are shown in Table XV.

TABLE XV  
EFFECT OF SINTERING ATMOSPHERE ON FLEXURAL  
PROPERTIES OF  $\text{Mo}-(\text{HfO}_2 \cdot 5\text{CeO}_2)$  COMPOSITES

Sintering Atmosphere	UFS, psi <span style="border: 1px solid black; padding: 0 2px;">3</span>
Vacuum ( $1 \times 10^{-4}$ Torr) <span style="border: 1px solid black; padding: 0 2px;">1</span>	72,250 66,080
Argon	33,200 55,000
Argon <span style="border: 1px solid black; padding: 0 2px;">2</span>	58,700 51,800
Hydrogen (Tank)	34,500 42,900
Hydrogen (Dried & Purified)	46,500 50,300

<span style="border: 1px solid black; padding: 0 2px;">1</span>	Binder removed in argon using cycle shown in Figure 9(a)
<span style="border: 1px solid black; padding: 0 2px;">2</span>	Binder removed in vacuum (20" Hg) at $1000^\circ\text{F}$
<span style="border: 1px solid black; padding: 0 2px;">3</span>	No yield point reached

The vacuum-sintering cycle provided the best properties that were obtained for the Mo-(HfO<sub>2</sub> · 5CeO<sub>2</sub>) composite. Control specimens of pure molybdenum were sintered in the same cycles. Yield strength of these specimens varied significantly (from 53 to 114 ksi) as did the degree of ductility. Only those specimens sintered in vacuum or in purified hydrogen had significant ductility. The molybdenum specimen sintered in vacuum bent 43 degrees before cracking, while the specimen sintered in purified hydrogen bent only 5 degrees. These specimens had yield strengths of 65 and 75 ksi, respectively. The variations in yield strength and ductility are attributed to interstitial contamination by oxygen.

A modified vacuum-sintering cycle was also evaluated for the fabrication of Mo-(HfO<sub>2</sub> · 5CeO<sub>2</sub>) composite flexural specimens. The cycle was similar to that described above except that a 2-hour holding plateau at 2400°F was incorporated during cooling, as shown in Figure 20.

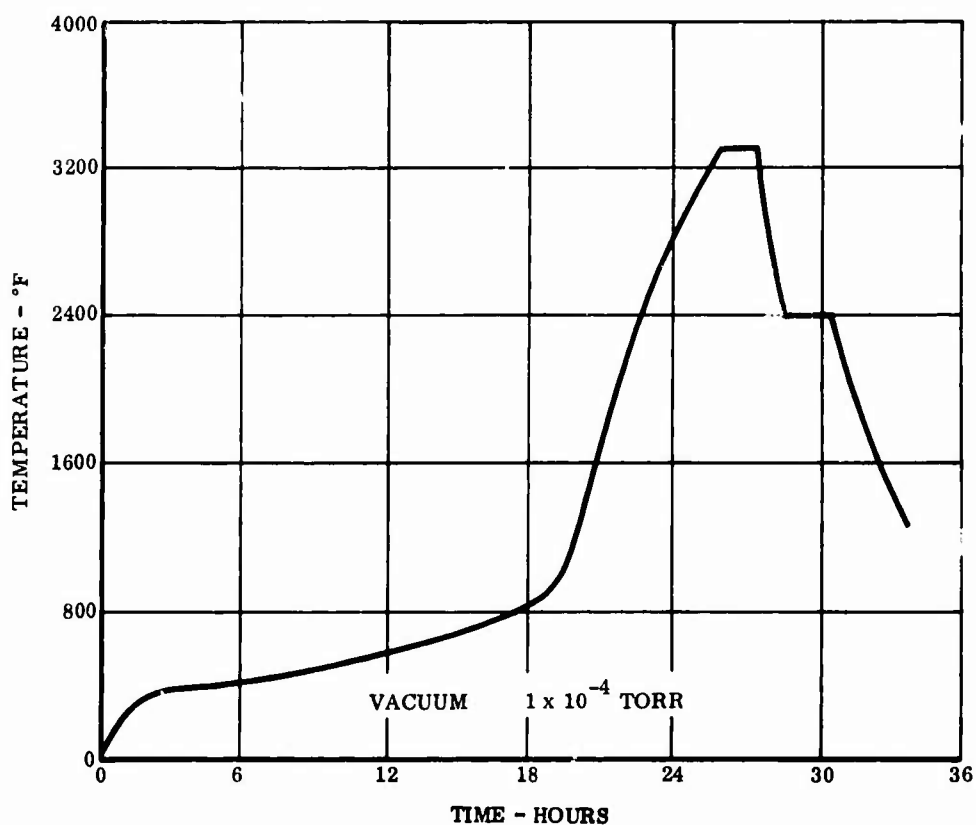


Figure 20. Modified Vacuum-Sintering Cycle.

The purpose of the plateau, which was just below the transformation temperature, was to act as a stress relief. A flexural strength of 53,600 psi (average of two tests) showed that the cycle was ineffective when compared to the results shown previously in Table XV.

Various sintering parameters, such as heating rate, temperature, holding time, and cooling rate, were evaluated for the fabrication of  $\text{Mo}(\text{HfO}_2 \cdot 5\text{CeO}_2)$  specimens. Sintering was conducted in a vacuum of  $1 \times 10^{-4}$  Torr, and the organic decomposition cycle used was the same as that described in Figure 18(a). The sintering parameters used and the results of room temperature flexural tests are given in Table XVI.

TABLE XVI  
EFFECT OF VARIOUS SINTERING PARAMETERS ON  
FLEXURAL PROPERTIES

Heat Rate, °F/hr	Sinter Temp, °F	Time @ Temp, Hrs.	Cool Rate, °F/hr.	Apparent Porosity %	FYS, ksi	UFS, ksi	Def, in.
400	3400	0	100	1.3	53.1	54.5	.018
400	3400	0	100	0.5	48.0	52.5	.015
400	3300	6	700	1.0	-	60.6	-
400	3300	6	700	0.0	-	53.4	-
100	3400	12	700	0.0	-	58.8	-
100	3400	12	700	0.7	-	63.0	-
700	3300	12	100	0.2	59.0	64.5	.014
700	3300	12	100	0.0	56.0	58.7	.013

No improvement in ultimate strength was realized over that obtained from the original time-temperature cycle (see Table XV) in evaluating effect of atmosphere. It was, however, considered significant that all of the specimens cooled with the 100°F-per-hour rate reached a flexural yield point and showed slight deformation prior to failure.

### 3.1.4 Molybdenum-Mullite · Alumina Composites

A series of tests was conducted to evaluate the potential benefits that might be obtained by substituting a more stable ceramic for the  $(\text{HfO}_2 \cdot 5\text{CeO}_2)$  ceramic. The ceramic selected was 52-percent mullite, with a composition corresponding to  $(3\text{Al}_2\text{O}_3 \cdot 2\text{SiO}_2)$ , and 48-percent free  $\text{Al}_2\text{O}_3$ . The mullite-alumina composition was used by Tinklepaugh (Reference 11) for a molybdenum fiber-reinforced ceramic composite. The ceramic was reported to match closely the thermal expansion of molybdenum, and produced a composite free from microcracks. The mullite-alumina ceramic does not undergo a phase transformation.

Three formulations, based on different forms of alumina and silica to achieve the desired ratio of alumina to silica, were used to fabricate composites. The formulations are described in Table XVII.

TABLE XVII  
MULLITE · ALUMINA FORMULATIONS

<u>Code No.</u>	<u>Material</u>	<u>Parts by Weight</u>
MAT <sub>1</sub>	Shamva Mullite	51.0
	Linde A 0.3 Micron Alumina	48.0
	Alon C Alumina	0.5
	Cabosil Silica	0.5
MAT <sub>2</sub>	Shamva Mullite	51.0
	A-14 Alumina	48.0
	Alon C Alumina	0.5
	Cabosil Silica	0.5
MAT <sub>3</sub>	A-14 Alumina	84.5
	Silica	14.3
	Alon C Alumina	0.5
	Titania	0.2
	Cabosil Silica	0.5

Compositions MAT<sub>1</sub> and MAT<sub>2</sub> both used fused grain of mullite obtained from the Mullite Refractories Company. This material contained significant quantities of free iron and required washing in hydrochloric acid before use. The MAT<sub>1</sub> formulation contained Linde-A, which is a high-purity 0.3-micron Al<sub>2</sub>O<sub>3</sub> powder with large surface area. Alcoa A-14 Al<sub>2</sub>O<sub>3</sub>, which is a high-purity grade of calcined alpha Al<sub>2</sub>O<sub>3</sub>, was used in the MAT<sub>2</sub> formulation. Small percentages of colloidal gamma Al<sub>2</sub>O<sub>3</sub> and amorphous SiO<sub>2</sub> (Alon C and Cabosil) were used in all batches to provide highly active particles to aid sintering. Composition MAT<sub>3</sub> used Al<sub>2</sub>O<sub>3</sub> and SiO<sub>2</sub> in the ratio corresponding to that required to form mullite plus a 48-percent excess of Al<sub>2</sub>O<sub>3</sub>. A small quantity of TiO<sub>2</sub> was added to aid the formation of mullite and to promote sintering.

The Mo-MAT composites were sintered both in vacuum ( $1 \times 10^{-4}$  Torr) and hydrogen at a temperature of 3300°F, and in vacuum ( $1 \times 10^{-4}$  Torr) at a temperature of 3400°F. Lowest porosity and highest strength were obtained by hydrogen sintering.

The composition which used MAT<sub>3</sub> as the ceramic phase produced the highest strength composites, as shown in Table XVIII.

Plastic deformation prior to failure was obtained only from those specimens sintered in vacuum. During the 3400°F vacuum-sintering, the ceramic phase volatilized from the surface of these specimens to a depth of approximately 0.010 inch. The surfaces of these test specimens were ground beyond this depth to provide a solid composite surface. Other sintering conditions did not appear to volatilize the ceramic from the surface.

The Mo-MAT composite was approximately 30-percent lighter than the Mo-(HfO<sub>2</sub> · 5CeO<sub>2</sub>) composite, but had very poor oxidation resistance by comparison.

A weight loss of 500 mg/cm<sup>2</sup> resulted from exposing the molybdenum Mo-MAT composite to air at 2500°F for 1/2 hour, compared to an equivalent weight loss (550 mg/cm<sup>2</sup>) for the Mo-(HfO<sub>2</sub> · 5CeO<sub>2</sub>) composite tested for 24 hours under similar conditions. There was no apparent reaction between the oxides of molybdenum and the mullite-alumina ceramic to retard oxidation, as was the case with the Mo-HfO<sub>2</sub> composites.

**TABLE XVIII**  
**FLEXURAL PROPERTIES OF Mo-MAT COMPOSITES**

<u>Composition</u>	<u>Sinter Temp, °F</u>	<u>Atm</u>	<u>Apparent Porosity, %</u>	<u>FYS, ksi</u>	<u>UFS, ksi</u>	<u>Def, in.</u>
Mo-MAT <sub>1</sub>	3300	Vac	11.8	30.5	41.1	.015
	3400	Vac	22.8	37.5	44.4	.015
	3300	H <sub>2</sub>	1.6	-	64.8	-
Mo-MAT <sub>2</sub>	3300	Vac	11.2	33.1	39.4	.016
	3400	Vac	17.9	42.9	56.4	-
	3300	H <sub>2</sub>	2.3	-	59.6	-
Mo-MAT <sub>3</sub>	3300	Vac	13.8	31.6	42.8	.016
	3400	Vac	14.5	45.5	58.9	.019
	3300	H <sub>2</sub>	1.4	-	77.7	-

The series of tests indicated that higher flexural strengths could be obtained with a strong, stable ceramic. The very poor oxidation resistance of the Mo-MAT system, however, precluded its use in a high-temperature oxidizing environment.

### 3.1.5 Oxidation Studies

In addition to the investigation of basic factors influencing the strength of the composite, a simultaneous study was made to determine the effect of various oxide additives on the oxidation resistance of the Mo-HfO<sub>2</sub>-based composite.

Prior Boeing work had shown that additions of MgO, SrO, BaO, Cr<sub>2</sub>O<sub>3</sub>, and HfSiO<sub>4</sub> were capable of improving oxidation resistance of the basic Mo-(HfO<sub>2</sub> · 5CeO<sub>2</sub>) macrolaminate composite at temperatures of 2500°F and below. An empirical, multiple composition level experiment was set up to evaluate progressive and

arbitrary additions of each of the above materials to a base ceramic phase. Ceramic alloy powder for each composition was prepared by prereacting the various constituents at 2700°F in air and grinding to pigment-sized particles. MgO, SrO, and BaO were added as carbonates and decomposed to oxide during the prereaction operation at 2700°F. HfSiO<sub>4</sub> prepared by reacting equal molar quantities of HfO<sub>2</sub> and SiO<sub>2</sub> at 3000°F was also added as a powder.

For the first composition level, 2-, 5-, and 10-weight-percent of each of the above five additives was added to a (HfO<sub>2</sub> · 5CeO<sub>2</sub>)-base ceramic. Oxidation and flexural test specimens were sintered at 3500°F using the cycle described in Figure 17. The results of tests on the first composition level indicated that the Mo-(HfO<sub>2</sub> · 4.8CeO<sub>2</sub> · 5SrO) composite had the best balance of properties, as shown in Table XIX. Several composites had higher strengths, notably those with BaO additions; however, these exhibited worse oxidation resistance at higher temperatures.

For the second-level composition oxidation tests, the (HfO<sub>2</sub> · 4.8CeO<sub>2</sub> · 5SrO) ceramic was used as the basic composition to which 2-, 5-, and 10-weight-percent additions of BaO, HfSiO<sub>4</sub>, Cr<sub>2</sub>O<sub>3</sub>, and MgO were made. The test results for the second-level composites showed that a 10-percent addition of Cr<sub>2</sub>O<sub>3</sub> was the most effective in improving oxidation resistance. As shown in Table XX(a), this composition showed weight losses of 16, 278, and 143 mg/cm<sup>2</sup> after 24-hour exposures in air at 1200°, 1800°, and 2500°F, respectively. The Mo-(HfO<sub>2</sub> · 4.3CeO<sub>2</sub> · 4.5SrO · 10Cr<sub>2</sub>O<sub>3</sub>) composite showed a significant improvement in oxidation resistance over the first-level composites, but only at some sacrifice in room-temperature flexural strength.

A third-level experiment was conducted using the (HfO<sub>2</sub> · 4.3CeO<sub>2</sub> · 4.5SrO · 10Cr<sub>2</sub>O<sub>3</sub>) as the basis of the ceramic phase, and additions of BaO, HfO, and MgO were made in 2-, 5-, and 10-weight-percent concentrations. Because all of the additives decreased the oxidation resistance of the best second-level composition, as shown in Table XX(b), no further additions were evaluated. The composite with a 10-percent addition of HfSiO<sub>4</sub> showed the best overall properties of the third-level compositions.

TABLE XIX  
OXIDATION RESISTANCE OF FIRST COMPOSITION LEVEL

Addition to Ceramic Phase	% Metal in Composite	Apparent Porosity, %	UFS, ksi	Weight Change After 24 Hr at Temperature, mg/cm <sup>2</sup>		
				1200°F	1800°F	2500°F
First Composition Level - (HfO <sub>2</sub> · 5CeO <sub>2</sub> ) Base Ceramic						
2% BaO	51.3	0.9	46.8	+ 9	-789	-1052
5% BaO	50.6	0.7	51.8	+ 22	-286	- 951
10% BaO	50.6	0.0	41.2	+ 18	-990	- 512
2% SrO	50.8	0.8	47.0	+ 25	-648	-1018
5% SrO	51.4	0.5	39.7	+ 6	-530	- 359
10% SrO	50.5	0.0	33.0	+ 10	-882	- 270
2% HfSiO <sub>4</sub>	50.7	0.0	32.9	+ 51	-302	- 923
5% HfSiO <sub>4</sub>	49.9	2.92	32.6	+ 42	-563	- 908
10% HfSiO <sub>4</sub>	51.0	5.8	29.9	+ 15	-853	- 270
2% Cr <sub>2</sub> O <sub>3</sub>	50.1	1.0	34.7	+ 7	-265	-1122
5% Cr <sub>2</sub> O <sub>3</sub>	50.1	0.3	36.1	+ 6	-394	- 648
10% Cr <sub>2</sub> O <sub>3</sub>	50.3	4.7	32.0	+ 6	-900	- 268
2% MgO	51.3	1.2	31.6	+ 49	-794	- 298
5% MgO	51.6	1.4	30.0	+137	-437	- 392
10% MgO	50.6	2.1	21.3	+ 15	-757	- 411
 No yield point reached.						

TABLE XX  
OXIDATION RESISTANCE OF SECOND AND  
THIRD COMPOSITION LEVELS

Addition to Ceramic Phase	% Metal in Composite	Apparent Porosity, %	UFS, ksi	Weight Change After 24 Hr at Temperature, mg/cm <sup>2</sup>		
				1200°F	1800°F	2500°F
(a) Second Composition Level - (HfO <sub>2</sub> · 4.3CeO <sub>2</sub> · 5SrO) Base Ceramic						
2% BaO	50.7	0.5	23.8	+ 69	-994	-457
5% BaO	50.3	0.0	35.5	+114	-813	-820
10% BaO	50.0	0.5	27.2	+128	-369	-649
2% HfSiO <sub>4</sub>	51.2	1.1	24.5	- 2	-1021	-439
5% HfSiO <sub>4</sub>	51.1	0.8	30.7	+ 3	-567	-448
10% HfSiO <sub>4</sub>	50.4	0.8	21.0	- 5	-807	-387
2% Cr <sub>2</sub> O <sub>3</sub>	50.1	0.7	23.2	- 20	-840	-453
5% Cr <sub>2</sub> O <sub>3</sub>	50.5	0.0	32.9	- 14	-455	-240
10% Cr <sub>2</sub> O <sub>3</sub>	51.5	1.3	30.3	- 16	-278	-143
2% MgO	50.0	1.3	21.0	- 0.4	-960	-424
5% MgO	51.0	0.2	22.4	+ 0.1	-241	-513
10% MgO	51.5	0.0	34.4	+ 0.3	-288	-347
(b) Third Composition Level - (HfO <sub>2</sub> · 4.3CeO <sub>2</sub> · 4.5SrO · 10Cr <sub>2</sub> O <sub>3</sub> ) Base Ceramic						
2% BaO	52.0	4.2	26.5	- 2.9	-381	-168
5% BaO	50.8	4.3	30.5	+ 16.6	-350	-151
10% BaO	50.7	4.2	28.1	+ 51.7	-655	-458

TABLE XX (Continued)

Addition to Ceramic Phase	% Metal In Composite	Apparent Porosity, %	UFS, ksi	Weight Change After 24 Hr at Temperature, mg/cm <sup>2</sup>		
				1200°F	1800°F	2500°F
2% HfSiO <sub>4</sub>	51.2	4.3	31.6	- 6.5	-556	-161
5% HfSiO <sub>4</sub>	51.1	4.2	31.1	- 3.8	-408	-178
10% HfSiO <sub>4</sub>	50.1	3.3	37.3	- 1.2	-459	-198
2% MgO	51.3	3.9	34.8	+ 0.4	-520	-490
5% MgO	50.9	1.7	39.2	+ 3.5	-125	-428
10% MgO	50.8	2.4	27.5	+ 2.2	+ 40.3	-336

1 ▷ See Table XIX for oxidation data of first level composite.

2 ▷ Specimen bloated

3 ▷ No yield point reached.

The data in Tables XIX and XX frequently showed that the oxidation resistance at 1800°F for a particular composite was lower than it was at either 1200° or 2500°F. At 1200°F, this is attributed to the fact that the oxidation rate of molybdenum is relatively low, as this is below the sublimation temperature of molybdenum oxide, 1462°F, the point where molybdenum begins to oxidize rapidly. At 2500°F, the reaction rate between the volatile molybdenum oxide and the ceramic phase is apparently more effective than it is at 1800°F; a more protective oxidation layer formed as a result.

The oxidation data were somewhat erratic in nature and did not always follow compositional trends. This behavior was attributed in part to differences in lamellae orientation between specimens. The results did, however, indicate the limited amount of improvement in oxidation resistance that can be obtained through modification of the ceramic phase.

### 3.1.6 Protective Coatings

Four types of protective coatings were evaluated for their ability to protect the Mo-(HfO<sub>2</sub> · 5CeO<sub>2</sub>) composite as follows:

1. Disilicide coating (MoSi<sub>2</sub>) applied by the fluidized bed process.
2. Solution-sprayed coatings of zirconia and chromia, applied as solutions of ammonium-zirconyl-carbonate and chromium nitrate on heated parts.
3. Ceramic glazes applied by spraying parts with water suspensions of calcia, alumina, and silica and fusing them at temperatures of 2800° to 3000°F in an inert atmosphere.
4. TiB<sub>2</sub> · MoSi<sub>2</sub> coatings applied as slurries using silicic acid and sodium silicate as binders.

Disilicide Coating - The disilicide coating is a conversion-type coating consisting of a MoSi<sub>2</sub> layer on the surface of the metal phase only. The coating was applied by the Boeing-developed fluidized bed process (DiSil) and is produced by the reaction of silicon iodide vapor with the molybdenum metal surface.

Examination of the disilicide-coated specimens showed that the coating on the metal phase protruded approximately 1 mil beyond the surface of the ceramic. During the coating process, a net loss of weight occurred and the ceramic phase was rough, indicating that it was attacked during the process by the iodide vapor. The coating provided some oxidation protection, but was inadequate by itself. A coated specimen lost 255 mg/cm<sup>2</sup> after 24 hours at 2500°F, and an uncoated specimen lost 550 mg/cm<sup>2</sup>.

Solution-Sprayed Coatings - Formation of ZrO<sub>2</sub> coatings on composite specimens was attempted by solution-spraying with ammonium-zirconyl carbonate. The best-appearing coatings of ZrO<sub>2</sub> were achieved with the part preheated to 400°F. Because the coating did not adhere to the smooth ground surface of the composite specimens and coverage was inadequate, no tests were run.

A uniform coating of Cr<sub>2</sub>O<sub>3</sub> was obtained by spraying composite specimens heated to 1000°F with a solution consisting of equal parts of chromium nitrate and water. The coated composite specimen was then heated to 2800°F in argon to allow the Cr<sub>2</sub>O<sub>3</sub> to diffuse into the surface of the specimen. This coating provided essentially no protection. After 24 hours at 2500°F in air, the coated specimens lost 510 mg/cm<sup>2</sup> and the uncoated specimen lost 550 mg/cm<sup>2</sup>.

Ceramic Glaze Coatings - A stable glass composition with a melting temperature above 2500°F was required as the basis of the glaze. To provide protection, its coefficient of thermal expansion should be the same or slightly lower than the substrate composite. A glaze with a higher expansion than the substrate will be in tension when solidification occurs and will crack. A glaze with too low a thermal expansion is placed under such high compression that shear forces at the interface cause it to spall.

The CaO - Al<sub>2</sub>O<sub>3</sub> - SiO<sub>2</sub> ternary system was selected for investigation, as compositions in the high SiO<sub>2</sub> region form very stable glasses that melt above 2500°F and have sufficient latitude in chemistry that the coefficient of expansion could be adjusted to fit that of the Mo-HfO<sub>2</sub> composites. The initial composition investigated contained 4-percent CaO, 13-percent Al<sub>2</sub>O<sub>3</sub> and 83-percent SiO<sub>2</sub>. The phase diagram of the ternary system indicated that this composition should melt at 2740°F and that its calculated coefficient of thermal expansion was  $5 \times 10^{-6}$  inches/inch/°C, which is essentially the same as that of the Mo-HfO<sub>2</sub> composite. It was prepared by ball-milling the constituents with water for 18 hours to form a slurry. The slurry was applied to the specimen by spraying and was fused at 2800°F in an argon atmosphere.

A perfectly clear glaze, which wet the specimen uniformly on the top and sides, resulted. The bottom side appeared to be void of coating in the center, because there was a tendency for the glass to gather near the edges at the points where a supporting screen contacted the bottom surface.

This coating offered considerable protection, reducing the weight loss after exposure at 2500°F for 24 hours to 216 mg/cm<sup>2</sup>, compared to 550 mg/cm<sup>2</sup> for an uncoated specimen. After testing, the specimen had numerous nodules of a slag material, and also had two scars where the specimen had contacted the platinum holder.

Two glaze coatings were prepared with reduced CaO contents as follows:

1. 2% CaO, 15% Al<sub>2</sub>O<sub>3</sub>, 83% SiO<sub>2</sub>
2. 1% CaO, 15% Al<sub>2</sub>O<sub>3</sub>, 84% SiO<sub>2</sub>

These modifications increased the fusion temperature to approximately 3000°F. Both glazes wet the composite but failed to provide complete protection on the ends of the specimens. A certain

amount of the glaze appeared to have diffused into the end of the specimens and left areas void of an exterior glass coating. Testing at 2500°F in air for 24 hours showed that these coatings were detrimental. Single specimens with each coating lost 772 and 820 mg/cm<sup>2</sup>, respectively, compared to 550 mg/cm<sup>2</sup> for an uncoated specimen.

Three additional ceramic glaze modifications, consisting of a 20-percent addition each of Cr<sub>2</sub>O<sub>3</sub>, ZrO<sub>2</sub>, and HfO<sub>2</sub> to the 4CaO · 13Al<sub>2</sub>O<sub>3</sub> · 83SiO<sub>2</sub> formulation, were prepared and applied to cylindrical test specimens of the Mo-(HfO<sub>2</sub> · 5CeO<sub>2</sub>). Coatings containing Cr<sub>2</sub>O<sub>3</sub> or ZrO<sub>2</sub> both formed mat surfaces. No problems in wetting were observed. The glaze containing HfO<sub>2</sub> formed opaque glass globules which wet the ceramic phase but not the molybdenum. The glaze formulation containing 20-percent ZrO<sub>2</sub> produced the greatest degree of protection of the three compositions but was not as good as the basic glaze formulation (450 mg/cm<sup>2</sup> weight loss compared to 216 mg/cm<sup>2</sup> weight loss after a 24-hour oxidation test at 2500°F). Specimens coated with glazes containing Cr<sub>2</sub>O<sub>3</sub> and HfO<sub>2</sub> showed weight losses of 493 and 545 mg/cm<sup>2</sup>, respectively, after oxidation testing.

TiB<sub>2</sub> · MoSi<sub>2</sub> Coatings - This type of coating has been found to produce a self-healing coating for graphite at temperatures up to 2600°F. When exposed to an oxidizing environment, the TiB<sub>2</sub> and MoSi<sub>2</sub> react to form a titanium borosilicate glass.

The coating was applied as a slurry consisting of 50-percent TiB<sub>2</sub> and 50-percent MoSi<sub>2</sub> with a silicic acid sol (Penn Salt Sytar) as the binder. The coating provided some improvement in oxidation resistance of the composite; weight loss was reduced from 550 mg/cm<sup>2</sup> for the uncoated specimen to 285 mg/cm<sup>2</sup> for the coated specimen after 24 hours at 2500°F.

Substitution of sodium silicate (water glass) for the silicic acid sol in an attempt to form a seal glass at lower temperature was not successful. This coating proved detrimental to the oxidation resistance of the composite; weight loss was 770 mg/cm<sup>2</sup> after 24 hours at 2500°F.

### 3.1.7 Summary of Mo-HfO<sub>2</sub> Macrolaminate Composite Results

The effort conducted on the Mo-HfO<sub>2</sub> composite system was concerned with improving the strength and oxidation resistance of the composites. Studies related to improving the strength primarily involved the evaluation of various fabrication parameters to define

a suitable fabrication process. Methods to improve the oxidation resistance involved modifying the ceramic phase with various oxide additives and applying additional coatings on the surface of the composites.

Phase transformation studies on the  $\text{CeO}_2$ -modified  $\text{HfO}_2$  ceramic phase showed that a reversible monoclinic-to-tetragonal transformation was occurring in the fabrication temperature range, and it was reasoned that this transformation could be contributing to low strength in the ceramic phase. Studies were conducted in an attempt either to fabricate below the transformation temperature or to raise the transformation temperature above the fabrication temperature range by reducing the  $\text{CeO}_2$  content. Hot-pressing at temperatures below or near the transformation temperature generally was not successful because of a reaction between the graphite die and the material being hot-pressed. Composites with reduced  $\text{CeO}_2$  contents had lower properties because of the poorer sintering response in the ceramic phase.

Using the basic  $\text{Mo}-(\text{HfO}_2 \cdot 5\text{CeO}_2)$  system, composites with near theoretical densities and flexural strengths approaching 70 ksi were achieved with vacuum-sintering techniques. Evidence of ductility was obtained by modifying the vacuum-sintering cycle to include a slow cooling rate.

A series of macrolaminate composites was fabricated in which a mullite · alumina ceramic was substituted for the  $(\text{HfO}_2 \cdot 5\text{CeO}_2)$  ceramic. Mullite · alumina is a strong, stable ceramic and undergoes no phase transformations. Tests on composites indicated that higher flexural strengths could be obtained; however, the poor oxidation resistance of the molybdenum-mullite · alumina system would preclude its use in a high-temperature oxidizing environment.

The oxidation resistance of the  $\text{Mo}-\text{HfO}_2$  system is based on the ability of the ceramic phase to react with the volatile metal oxide during the oxidation process and to form a protective oxide layer. A series of five oxide additives, i. e.,  $\text{MgO}$ ,  $\text{Cr}_2\text{O}_3$ ,  $\text{SrO}$ ,  $\text{BaO}$  and  $\text{HfSiO}_4$ , were added to the basic  $\text{Mo}-(\text{HfO}_2 \cdot 5\text{CeO}_2)$  system in progressive amounts in a three-level experiment. The addition of 5-percent  $\text{SrO}$  and 10-percent  $\text{Cr}_2\text{O}_3$  produced approximately a 400-percent improvement in oxidation resistance at 2500° F. The unmodified  $\text{Mo}-(\text{HfO}_2 \cdot 5\text{CeO}_2)$  composite had a weight loss of 550  $\text{mg}/\text{cm}^2$  after 24-hour static tests in air compared to a 143  $\text{mg}/\text{cm}^2$  weight loss for the modified composite. The study was

discontinued after the third level when it was apparent that further oxide additions to the  $\text{HfO}_2$ -base ceramic would decrease both strength and oxidation resistance.

The application of coatings on a  $\text{Mo}-(\text{HfO}_2 \cdot 5\text{CeO}_2)$  composite was evaluated using four different coating systems. Of the coatings evaluated, an  $\text{Al}_2\text{O}_3$ - $\text{SiO}_2$ - $\text{CaO}$  ceramic glaze coating, a  $\text{TiB}_2$ - $\text{MoSi}_2$  slurry coating, and a  $\text{MoSi}_2$  conversion coating (DiSil) all showed improvements in oxidation resistance at  $2500^\circ\text{F}$ . The best protection was shown by a ceramic glaze coating, with a 24-hour oxidation weight loss of  $216 \text{ mg/cm}^2$  at  $2500^\circ\text{F}$ , compared with a loss of  $550 \text{ mg/cm}^2$  for an uncoated specimen.

Based on the oxidation data obtained, it could be projected that oxidation rates of about  $100 \text{ mg/cm}^2$  for a 24-hour test at  $2500^\circ\text{F}$  would be expected by modifying the  $\text{HfO}_2$  ceramic phase and by applying a protective coating over the composite. However, it was anticipated that an oxidation rate of about  $1.0 - 2.0 \text{ mg/cm}^2$  at the above conditions would be required for a suitable nozzle vane material. Additional work on the  $\text{Mo-HfO}_2$  composite system to attain improvements of this nature was considered beyond the scope of this program.

### 3.2 Ni-MgO MACROLAMINATE COMPOSITES

As previously discussed in Section 2.1, Ni and MgO were found to be compatible with each other and suitable for the fabrication techniques employed for macrolaminate composites. Hot-pressing at temperatures of from  $2150^\circ$  to  $2350^\circ\text{F}$  showed potential for producing dense composites with no measurable apparent porosity.

The research and development effort conducted on Ni-MgO composites involved evaluating compositional variables and improving the processing techniques. Laboratory tests on selected composites were also conducted to determine tensile properties and resistance to oxidation and thermal fatigue. General items of work, discussed in subsequent paragraphs, are as follows:

Baseline Property Study

Ceramic Phase Study

Metal-Ceramic Bond Studies

Metal Phase Studies

Combined Additions to Macrolaminate Composites  
Metallographic Bend Studies  
Process Improvement  
Metal-Ceramic Ratio Evaluation

3.2.1 Baseline Property Study

To establish some baseline properties for Ni-MgO composites and the separate Ni and MgO phases, flexural test specimens of each material were prepared using the general macrolaminate composite fabrication procedures described in Section 2.1.2. For hot-pressing the initial test specimens, a cycle of 15 minutes at 2350°F with 4-ksi pressure was selected. The room-temperature flexural properties of these materials are shown in Table XXI.

TABLE XXI  
FLEXURAL PROPERTIES OF Ni-MgO AND SEPARATE PHASES

Material	FYS, psi	UFS, psi	Deflection, in.
Ni	15,000	-	0.035
MgO	*	22,100	-
Ni-MgO	*	38,100	-

\*No yield point reached

The strength of the composite was higher than the strengths of the components, indicating that reinforcement of the metal was occurring. Subsequent work on the separate metal and ceramic phases was conducted as a means of improving the strength of the Ni-MgO composite.

### 3. 2. 2 MgO Ceramic Phase Studies

Various ceramic phase additives were evaluated for their ability to improve the strength of MgO. The additives evaluated were as follows:

1. LiF - A fugitive sintering aid added to reduce porosity.
2. Cr<sub>2</sub>O<sub>3</sub> - Added to solid solution to strengthen the MgO matrix.
3. ZrO<sub>2</sub> and HfO<sub>2</sub> - Dispersed, insoluble particles added to control grain size in the MgO matrix.

A group of ceramic specimens was hot-pressed from powder containing the various additives. A (MgO · 10Cr<sub>2</sub>O<sub>3</sub>) powder was ground to an average particle size of 5 microns from a fused ingot. Powders of (MgO · 0.5ZrO<sub>2</sub>) and (MgO · 3ZrO<sub>2</sub>) were prepared by precipitating Mg(OH)<sub>2</sub> from a nitrate solution containing duPont No. 180 colloidal ZrO<sub>2</sub>. The precipitate was calcined in air at 1000°F and ground to a particle size of 5 microns. A (MgO · 5HfO<sub>2</sub>) powder was prepared by coprecipitating the hydroxides from an aqueous solution of magnesium nitrate and hafnium chloride. The hydroxides were washed, calcined in air at 1000°F, and ground to an average particle size of 5 microns. Additional studies to develop improved chemical processes for preparing (MgO · 5HfO<sub>2</sub>) powder were subsequently conducted, and are discussed in Section 3. 2. 6. LiF was added to MgO by ball-milling.

The specimens were hot-pressed at 2350°F and 4-ksi pressure. Following hot-pressing, representative specimens were post-treated by slow heating to 2400°F using a 24-hour cycle. Previous Boeing-sponsored work with pure MgO showed that post-treating would allow further sintering and thereby would improve density and strength. Flexural test results of the ceramic specimens are given in Table XXII.

The post-treated specimens with 3-percent ZrO<sub>2</sub> and 5-percent HfO<sub>2</sub> additions showed strength improvements of about 50 percent over the flexural strength (22, 100 psi) reported initially for pure MgO in Table XXI. This strength increase was attributed to the retention of a fine grain size and increased sintering obtained with the post-treat cycle, as determined by transmission microscopy. This work was conducted on thin sections prepared from samples with ZrO<sub>2</sub> and HfO<sub>2</sub> additions. The hot-pressed material was quite opaque, with no grain structure apparent. After post-treating at 2400°F, the material was more transparent, having a uniform

TABLE XXII  
EFFECT OF ADDITIVES ON FLEXURAL STRENGTH OF MgO

Ceramic Additive, %	As Hot-Pressed UFS, psi	Post Treated, 2400°F UFS, psi
2 LiF	20,400 (avg of 2)	19,800
10 Cr <sub>2</sub> O <sub>3</sub>	9,200	-
10 Cr <sub>2</sub> O <sub>3</sub> + 2 LiF	12,200 (avg of 2)	19,200
0.5 ZrO <sub>2</sub>	21,200 (avg of 2)	20,320
3 ZrO <sub>2</sub>	19,300 (avg of 2)	32,400
5 HfO <sub>2</sub>	21,300 (avg of 2)	34,200

grain size of less than 2 microns and uniformly distributed particles of about the same size. Grain growth to 10 or 20 microns takes place in pure MgO post treated under the same conditions. The results indicate that 3- to 5-percent additions of either ZrO<sub>2</sub> or HfO<sub>2</sub> will effectively control the grain size.

### 3.2.3 Metal-Ceramic Bond Studies

A review of literature on metal-ceramic bond was conducted. Early investigation of Ni-MgO cermets showed that liquid-phase sintering was not successful, as the liquid nickel did not wet the MgO. Economos and Kingery (Reference 12) investigated the metal-ceramic interaction and found that MgO and Ni did not react at temperatures below 1600°C (2922°F). Hower (Reference 13) investigated the addition of intermediate compounds, e. g. , nitrides, carbides, borides, and hydrides, in promoting a chemical bond between oxides and metals. Based on similarity of crystal structure, radii of atoms and ions involved, and type of bond, Hower selected TiN for use with Ni-MgO cermets and found it effective in promoting a bond. Sutton (Reference 14) reported that titanium, zirconium, and chromium additions to nickel increased its wetting in contact with Al<sub>2</sub>O<sub>3</sub>. Titanium hydride, which disassociates and leaves free titanium, is frequently used in preparing metal-ceramic joints because of the ability of titanium to promote a bond.

In this program, titanium and TiN additions to the metal phase, and TiO<sub>2</sub> additions to the ceramic phase, were evaluated for their ability to promote bonding in a Ni-MgO macrolaminate composite. Flexural test specimens were prepared by hot-pressing at temperatures ranging from 2200° to 2300°F using a pressure of 4 ksi. Included in this group of specimens were composites with ZrO<sub>2</sub> and HfO<sub>2</sub> additions to the ceramic phase. These were prepared as previously described in Section 3.2.2. The results of flexural tests on these composite specimens are shown in Table XXIII.

TABLE XXIII  
EFFECT OF ADDITIONS ON FLEXURAL STRENGTH OF Ni-MgO

Addition to Ni Phase, %	Addition to MgO Phase, %	FYS, ksi	UFS, ksi	Deformation, in.
None	None	-	38.1	-
None	1 TiO <sub>2</sub>	42.6	52.4	0.017
2 Ti	0.5 TiO <sub>2</sub>	29.2	46.6	0.013
2 TiN	0.5 TiO <sub>2</sub>	33.9	47.0	0.013
2 TiN	1 TiO <sub>2</sub>	43.0	54.7	0.014
None	3 ZrO <sub>2</sub>	12.2	14.0	0.010
2 TiN	3 ZrO <sub>2</sub>	37.7	49.1	0.015
None	5 HfO <sub>2</sub>	-	27.4	-
2 TiN	5 HfO <sub>2</sub>	36.9	42.2	0.025

1 ▷ From Table XII

The presence of the titanium ion definitely improved the room temperature flexural strength and ductility of the composite; 1-percent TiO<sub>2</sub> additions to MgO and 2-percent TiN additions to Ni-MgO composite specimens showed that TiN additions improved the metal-ceramic bond in the composite. The description and results of these tests are presented in Section 3.2.6.

### 3.2.4 Metal Phase Studies

General work with dispersion-strengthened alloys has shown that hard, insoluble particles uniformly dispersed in a metal matrix can improve high-temperature strength. Dispersion-strengthening is most effective when the material can be cold-worked. A proper cold-working procedure can improve the uniformity of dispersoid distribution and develop a subgrain microstructure. Such a structure in SAP alloy has been attributed for producing the good elevated temperature properties of this material (Reference 15). In a macrolaminate composite, there is no opportunity to cold-work the metal phase. However, the presence of a uniformly distributed dispersoid in the metal phase could be expected to make modest improvements in the strength of the composite system.

To determine the compatibility and effectiveness of various dispersoid materials with the metal phase of the Ni-MgO composite, a study was initiated with  $\text{ThO}_2$ ,  $\text{Y}_2\text{O}_3$ , MgO and CaO additions to nickel. Initial work was done using Sherritt-Gordon Type NF-1M nickel, a 99.82-percent pure material with a nominal particle size of 1 micron. Nitrates of thorium, yttrium, magnesium, and calcium were added to separate batches in concentrations adjusted to provide equal volume fractions of the oxide on decomposition of the nitrate.

The amount of water required to wet the nickel powder was determined by adding water from a burette to a weighed quantity of powder while mechanically mixing it. The end point, established with the first drop which caused puddling, was found to be 40 cubic centimeters of water per 100 grams of nickel powder. The quantity of nitrate of the selected additive was then dissolved in the quantity of water required for a particular batch size. This solution was added to the nickel slowly while it was being mixed to ensure uniform wetting of all particles. The wet powder was then spread over the bottom of a nickel tray and placed in an oven at  $220^\circ\text{F}$  for rapid drying. The dry powder then was transferred to a tube furnace and heated for 3 hours at  $1000^\circ\text{F}$  in hydrogen to decompose the nitrate.

Metal phase specimens of  $(\text{Ni} \cdot 2\text{ThO}_2)$  were prepared by hot-pressing for 20 minutes at temperatures of  $2300^\circ$  and  $2350^\circ\text{F}$  with 4-ksi pressure; flexural yield strengths of 25 and 32 ksi, respectively, were measured on two specimens. These values show an improvement over the 15-ksi yield strength obtained from pure nickel. It was noted during the hot-pressing cycle that on reaching a temperature of  $2100^\circ\text{F}$ , ram travel reversed, indicating that consolidation

of the specimen was essentially completed at that point. Based on this result, a third cycle was used in which the hot-press temperature was limited to 2100°F. The pressure used in this cycle was applied and built up gradually to 4 ksi. The specimen pressed in this manner showed a considerable improvement in properties, with a flexural yield strength of 147 ksi. Specimens with MgO, CaO, and Y<sub>2</sub>O and specimens with Y<sub>2</sub>O<sub>3</sub> additions were similarly prepared with 2100°F hot-press cycles used. The hot-press cycles and the data obtained are shown in Figure 21 and Table XXIV, respectively.

TABLE XXIV  
EFFECT OF OXIDE ADDITIONS ON FLEXURAL STRENGTH OF METAL PHASE

Composition	Hot-Press Cycle *	FYS, psi	Deflection, in.
Ni	1	15,000	-
Ni · 2ThO <sub>2</sub>	1	25,000	.015
Ni · 2ThO <sub>2</sub>	2	32,500	.011
Ni	3	38,400	.050
Ni · 2ThO <sub>2</sub>	3	147,000	.028
Ni · 1.05Y <sub>2</sub> O <sub>3</sub>	3	109,000	.030
Ni · 1.05Y <sub>2</sub> O <sub>3</sub>	3	73,000	.038
Ni · 0.77MgO	3	122,900	.030
Ni · 0.77MgO	3	136,600	.027
Ni · 0.72CaO	3	47,500	53° total bend

\*Described in Figure 21

Metallographic evaluation of representative specimens showed that hot-pressing at temperatures of 2300° and 2350°F produced an irregular grain size between 5 and 20 microns, whereas

specimens hot-pressed at 2100°F had a uniform grain size of 1 to 2 microns. Pure nickel without oxide additions and hot-pressed at 2100°F had large grains up to 80 microns. Based on these results, ThO<sub>2</sub>, MgO, and CaO additions to NF-1M nickel powder were subsequently evaluated in composite test specimens (Section 3.2.5). CaO was included because it showed the best ductility.

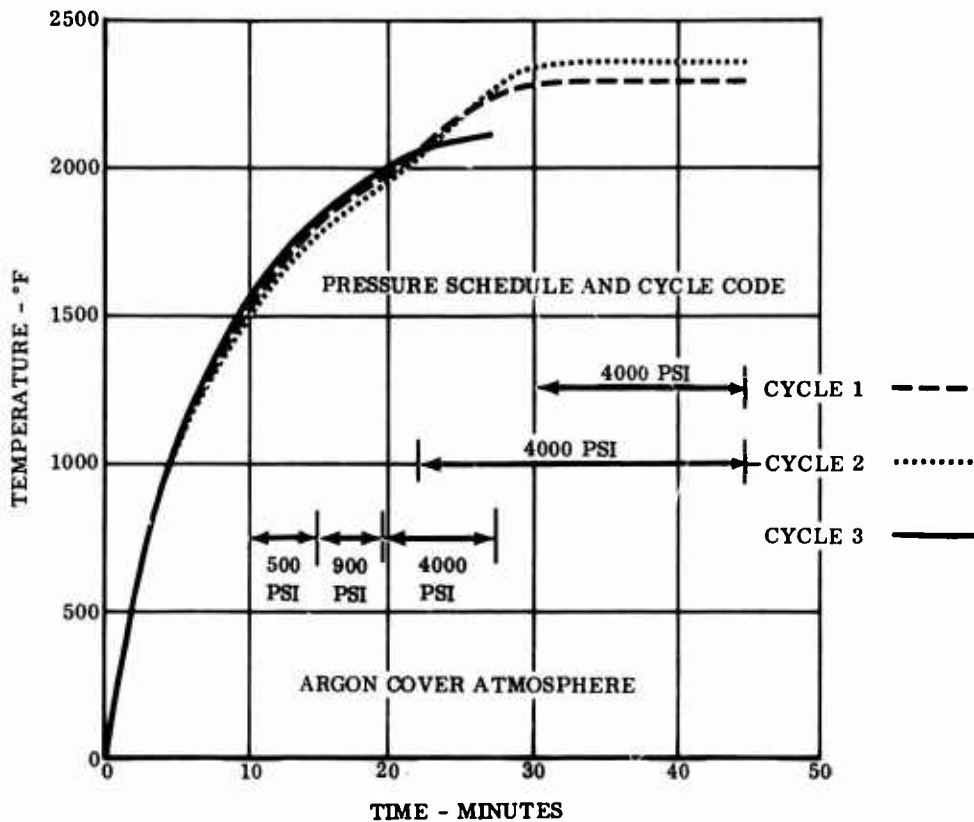


Figure 21. Hot-Press Cycles for Nickel Specimens.

Post-Heat-Treat Study - As discussed previously in Section 3.2.2, a post-treat cycle at 2400°F was effective in increasing the flexural strength of ceramic specimens. To determine the effect of a post-treat cycle on metal phase specimens, portions of the specimens described above in Table XXIV were subjected to the 2400°F post-treat cycle shown in Figure 22. Specimens with oxide additions that previously had been hot-pressed at 2100°F showed various degrees of bloating during post-treating because of internal gas pressure. Specimens with ThO<sub>2</sub> and Y<sub>2</sub>O<sub>3</sub> additions formed large internal voids, while the specimens that contained CaO and

MgO formed smaller voids near the surface.  $(\text{Ni} \cdot 2\text{ThO}_2)$  specimens hot-pressed at 2300° and 2350° F and the pure nickel specimens were not affected by the post-treat cycle.

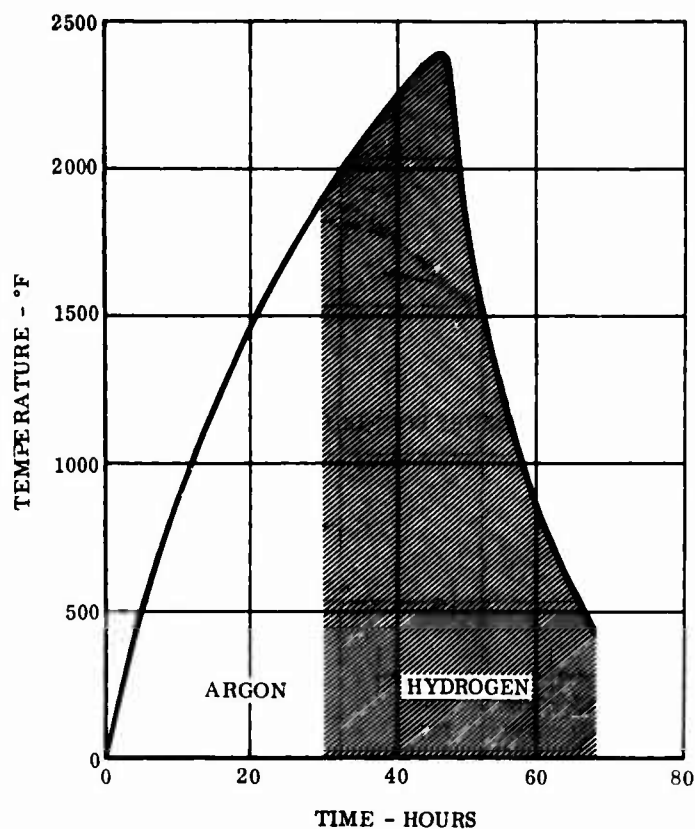


Figure 22. Post-Treat Cycle.

To determine the nature of the gas being released, samples of the pure nickel and  $(\text{Ni} \cdot 2\text{ThO}_2)$  were heated in combustion tubes to 2400° F. The gases liberated were collected and analyzed with a Bendix time-of-flight mass spectrometer and a chromatograph. The major gas given off by both samples was carbon dioxide. A trace of sulfur dioxide also was present in the  $(\text{Ni} \cdot 2\text{ThO}_2)$  sample.

These gases were part of the environment inside the graphite die and became entrapped during the hot-pressing process. This condition could be alleviated by replacing the graphite dies with metal or ceramic dies; however, graphite dies had proved to be generally more practical. Metal dies had the problem of part adherence and gave poor service life. Ceramic insert dies would

have required the use of high density, high strength alumina. The high cost of this material in the sizes necessary for experimental die inserts was not believed to be justified.

An effort was made to avoid the effect of gaseous contaminants by modifying the hot-pressing and the post-treating cycles. Additional ( $\text{Ni} \cdot 2\text{ThO}_2$ ) specimens were prepared using modified hot-press and post-treat cycle. By increasing the time at  $2100^\circ\text{F}$  to 20 minutes during hot-pressing and extending the post-treat cycle to 69 hours, as shown in Figure 23, bloating of specimens was eliminated.

However, the specimens produced with this modified procedure had a very coarse ( $1/32$ - to  $1/16$ -inch diameter) microstructure, which resulted in a flexural yield strength of only 21.5 ksi. The use of carbonyl-nickel powder was studied in an effort to obtain an improvement in the large grain size and attendant low properties.

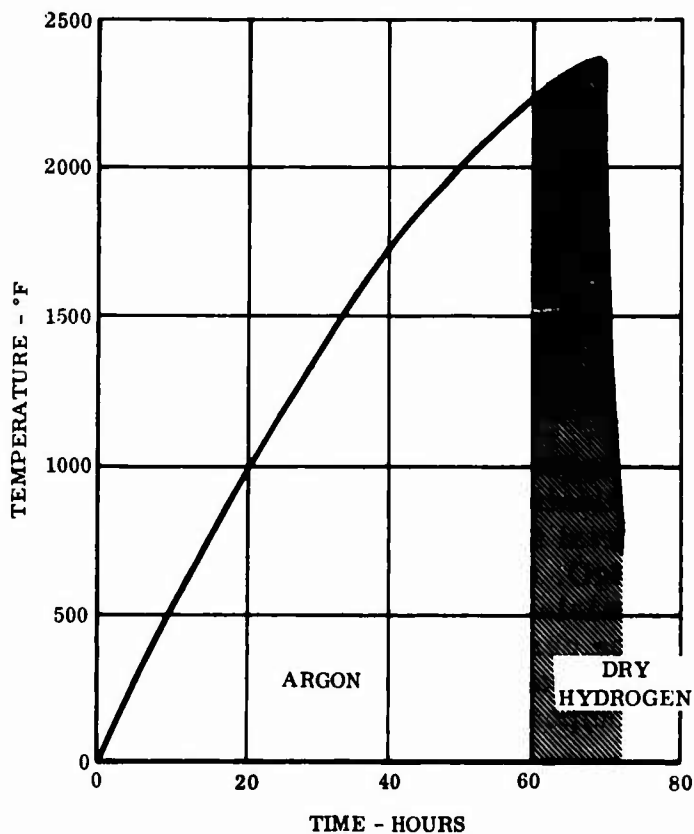


Figure 23. Modified Post-Treat Cycle.

Carbonyl-Nickel Powders - A carbonyl-nickel powder, Mond type 255, was evaluated as a substitute for NF-1M powder. The type 255 powder has a chainlike structure of irregularly shaped particles, with a typical particle size of 2.83 microns. The NF-1M powder has spherically shaped particles with a typical particle size of 0.94 micron.

Specimens of  $(\text{Ni} \cdot 2\text{ThO}_2)$  were hot-pressed at  $2100^\circ\text{F}$ , holding 30 minutes at temperature and using a pressure of 4 ksi. Flexural yield strengths after hot-pressing and after post-treating at  $2400^\circ\text{F}$  using the cycle in Figure 23 are as follows:

As pressed - 83,500 psi

Post treated - 74,100 psi

In both conditions, specimens were deformed 90 degrees without cracking. Metallographic evaluation of a post-treated sample showed that a fine grain size of 2 to 3 microns was retained. The ability of the type 255 nickel powder to retain a finer grain size than the NF-1M powder was attributed to the shape and surface area difference between the two powders. Although the type 255 powder has a larger particle size (2.83 microns compared to 0.94 micron for the NF-1M), its bulk packaging density is much lower (0.48 gm/cc compared to 1.12 gm/cc for the NF-1M). The lower bulk packing density is indicative of a larger surface area, which would tend to promote a more uniform and effective distribution of the  $\text{ThO}_2$  particles.

### 3.2.5 Combined Additions to Macrolaminate Composites

The work conducted in Sections 3.2.2 and 3.2.4 was associated with the evaluation of methods to improve the strength of the separate metal and ceramic phases. It was found that the addition of  $\text{ThO}_2$ ,  $\text{MgO}$ , and  $\text{CaO}$  particles to the metal phase, the addition of  $\text{HfO}_2$  particles to the ceramic phase, and a post-heat-treat cycle for the ceramic phase were the most effective. Work was conducted to evaluate the effect of combined additions to a macrolaminate composite.

Before the evaluation of the type 255 carbonyl-nickel powder described above, a series of macrolaminate composite specimens was prepared using the NF-1M nickel powder with  $\text{CaO}$ ,  $\text{MgO}$  and  $\text{ThO}_2$  additions as the metal phase and pure  $\text{MgO}$  as the ceramic phase. The metal phase powders with the oxide additions were prepared using techniques described previously in Section 3.2.4.

The binder in the laminate particles was removed by heating in nitrogen for 3 hours at 1100°F. Hot-pressing temperatures of 2100°, 2200°, and 2300°F were evaluated. Portions of the samples were subsequently post-treated at 2400°F using the 69-hour cycle described in Figure 23. Flexural properties of the specimens are given in Table XXV.

TABLE XXV  
FLEXURAL PROPERTIES OF Ni-MgO COMPOSITES  
WITH METAL PHASE OXIDE ADDITIONS

Hot- Press Cycle *	As-Pressed Properties			Post-Treated Properties			Apparent Porosity	
	FYS, ksi	UFS, ksi	Def, in.	FYS, ksi	UFS, ksi	Def, in.	As Pressed %	Post Treated %
<u>(Ni · 0.72 CaO) - MgO Composite</u>								
A	-	29.7	-	47.1	53.1	.012	4.4	2.6
A	-	37.0	-	45.5	52.5	.011	4.6	1.3
B	-	49.7	-	45.7	51.3	.010	1.4	0.0
B	-	56.2	-	43.6	49.1	.010	1.6	0.0
C	-	51.8	-	43.6	49.1	.010	0.0	0.0
C	68.9	72.0	.007	40.6	53.0	.011	0.0	1.7
<u>(Ni · 0.77 MgO) - MgO Composite</u>								
A	-	54.1	-	42.7	50.5	.015	4.1	7.1
A	-	37.4	-	40.6	59.4	.020	5.3	6.2
B	-	36.6	-	30.4	43.9	.021	0.0	6.2
B	-	44.6	-	28.5	36.7	.012	0.0	9.4
C	-	33.6	-	34.6	47.8	.012	3.0	3.6
C	33.5	35.9	.006	30.1	39.0	.012	0.0	5.1
<u>(Ni · 2ThO<sub>2</sub>) - MgO Composite</u>								
A	-	32.7	-	43.2	57.0	.015	5.7	6.3
A	-	29.9	-	44.6	53.0	.013	7.3	6.2
B	-	41.4	-	38.3	54.0	.010	1.9	3.9
B	-	51.8	-	36.2	45.0	.021	1.7	6.8
C	-	61.9	-	43.0	43.4	.006	1.8	4.9
C	-	62.8	-	32.3	47.8	.012	0.0	5.1

\*See Figure 24

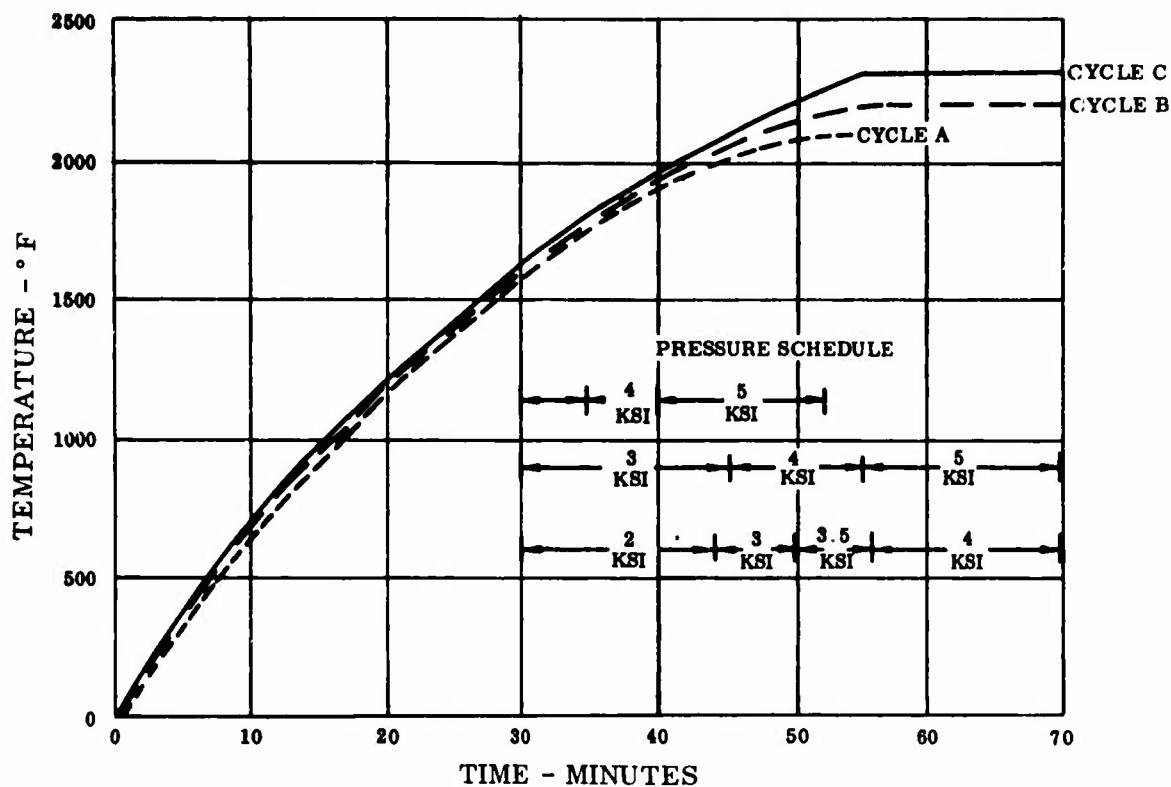


Figure 24. Hot-Press Cycles for Ni-MgO Composites.

The as-pressed specimens showed a fairly wide variation in properties and had little or no ductility. After post-treating, the variation in properties was reduced, and all specimens showed yield points, with the best strengths demonstrated by the composites with  $\text{ThO}_2$  and  $\text{CaO}$  additions to the metal phase. There was no apparent correlation between porosity and strength. The  $2100^\circ\text{F}$  hot-press temperature (Cycle A) showed somewhat better strengths. Also, the post-treatment was observed to increase strength in some specimens, while in other specimens the reverse was true; porosity was generally increased by post-treating.

A second series of macrolaminate composite specimens was prepared using Mond type 255 nickel with 2-percent  $\text{ThO}_2$  additions as the metal phase and both pure  $\text{MgO}$  and  $(\text{MgO} \cdot 5\text{HfO}_2)$  as the ceramic phase. The  $(\text{MgO} \cdot 5\text{HfO}_2)$  was prepared using the coprecipitation technique described in Section 3.2.2. The organic binder was decomposed from the laminate particles prior to hot-pressing by heating in nitrogen at  $900^\circ\text{F}$  for 3 hours. Specimens were hot-pressed at  $2100^\circ$  and  $2300^\circ\text{F}$  and post-treated at  $2400^\circ\text{F}$ ,

using the 69-hour cycle described in Figure 23. The flexural properties for these specimens are shown in Table XXVI.

TABLE XXVI  
FLEXURAL PROPERTIES OF Ni-MgO COMPOSITES  
WITH ADDITIONS TO BOTH PHASES

Composition	Hot- Press Cycle	Flexural Properties		Apparent Porosity	
		As Pressed UFS, ksi	Post Treated UFS, ksi	As Pressed, %	Post Treated, %
(Ni · 2ThO <sub>2</sub> ) -	D	26.2	40.1	3.2	1.6
MgO	D	36.6	39.3	0.6	3.3
↓	E	38.1	39.2	1.2	1.9
↓	E	37.0	34.5	4.4	6.4
(Ni · 2ThO <sub>2</sub> ) -	D	32.5	45.6	0.7	4.2
(MgO · 5HfO <sub>2</sub> )	D	35.8	42.9	0.9	3.7
↓	E	35.5	46.5	1.1	4.2

1 No yield point reached.

2 See Figure 25

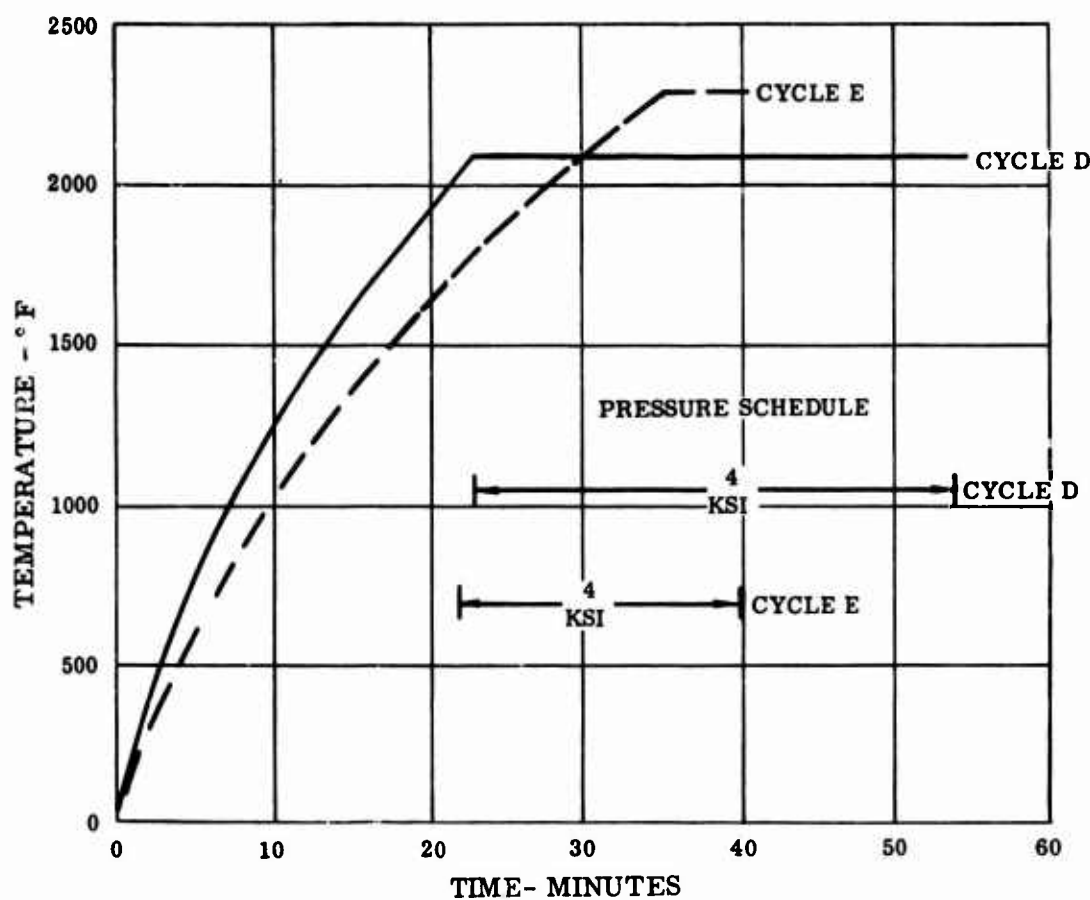


Figure 25. Hot-Press Cycles for Ni-MgO Composites.

In both compositions, the higher properties that were anticipated by using the type 255 carbonyl-nickel powder were not realized. Failure occurred prior to reaching a flexural yield point. No significant difference in properties was noted as a result of using the 2100° or 2300° F hot-press cycles. Although the post-treat cycle improved the properties of the  $(\text{Ni} \cdot 2\text{ThO}_2) - (\text{MgO} \cdot 5\text{HfO}_2)$  specimens, the strength level was lower than that of the previous specimens reported in Table XXV.

A group of  $(\text{Ni} \cdot 0.72\text{CaO}) - (\text{MgO} \cdot 5\text{HfO}_2)$  composite specimens, using type 255 nickel powder, was similarly prepared. Processing parameters were the same as described above except that only the 2100° F hot-press cycle (Cycle D in Figure 25) was used. The flexural test results of these specimens are given in Table XXVII.

**TABLE XXVII**  
**FLEXURAL PROPERTIES OF (Ni · 0.72CaO) -- (MgO · 5HfO<sub>2</sub>)**  
**COMPOSITES**

<u>As Pressed Properties</u>			<u>Post-Treated Properties</u>			<u>Apparent Porosity</u>	
FYS, ksi	UFS, ksi	Deflection, in.	FYS, ksi	UFS, ksi	Deflection, in.	As Pressed, %	Post Treated, %
34.5	39.4	.012	41.2	53.4	.006	3.4	2.2
36.8	41.4	.014	46.2	53.1	.007	1.8	1.0

The test results of the above specimens were somewhat improved over the results of the similar group shown in Table XXVI, in that flexural yield points were reached in specimens with the (MgO · 5HfO<sub>2</sub>) ceramic phase.

The general level of properties of specimens shown in Tables XXV to XXVII was lower than anticipated from work with the separate metal and ceramic phases. The relatively high porosity measured in most samples indicated that entrapped gases or gaseous reactions during post-treating were contributing to the lower properties.

It was observed that a feathery whisker growth had occurred on some of the post-treated specimens. X-ray diffraction identified the whiskers as pure MgO. Examination of the specimens indicated that this phenomenon was primarily a surface reaction. Ceramic lamellae located at the surface of the specimens were providing the material for the whisker growth. A carbon analysis conducted on one of the specimens evaluated showed a carbon content of 1.87 percent. Carbon contamination of a specimen could result in a MgO - MgCO<sub>3</sub> reaction and produce the whisker growth that was observed.

Minor variations in mechanically processing the material may have been a factor in producing the scatter evident in some of the data. Some possible variations include the manner in which material was distributed on trays for the decomposition and organic binder burnout cycles, and the quantity of material being processed for a given test.

The fabrication procedures, including the preparation of ceramic powder, painting of laminate sheets, organic binder burnout cycles, and hot-pressing dies, were subsequently improved to minimize contamination and some of the process variables.

### 3.2.6 Metallographic Bend Studies

Studies were conducted on macrolaminate composite specimens to determine the nature of crack propagation. Small bend specimens, measuring approximately 0.05 x 0.25 x 1.2 inches, were polished using standard metallographic techniques. The specimens were evaluated in a 1-inch bend fixture which applied a load by means of a micrometer screw. The tension side of the specimen was viewed on a metallograph while under stress.

Three specimens initially evaluated were Ni-MgO composites with 50:50 metal-ceramic ratios. The first evidence of cracking in all cases was observed in ceramic lamellae oriented parallel to the direction of principal stress. These cracks were very fine and occasionally were apparent only under polarized light. Evidence of plastic strain in the metal lamellae was not visually apparent until after cracking had occurred in the ceramic. Cracking also propagated into the adjacent metal lamellae if they were oriented generally parallel to the direction of stress. If the orientation of lamellae was approximately 45 degrees or more with respect to the direction of stress, cracks propagated along a metal-ceramic interface. Figure 26 illustrates the type of cracking that was observed under load.

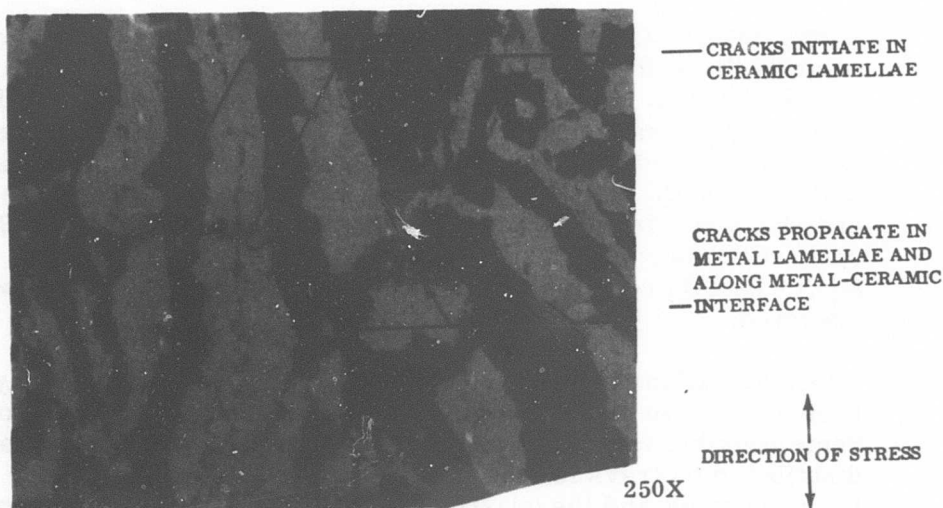


Figure 26. Fracture in a Ni-MgO Specimen.

Visual evaluation of the fracture surfaces showed that considerable metal-ceramic interface cracking, which would indicate that the metal-ceramic bond was relatively weak, had occurred.

After the above tests, additional studies were conducted on the following composites:

1.  $(\text{Ni} \cdot 2\text{ThO}_2) \cdot 2\text{TiN} - (\text{MgO} \cdot 5\text{HfO}_2)$
2.  $(\text{Ni} \cdot 0.72 \text{CaO}) \cdot 2\text{TiN} - (\text{MgO} \cdot 5\text{HfO}_2)$

In each of the materials, TiN was added to improve the metal-ceramic bond. The purpose of the HfO<sub>2</sub> addition to the ceramic phase was to control the grain size of the MgO. The grain size was 2 to 4 microns in composition No. 1, and 6 to 12 microns in composition No. 2.

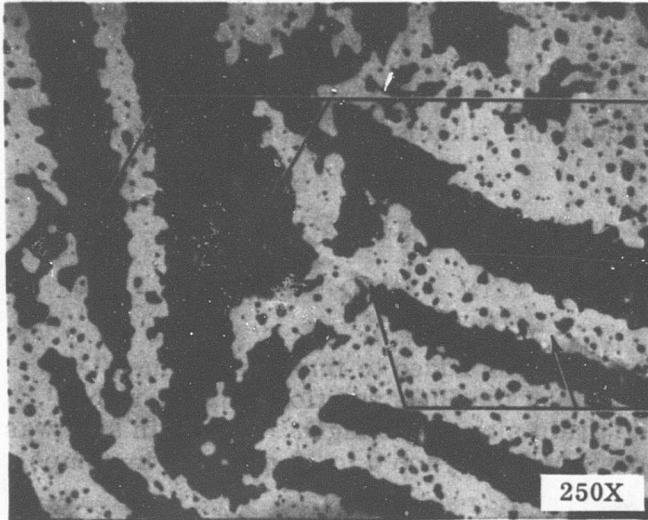
For both composites, cracking initiated in a number of ceramic lamellae which were more randomly oriented than the Ni-MgO specimens evaluated previously. No metal-ceramic interface cracking was observed initially, regardless of the orientation of lamellae with respect to direction of stress. Fracture in the ceramic was observed to be predominately intergranular, which is characteristic of a grain size of 10 microns or less. As deflection increased, cracking propagated along some metal-ceramic interfaces. These interfaces frequently showed some evidence of local ceramic porosity. Examples of fracture in these specimens is shown in Figure 27.

Visual evaluation of the fracture surface indicated that there was less metal-ceramic interface cracking by comparison with the plain Ni-MgO specimens. The improvement in metal-ceramic bond was attributed to TiN.

### 3.2.7 Process Improvement

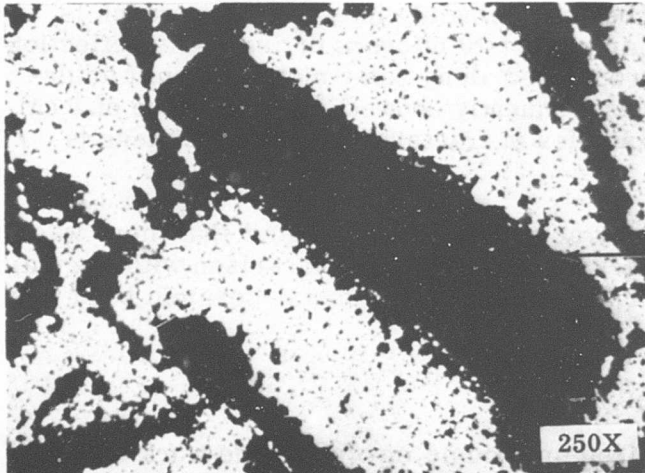
Various studies described previously involved some work related to the evaluation of selected processing parameters such as time, temperature, pressure, and atmosphere. In addition, work also was conducted to improve the fabrication procedures for macro-laminate composites in specific areas as follows:

1. Process to prepare  $(\text{MgO} \cdot 5\text{HfO}_2)$  ceramic powder
2. Process to prepare laminate sheets
3. Organic binder burnout cycle
4. Double-acting hot-press dies



-CRACKS INITIATE IN  
RANDOMLY ORIENTED  
CERAMIC LAMELLAE

-PLASTIC STRAIN OBSERVED  
IN METAL PRIOR TO INTER-  
FACE CRACKING



CRACKS PROPAGATE ALONG  
METAL-CERAMIC INTERFACE  
AFTER EXTENSIVE CERAMIC  
CRACKING

↑  
DIRECTION OF STRESS  
↓



Figure 27. Fracture in Macrolaminate Composites.

Ceramic Powder Process - An evaluation of the process used initially to prepare the  $(\text{MgO} \cdot 5\text{HfO}_2)$  powder indicated that contamination by sodium and chloride ions was possible. The process involved coprecipitating magnesium and hafnium hydroxides from an aqueous solution with a strong alkali, such as NaOH. Ammonium hydroxide was not suitable, because it formed a soluble complex with magnesium. Reagent grade  $\text{Mg}(\text{NO}_3)_2$  and reactor grade II  $\text{HfCl}_4$ , the only soluble salt of hafnium available, were used for the starting materials. A chloride salt normally would be undesirable, as chloride ion carryover with the precipitates results in the formation of NaCl and  $\text{MgCl}_2$ . Both compounds reduce the strength of MgO and cannot be eliminated by heat-treatment at temperatures below the melting point of nickel.

To avoid contamination, the coprecipitation technique was replaced by one which involved decomposition of a hafnium salt on MgO. The initial step in the process was to prepare a water-soluble salt of hafnium which was free of chloride ion. This was accomplished by precipitating  $\text{Hf}(\text{OH})_4$  from a  $\text{HfCl}_4$  solution with  $\text{NH}_4\text{OH}$  and washing with distilled water until, using the silver nitrate test, no trace of chloride was evident. The  $\text{Hf}(\text{OH})_4$  was then dissolved in a nitric acid solution to form  $\text{Hf}(\text{NO}_3)_4$ . An appropriate amount of the  $\text{Hf}(\text{NO}_3)_4$  solution was used to wet MgO powder. This material was then calcined in air at  $1000^\circ\text{F}$  to decompose the nitrate and remove the water, leaving a uniform mixture of MgO and  $\text{HfO}_2$  powders. Ceramic powder prepared in this manner was used for the metal-ceramic ratio study described in Section 3.2.8.

Laminate Sheet Process - Laminate sheet material was prepared during the initial portion of the program by using manual brushing techniques. Control of the layer thicknesses by brushing was maintained by weighing the laminate sheet after each paint layer was applied and dried.

A draw-knife apparatus, shown in Figure 28, was evaluated to determine its ability to achieve better uniformity and thickness control of the laminate layers. The baseplate for the apparatus was machined and lapped from 355-T71 cast aluminum.

The laminate sheets were applied over an aluminum-coated mylar film. A thin film of grease was used to hold the mylar film to the baseplate. Between the application of each layer, the sheets were warm-air dried for 7 to 8 minutes while still on the baseplate.

Several laminate sheets, each consisting of 12 layers, were prepared using the above process to determine the variation in layer

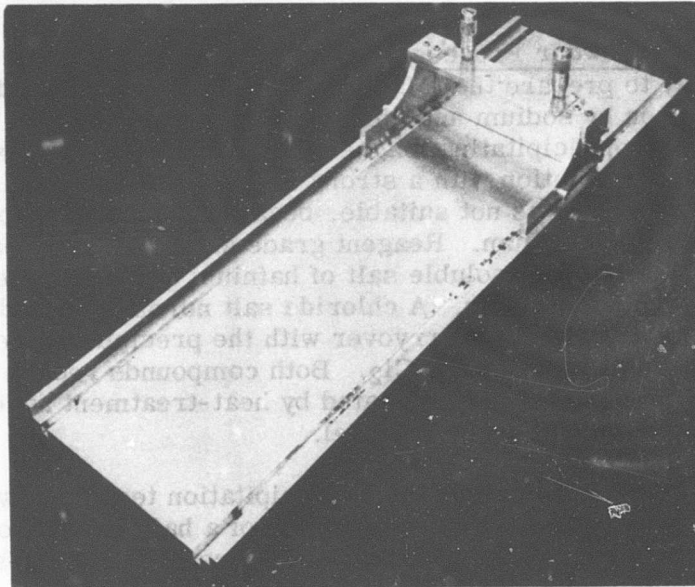


Figure 28. Draw-Knife Apparatus.

thicknesses. The thickness data of the laminate sheets were obtained by checking a cross-sectional sample with a microscope equipped with a filar micrometer.

The data are shown in Table XXVIII.

The metal volume was calculated on the basis of the observed metal layer thicknesses. Subsequent metal-ceramic ratio determinations were made by checking the specific gravity of the macrolaminate particles with an air pycnometer. As shown by the data, variations in thickness for the first three samples averaged about  $\pm 0.6$  mil for the metal and ceramic layers. Through experience gained in the use of the draw-knife apparatus, this variation was reduced to about  $\pm 0.35$  mil on later samples. While this variation was large when considered on a percentage basis, overall control of the average layer thickness was good, and metal-ceramic ratios within 5 percent of the aim point generally were achieved.

Organic Binder Burnout Cycle - As previously discussed in Section 3.2.4, high carbon contents were found in specimens which had been hot-pressed and post-treated. To determine if the organic binder decomposition cycle had contributed to the high residual carbon content, two modified burnout cycles were evaluated. As shown in Table XXIX, carbon analysis data indicated that an air

**TABLE XXVIII**  
**THICKNESS DATA FOR KNIFE-COATED LAMINATE SHEETS**

Sample No.	Metal Layer Thick, Mils			Ceramic Layer Thick, Mils			Metal Volume, %
	Average	Min	Max	Average	Min	Max	
1	1.16	.60	1.81	.94	.69	1.33	57.8
2	.94	.44	1.88	.93	.60	1.65	52.8
3	1.23	.68	2.32	.72	.34	1.33	63.1
4	1.15	.85	1.67	.78	.50	1.05	59.6
5	1.00	.63	1.24	.92	.62	1.33	51
6	.77	.42	1.12	1.21	.79	1.46	39.0
7	1.00	.58	1.21	1.06	.80	1.41	47.7
8	.89	.40	1.60	1.04	.84	1.40	46.3

1 Samples 1-5: (Ni · 2ThO<sub>2</sub>) - MgO  
2 Samples 6-8: (Ni · 0.72CaO) - MgO  
2 Average value based on measurements at both ends and center of the laminate sheets

**TABLE XXIX**  
**CARBON CONTAMINATION RESULTING**  
**FROM VARIOUS ORGANIC BURNOUT CYCLES**

<u>Decomposition Cycle</u>	<u>Percent C*</u>
4 hours at 900°F in N <sub>2</sub>	1.87
3 hours at 1100°F in vacuum (200-500 microns)	0.246
3 hours at 1200°F in air + 3 hours at 1000°F in H <sub>2</sub>	0.075

\*Measured after hot-pressing and post-treating.

burnout cycle and a vacuum burnout cycle were effective in reducing the high carbon content associated with the nitrogen burnout cycle used initially.

The vacuum burnout cycle produced what was believed to be an acceptable carbon level and also avoided the possibility, present with the air burnout cycle, of excessively oxidizing the metal phase.

A series of macrolaminate composite test specimens was prepared to evaluate further the effect of the vacuum and nitrogen burnout cycles described in Table XXIX. The specimens were hot-pressed as shown in Figure 29 and post-treated using the 69-hour cycle at 2400°F described in Figure 23. The results of flexural tests on these specimens are shown in Table XXX.

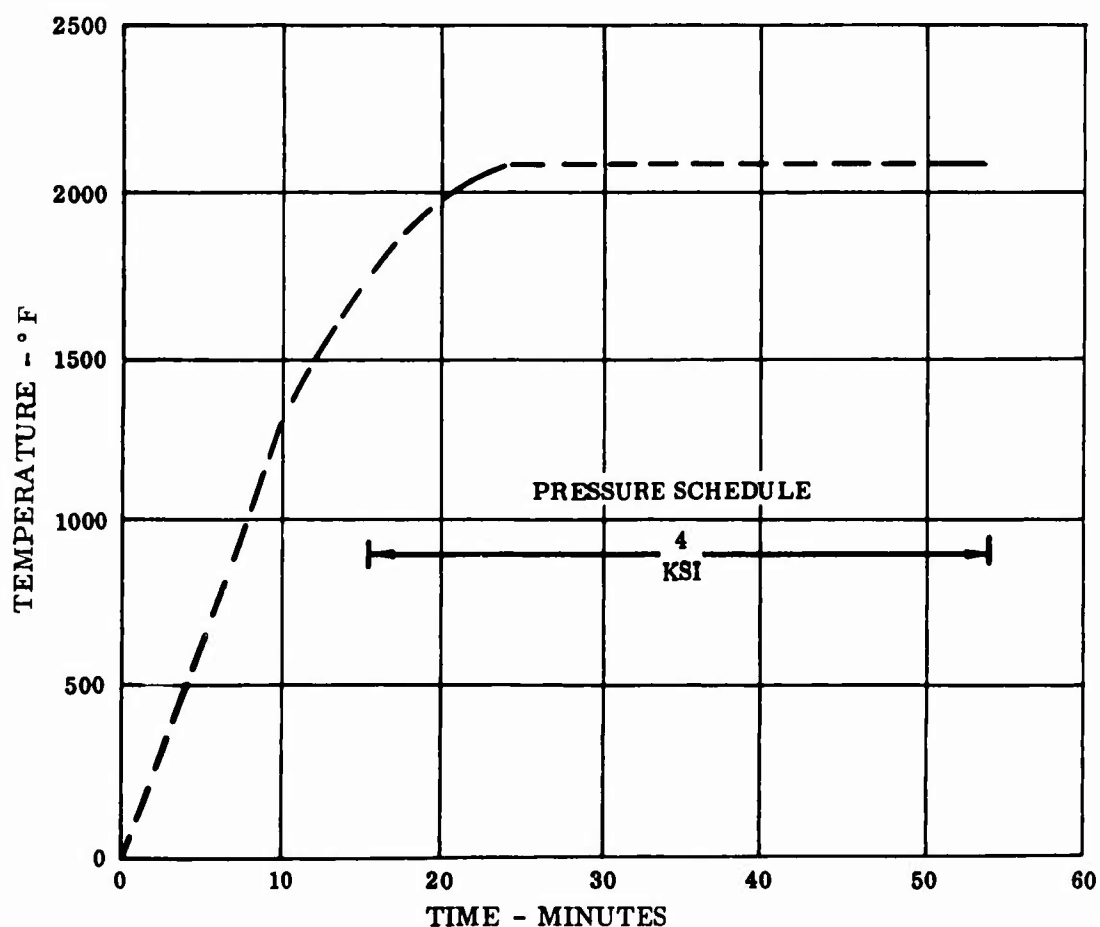


Figure 29. Hot-Press Cycle for Ni-MgO Composites.

TABLE XXX  
EFFECT OF ORGANIC BURNOUT CYCLES  
ON FLEXURAL PROPERTIES

Organic Burnout Cycle	Condition	FYS, ksi	UFS, ksi	Deformation, in.	Apparent Porosity, %
<u>(Ni · 2ThO<sub>2</sub>) · 2TiN - (MgO · 5HfO<sub>2</sub>) Composite</u>					
900°F-N <sub>2</sub>	As Pressed	-	55.3	-	1.9
"	Post Treated	42.2	46.7	0.007	7.2
"	As Pressed	-	45.6	-	2.8
"	Post Treated	49.7	53.3	0.009	6.1
1100°F-Vac	As Pressed	-	68.1	-	1.5
"	Post Treated	44.7	47.0	0.007	3.0
"	As Pressed	-	48.2	-	1.1
"	Post Treated	52.5	54.5	0.007	2.9
<u>(Ni · 0.72 CaO) · 2TiN - (MgO · 5HfO<sub>2</sub>) Composite</u>					
900°F-N <sub>2</sub>	As Pressed	-	45.5	-	3.6
"	Post Treated	53.2	54.0	0.006	0.6
"	As Pressed	-	54.7	-	0.3
"	Post Treated	50.1	55.0	0.007	0.2
1100°F-Vac	As Pressed	-	51.5	-	0.1
"	Post Treated	47.6	49.6	0.007	0.2
"	As Pressed	-	48.1	-	0.0
"	Post Treated	50.0	52.0	0.007	0.0

The data in Table XXX indicate that there was little or no improvement in flexural strength for the specimens which were prepared using the vacuum burnout cycle. Apparent porosity, however, was definitely improved when the vacuum burnout cycle was used, and no evidence of whisker growth was observed.

**Hot-Press Dies** - Hot-pressing normally was conducted using single-acting graphite dies. This procedure was found to be satisfactory when the resulting specimens were thin (less than 0.2 inch thick). For thicker specimens, however, a nonuniform density occurred across the specimen cross section. Visually apparent porosity was observed on the lower surface of ground tensile specimens. Increased sidewall friction associated with the larger quantity of material being pressed was apparently resulting in a nonuniform distribution of pressure to the material in the die cavity.

To provide more uniform pressure, ram travel from top and bottom was required and was achieved by using a suspended die. After the die cavity was charged with laminate particles, the die was assembled with the upper and lower rams extending from the die body. The die assembly was then prepressed at room temperature, while supporting the die body, to build up sufficient sidewall friction to hold it together during hot-pressing. Heating in the induction furnace was accomplished in the normal manner. A sketch illustrating the single- and double-acting dies is shown in Figure 30.

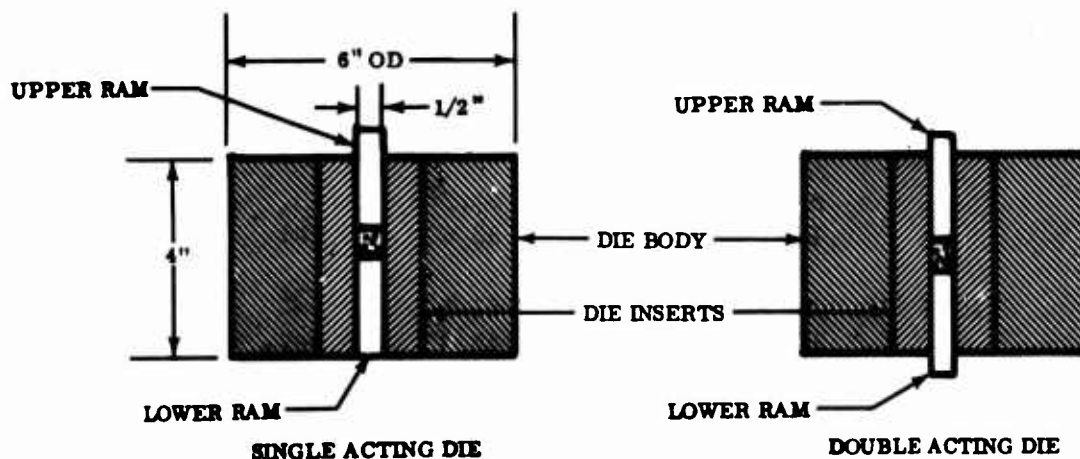


Figure 30. Modified Method of Assembling Hot-Press Die.

This procedure proved effective in minimizing porosity and was utilized for preparing specimens used in the metal-ceramic ratio studies for both the Ni-MgO and the Ni-Al<sub>2</sub>O<sub>3</sub> composite systems.

### 3.2.8 Metal-Ceramic Ratio Study

The metal-ceramic ratio study conducted in this part of the program involved room temperature flexural tests, elevated temperature tensile tests, oxidation tests, and thermal-fatigue tests. The purpose of these tests was to evaluate the suitability of composites of the Ni-MgO system for stator vane application. Based on the results of previous work, a  $(\text{Ni} \cdot 2\text{ThO}_2) \cdot 2\text{TiN} - (\text{MgO} \cdot 5\text{HfO}_2)$  composite was selected for this study.

Mond type 255 carbonyl-nickel powder was used in the metal phase. The  $(\text{Ni} \cdot 2\text{ThO}_2)$  metal phase powder was prepared using a decomposition cycle at  $1000^\circ\text{F}$  for 3 hours in hydrogen. TiN was added to the metal phase powder mechanically by ball-milling while mixing with the organic binder. The ceramic phase powder was prepared using the procedure described in Section 3.2.7. Laminate sheets with metal-ceramic ratios of 70:30, 50:50, and 30:70 on a volume basis were prepared using draw-knife techniques also described in Section 3.2.7.

Prior to hot-pressing, the organic binder was decomposed by heating in vacuum at  $1100^\circ\text{F}$  for a period of 3 hours. The particles were prepressed at room temperature in graphite dies using a pressure of 3 ksi. All specimens were hot-pressed using the suspended die technique at  $2100^\circ\text{F}$ , holding the specimen at this temperature for 30 minutes under a pressure of 4 ksi. After hot-pressing, flexural test specimens were post-treated at  $1850^\circ\text{F}$  using the cycle shown in Figure 31. Previous results obtained with specimens post-treated at  $2400^\circ\text{F}$  indicated that the  $2400^\circ\text{F}$  cycle generally was not effective in improving the properties of composites. The  $1850^\circ\text{F}$  post-treat cycle was found to be effective in improving the strength of the flexural test specimens, and on this basis was used for the remainder of the specimens.

Procedures that were used to finish the test specimens and conduct the tests are described in Section 2.3.

Flexural Tests - Room temperature flexural strength increased rapidly with increasing metal content in both the as-pressed and post-treated conditions. Specimens with higher ceramic contents showed the best relative improvement in flexural strength as a result of the  $1850^\circ\text{F}$  post-treatment. Figure 32 shows a plot of flexural strength as a function of metal content.

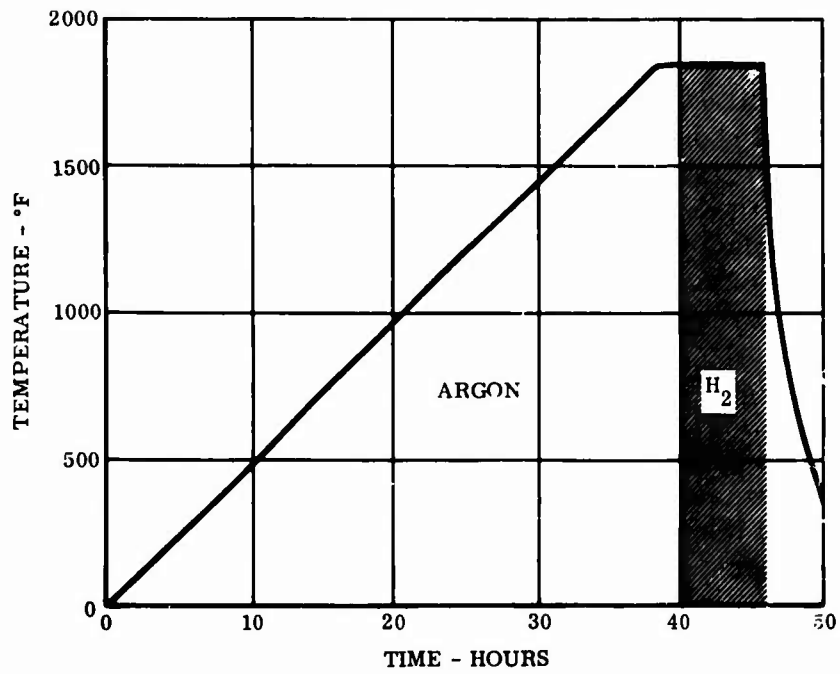


Figure 31. Post-Treat Cycle.

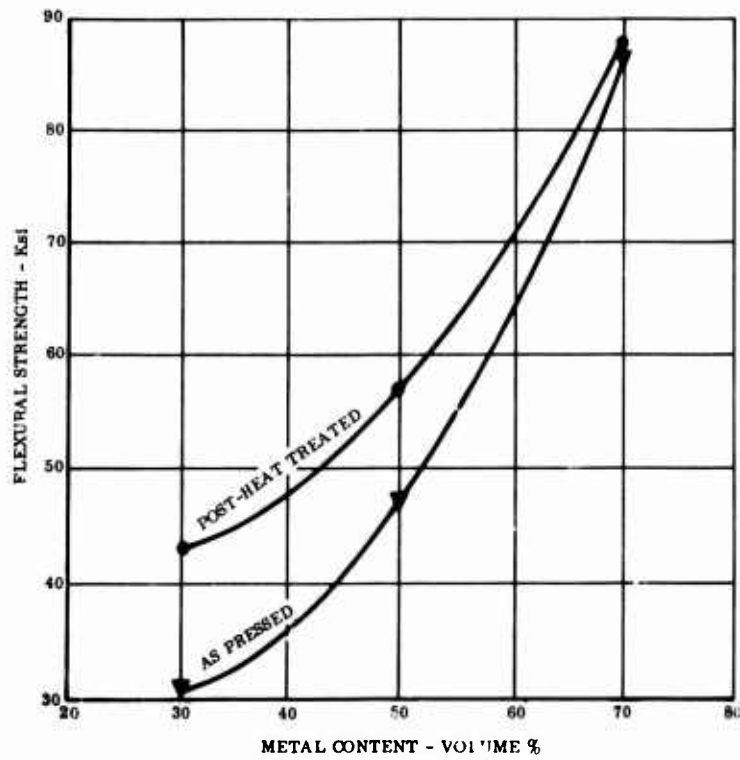


Figure 32. Flexural Strength Versus Metal Content for  $(\text{Ni} \cdot 2\text{ThO}_2) \cdot 2\text{TiN} - (\text{MgO} \cdot 5\text{HfO}_2)$  Composites.

The flexural strengths that approached 90,000 psi for the 70:30 metal-ceramic ratio specimens were the highest recorded for the Ni-MgO system in this program. Portions of these flexural test specimens were subsequently used for the oxidation and thermal-fatigue tests.

Oxidation Tests - Static oxidation tests at 2300° F in air for 24- and 100-hour durations were conducted with rectangular specimens which measured approximately 1/2 x 1/8 x 1 inch. Weight gain resulting from oxidation increased in a linear manner with respect to metal content over the range of 30- to 70-volume-percent metal, as shown in Figure 33.

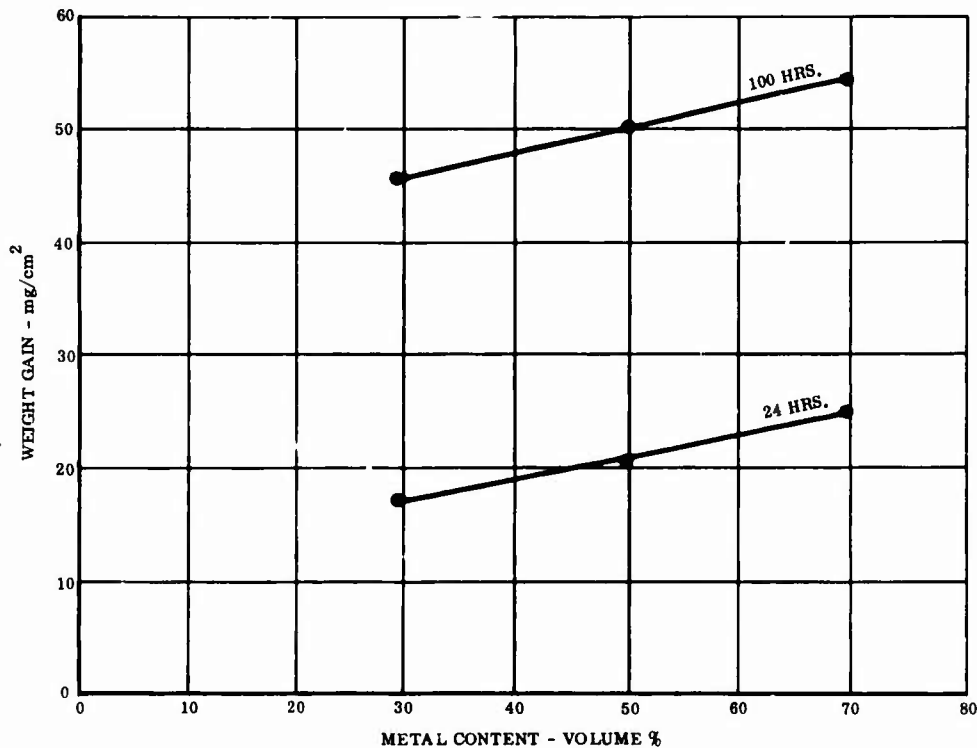
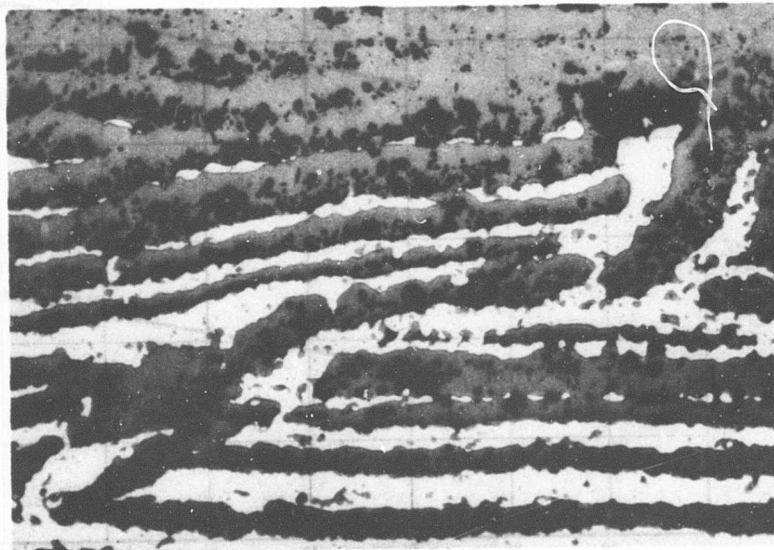


Figure 33. Oxidation Resistance at 2300° F Versus Metal Content for  $(\text{Ni} \cdot 2\text{ThO}_2) \cdot 2\text{TiN} - (\text{MgO} \cdot 5\text{HfO}_2)$  Composites.

The low metal content specimens showed a disproportionately high weight gain resulting from oxidation. For example, reducing the metal content from 70-volume-percent to 30-volume-percent produced only a 15-percent reduction in the weight gain. Since weight

gain by oxidation is a function of the surface area exposed, the ceramic phase was not an effective barrier to oxygen diffusion and was allowing subsurface oxidation to occur.

Evidence of subsurface oxidation of metal lamellae is shown in Figure 34. NiO, formed during the oxidation of the metal phase, dissolved in the ceramic phase and had the effect of increasing the thickness of the ceramic phase. NiO and MgO form a continuous solid solution, which is easily identified by its characteristic green color when viewed under polarized light. Porosity is evident in many ceramic lamellae below the heavy (0.022 inch) surface scale; however, there appears to be very little porosity actually at the metal-ceramic interface. This would indicate that the surface scale and the ceramic lamellae were offering inadequate resistance to the diffusion of oxygen.



Unetched

200X

Figure 34. Oxidation in a 50:50 Metal-Ceramic Ratio Specimen of  $(\text{Ni} \cdot 2\text{ThO}_2) \cdot 2\text{TiN}-(\text{MgO} \cdot 5\text{HfO}_2)$

**Thermal Fatigue** - Thermal-fatigue tests were conducted using a flame heating and air-blast cooling cycle as described in Section 2. 3. The temperature cycle ranged from 300° to 2300° F. The purpose of the tests was to determine whether the composites could withstand 500 cycles without failure. Duplicate specimens were used

for each of the metal-ceramic ratios. The test results, given in Table XXXI, show that thermal-fatigue properties improved with increasing metal content; however, none of the specimens tested were considered to have successfully withstood 500 cycles.

Thermal-fatigue testing of the type used in this program normally produced cracking in the center of the hot zone. These cracks resulted from alternate compressive and tensile strains produced in the edge of the specimen by thermal cycling, as illustrated in Figure 35.

TABLE XXXI  
THERMAL-FATIGUE TEST RESULTS FOR  
(Ni · 2ThO<sub>2</sub>) · 2TiN - (MgO · 5HfO<sub>2</sub>)  
COMPOSITES

Metal Content, Volume %	Cycles Tested	Remarks
30	3	Thermal shock crack
30	3	Thermal shock crack
50	490	0.025-inch erosion
50	490	0.025-inch erosion
70	512	No failure; 1/32-inch bow
70	512	No failure; 1/32-inch bow

On heating, higher relative thermal expansion in the hot zone causes compression upsetting. A tensile strain equivalent to the compressive strain is produced during the cooling cycle. The higher metal content specimens of this test group showed a visual amount of upsetting and bowing, as depicted in Figure 36, which is indicative of higher ductility and more resistance to crack formation.

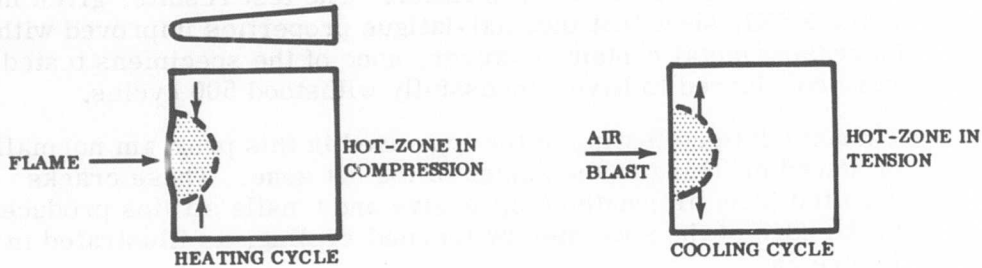


Figure 35. Thermal Strains in Test Specimen.

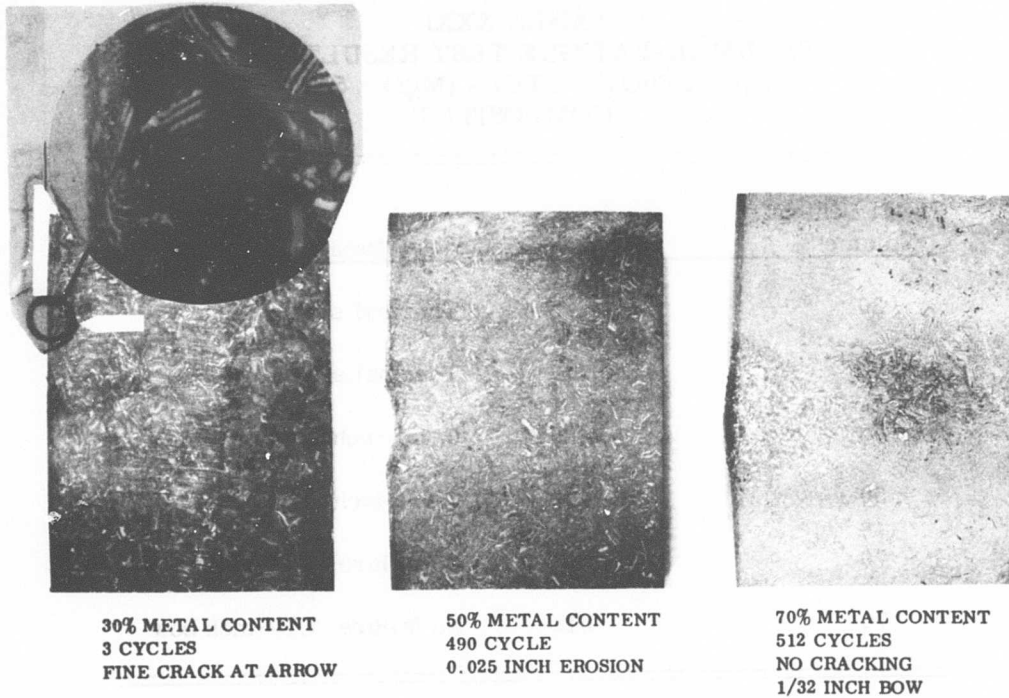


Figure 36. Thermal-Fatigue Test Specimens of  $(\text{Ni} \cdot 2\text{ThO}_2) \cdot 2\text{TiN} - (\text{MgO} \cdot 5\text{HfO}_2)$  Composites.

The 30:70 metal-ceramic specimens showed cracks after only a few cycles. This type of cracking was observed to occur at the edge of the hot zone and can be classified more correctly as a thermal-shock failure. The failure results from the inability of a nonductile material to accommodate thermal strains associated with a temperature gradient.

Tensile Test - Tensile tests at room temperature, 1800°F, and 2200°F also were conducted for the three metal-ceramic ratios. A plot of the test results is given in Figure 37.

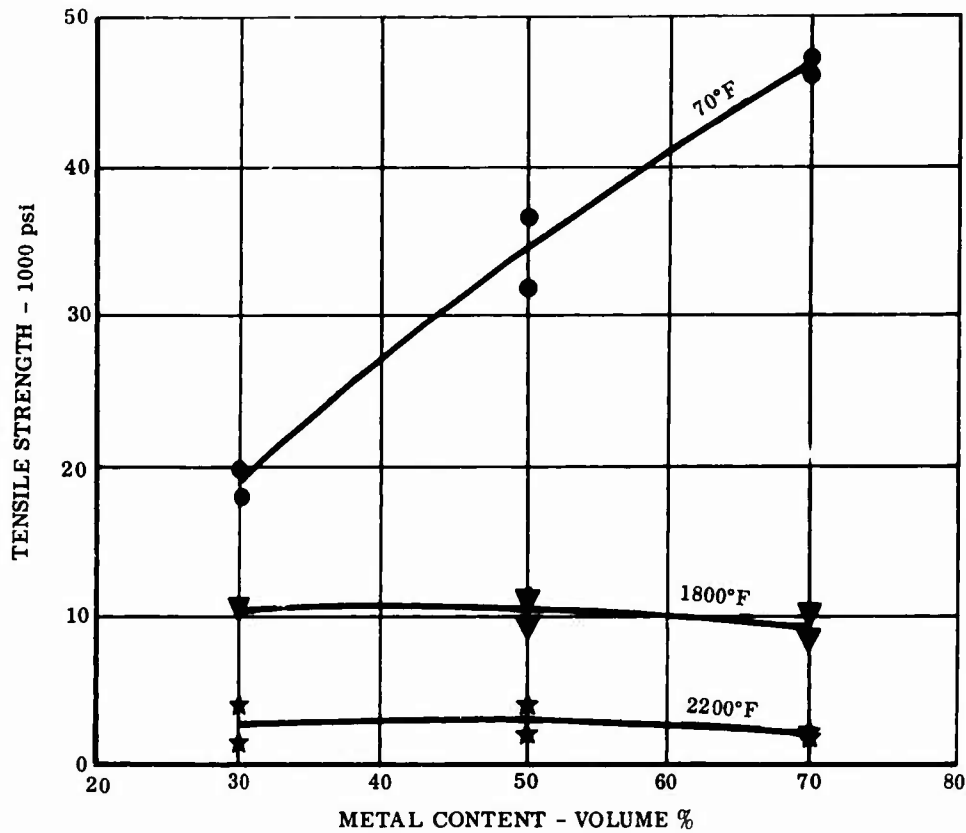
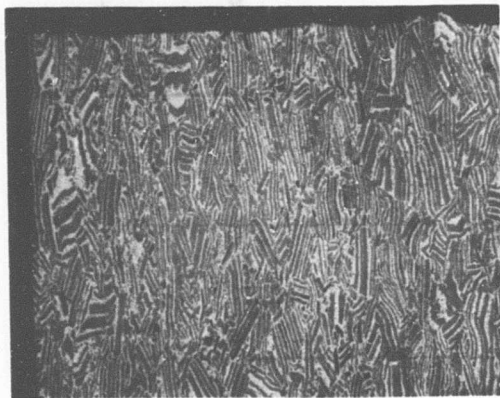


Figure 37. Tensile Strength Versus Metal Content for  $(\text{Ni} \cdot 2\text{ThO}_2) \cdot 2\text{TiN} - (\text{MgO} \cdot 5\text{HfO}_2)$  Composites.

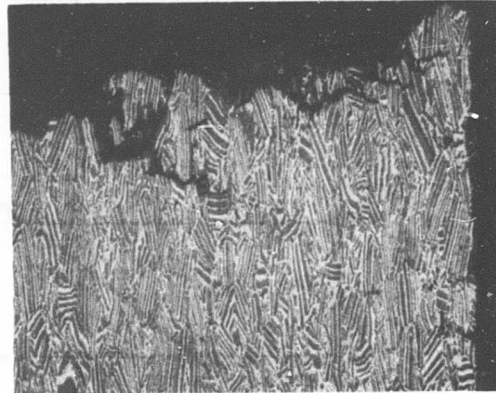
At room temperature, tensile strengths, like flexural strengths, increase significantly with metal content (Figure 32). The ratios of flexural strength to tensile strength were relatively consistent, with values of 1.75:1, 1.65:1, and 1.87:1 for metal-ceramic ratios of 30:70, 50:50, and 70:30, respectively. At the elevated temperatures, the metal-ceramic ratio had relatively little effect on the tensile strength.

The mode of tensile failure varied with the metal-ceramic ratio and test temperature. For specimens with 30- and 50-volume-percent metal, the fracture surface was flat in nature and occurred

perpendicular to the direction of stress in tests at room temperature and 1800°F. At 2200°F, the fracture for both of these metal-ceramic ratios had a fibrous appearance. Cross sections of specimens illustrating the types of fracture are shown in Figure 38. The fractures for the 2200°F tests generally occurred along metal-ceramic interfaces, with some of these being between laminate particles.



UNETCHED  
ROOM TEMPERATURE  
15X



UNETCHED  
2200°F  
15X

Figure 38. Effect of Temperature on Tensile Fracture of  $(\text{Ni} \cdot 2\text{ThO}_2) \cdot \text{TiN} - (\text{MgO} \cdot 5\text{HfO}_2)$  Specimens With 50:50 Metal-Ceramic Ratio.

For specimens with 70-volume-percent metal, the fracture was fibrous in appearance at all three temperatures. Measurable tensile elongation occurred only at 2200°F for the 50- and 70-volume-percent metal specimens.

A summary of the tensile test data and oxidation data for the  $(\text{Ni} \cdot 2\text{ThO}_2) \cdot \text{TiN} - (\text{MgO} \cdot 5\text{HfO}_2)$  macrolaminate composites with various metal-ceramic ratios is given in Table XXXII.

TABLE XXXII  
SUMMARY OF (Ni · 2ThO<sub>2</sub>) · 2TiN - (MgO · 5HfO<sub>2</sub>) COMPOSITE  
TEST DATA FOR VARIOUS METAL-CERAMIC RATIOS

Test Temperature, °F	0.2% YS, psi	UTS, psi	Elongation, %	Density, gm/cc	Apparent Porosity, %	Weight Gain Due to Oxidation, mg/cm <sup>2</sup>
<u>Metal Content - 30 Volume %</u>						
(Oxidation Specimen)				4.75	0.8	45.6
70	2	18,100	0	4.95	0.7	-
70	2	19,800	0	4.81	0.8	-
1800	2	10,200	0	4.82	0.1	-
1800	2	3,300	0	4.69	3.3	-
2200	2	4,000	0	4.77	1.4	-
2200	1,400	1,500	7	4.67	3.6	-
<u>Metal Content - 50 Volume %</u>						
(Oxidation Specimen)				5.86	0.0	50.0
70	2	36,700	0	5.95	0.4	-
70	2	33,700	0	5.24	0.3	-
1800	2	9,500	0	5.84	0.0	-
1800	2	11,300	0	5.69	0.1	-
2200	1,800	2,000	1.5	5.80	0.2	-
2200	3,900	4,000	1.6	5.67	0.5	-

TABLE XXXII (Continued)

Test Temperature, °F	0.2% YS, psi	UTS, psi	Elongation, %	Density, gm/cc	Apparent Porosity, %	Weight Gain Due to Oxidation, mg/cm <sup>2</sup>	
<u>Metal Content - 70 Volume %</u>							
	(Oxidation Specimen )			6.91	0	54.2	
70	2	47,400	0	7.03	0.4	-	
70	2	46,200	0	6.99	0.4	-	
1800	10,200	10,200	0.5	6.87	0.2	-	
1800	8,300	8,400	0.5	6.86	0.1	-	
2200	2,000	2,100	3	6.87	0.2	-	
2200	1,900	2,000	3	6.89	0.3	-	
							1
							2
							1
							2

1 Exposed 100 hours at 2300°F.

2 Yield point not reached.

### 3.2.9 Summary of Ni-MgO Macrolaminate Composite Results

The program conducted on the Ni-MgO composite system was aimed at improving the quality of the composite in terms of strength, density, and ductility and then evaluating the suitability of this material for high-temperature nozzle vane application. Studies were conducted to determine the effect of additives and process variables on properties of the separate metal and ceramic phases and subsequently on the properties of macrolaminate composites. Based on these studies, a composition was selected and a process defined for the preparation of specimens with various metal-ceramic ratios. Evaluation of these specimens included tensile, thermal-fatigue and oxidation tests.

Dispersed second-phase particles, i. e. ,  $\text{ThO}_2$  in the metal phase and  $\text{HfO}_2$  in the ceramic phase, were found to be the most effective in improving the strengths of the separate phases. The dispersed particles were observed to retain fine grain sizes, of about 10 microns, in both the metal and ceramic phases.

Additions of  $\text{TiN}$  to the metal phase of  $\text{TiO}_2$  to the ceramic phase improved the flexural strength of  $\text{Ni-MgO}$  composites. Metallographic studies conducted on specimens with and without  $\text{TiN}$  additions to the metal phase showed that  $\text{TiN}$  improved the metal-ceramic bond. Improving the metal-ceramic bond had the effect of promoting more deformation in the metal phase and, hence, allowing a better distribution of load to the ceramic phase.

Based on the initial studies, combinations of additions were selected and evaluated in macrolaminate composites. However, the combined additions produced only slight improvements in properties. The effects associated with individual additions were not additive when combined additions were evaluated in composites. Room-temperature flexural strengths of composites were found to be limited to about 60 ksi, regardless of the combination of additives evaluated.

Methods also were evaluated to improve the processing techniques used to prepare macrolaminate composites. The use of a draw-knife apparatus provided good control over the metal-ceramic ratio during the preparation of laminate sheets. Hot-pressing at  $2100^\circ\text{F}$  for 30 minutes produced composites with negligible porosity in thinner specimens; i. e. , specimens less than 0.2 inch thick. More porosity was apparent in larger specimens, although this condition was improved by the use of a double-acting suspended die during hot-pressing.

Post-treating at  $2400^\circ\text{F}$ , after hot-pressing, was effective in improving the strength of ceramic test specimens, but generally was not effective when used on macrolaminate composites. Initial post-treat cycles resulted in reactions of the  $\text{MgO}$  with both residual carbon and entrapped gases. These reactions produced whisker growth on the surface and bloating of the composites. The use of a vacuum organic burnout cycle and post-treat cycles with slower heating rates, and subsequently lower temperatures, essentially eliminated the reactions.

Based on the results of the previous work, a  $(\text{Ni} \cdot 2\text{ThO}_2) \cdot 2\text{TiN} - (\text{MgO} \cdot 5\text{HfO}_2)$  composite was selected for evaluation with various metal-ceramic ratios. Specimens with metal contents of 30, 50, and 70 volume-percent were prepared and evaluated by means of room and elevated temperature tensile tests, thermal-fatigue tests with a 300° to 2300° F cycle and 2300° F oxidation tests. These tests were conducted primarily to determine the suitability of this material system for nozzle vane application. Room temperature strength was observed to increase as the metal content of the composite increased; however, the elevated temperature strength was essentially independent of the metal-ceramic ratio. Tensile strengths were about 10,000 psi at 1800° F and 2,000 psi at 2200° F. Oxidation tests at 2300° F for 100 hours in static air showed that weight gains resulting from oxidation decreased from 54.2 to 45.6 mg/cm<sup>2</sup> as the ceramic content increased from 30 percent to 70 percent. The fact that oxidation resistance was not proportionately decreased as ceramic content increased was attributed to subsurface oxidation. Thermal-fatigue tests showed that this material system had inadequate resistance to severe thermal cycles. Specimens with low metal content failed by thermal shock because of insufficient ductility. Specimens with high metal content showed bowing, which resulted from compressive stress in the hot zone of the test specimen.

In general, the Ni-MgO system was amenable to fabrication processes developed for macrolaminate composites. The composites produced generally showed a low level of porosity. However, it must be concluded that the strength, oxidation resistance, and thermal-fatigue resistance of the Ni-MgO composite system are inadequate for nozzle vane application. Subsequent work on the Ni-Al<sub>2</sub>O<sub>3</sub> system indicated that it offered more potential for this application.

### 3.3 Ni-Al<sub>2</sub>O<sub>3</sub> MACROLAMINATE COMPOSITES

The Ni-Al<sub>2</sub>O<sub>3</sub> macrolaminate composite system was considered in this program because of the potential strength advantages of Al<sub>2</sub>O<sub>3</sub> over MgO, as previously discussed in Section 2.1.3. Because no background information was available on a Ni-Al<sub>2</sub>O<sub>3</sub> macrolaminate composite, a preliminary study was conducted to establish fabrication procedures. Information derived from the preliminary work was subsequently used to conduct studies related to investigating chromium additions to the metal phase and sintering-aid additions to the ceramic phase. A final series of tests was conducted to determine the effect of metal-ceramic ratio on tensile, oxidation, and thermal-fatigue properties.

The research and development items of work conducted on the Ni-Al<sub>2</sub>O<sub>3</sub> composites, and subsequently discussed in the following paragraphs, are as follows:

Preliminary Evaluation Studies

Compositional Development

Metal-Ceramic Ratio Study

### 3.3.1 Preliminary Evaluation Studies

General procedures for the preparation of laminate particles were the same as those used for the Ni-MgO system, and are described in Section 2.1.1. Initial composites were prepared using Sherritt-Gordon NF-1M nickel powder for the metal phase and Linde-A 0.3 micron Al<sub>2</sub>O<sub>3</sub> for the ceramic phase. Temperatures of 2350° F with holding times of 15 minutes at temperature were used to hot-press flexural test specimens, as shown in Figure 39. A 69-hour post-treat cycle at 2400° F, previously described in Figure 23, also was evaluated. Test results of these specimens, given in Table XXXIII, showed some improvement in properties over plain Ni-MgO composites.

TABLE XXXIII  
FLEXURAL PROPERTIES OF PRELIMINARY Ni-Al<sub>2</sub>O<sub>3</sub> COMPOSITES

Hot-Pressing Pressure Cycle	As-Pressed UFS, psi	Post-Treated UFS, psi	As-Pressed Apparent Porosity, %	Post-Treated Apparent Porosity, %
5.0 ksi for 15 min	43,800	42,400	10.9	15.1
5.0 ksi for 29 min	46,800	48,500	8.0	12.6

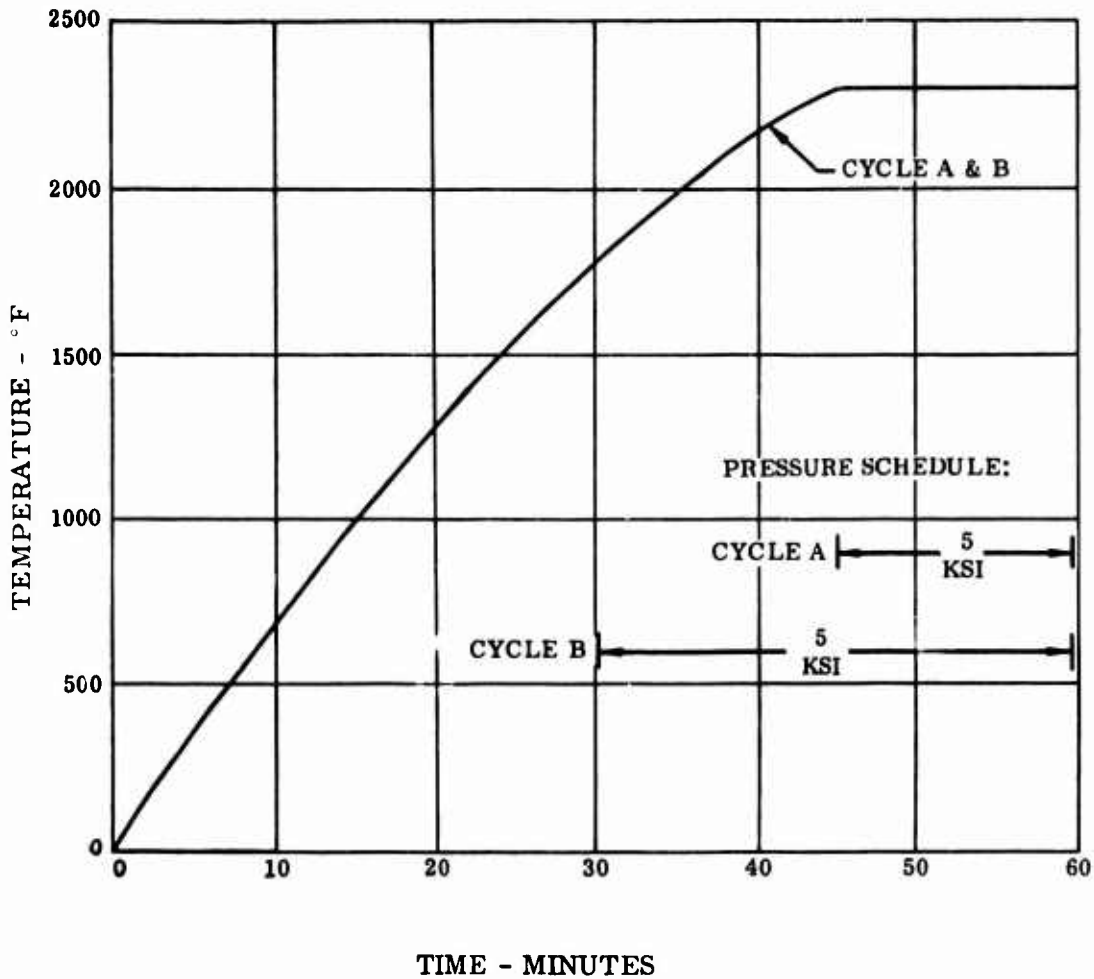


Figure 39. Hot-Press Cycle for Ni-Al<sub>2</sub>O<sub>3</sub> Composites.

The data indicated that the hot-pressing cycles used were generally inadequate and that higher hot-pressing temperatures and/or pressures should be capable of producing composites with lower porosity and, therefore, higher strength. Attempts to use pressures higher than 5 ksi were, however, not successful because of failure of the graphite dies. At the time this program was conducted, the availability of graphite die materials was limited to ATJ graphite and Graphitite G. Hot-pressing trials were also made using temperatures of 2400° and 2500° F; however, excessive extrusion of metal out of the die cavity resulted. These factors limited hot-pressing temperatures to 2350° F and pressures to 4.5 to 5.0 ksi. In view of these limitations, efforts

were concentrated on the use of sintering aids as a means of reducing porosity and improving strength, as discussed later in this section.

Two preliminary specimens also were prepared with chromium additions to the metal phase to improve oxidation resistance and provide some solid solution hardening. A macrolaminate composite corresponding to Ni · 13Cr · 0.7ThO<sub>2</sub>-Al<sub>2</sub>O<sub>3</sub> was hot-pressed for 1 hour at 2350° F with 4.5-ksi pressure. The metal phase powder was prepared by mixing proportions of (Ni · 2ThO<sub>2</sub>) powder with 80Ni-20Cr alloy powder. Flexural properties of the as-pressed specimens are given in Table XXXIV.

TABLE XXXIV  
FLEXURAL PROPERTIES OF  
Ni · 13Cr · 0.7ThO<sub>2</sub>-Al<sub>2</sub>O<sub>3</sub> COMPOSITES

Condition	FYS, ksi	UFS, ksi	Deflection, in.	Apparent Porosity, %
As Pressed	32.8	38.2	0.016	-
As Pressed	38.2	45.3	0.015	1.1

The properties obtained were approximately equivalent to those of the Ni-Al<sub>2</sub>O<sub>3</sub> composites described in the previous table. Specimens which were post-treated at 2400° F. using the cycle in Figure 23, showed evidence of incipient melting. The melting was attributed to excessive carbon content as the result of an inadequate organic binder decomposition cycle. Modified cycles were subsequently evaluated in Section 3.3.2. To improve the high porosity that was generally present in the ceramic phase, TiO<sub>2</sub> was evaluated as a sintering aid, as discussed below.

**Ceramic Phase Additive** - Minor additions of a second component which can form a solid solution have been found effective in promoting sintering in a number of materials.  $TiO_2$  has been reported to be effective in sintering pure  $Al_2O_3$ , and a preliminary study was conducted to determine its effectiveness in a macro-laminate composite. A ceramic phase was prepared in which 0.25-percent additions of Baker's reagent grade  $TiO_2$  were made to Linde-A 0.3 micron  $Al_2O_3$ . Type 255 carbonyl-nickel powder was used as the metal phase. A hot-pressing cycle of  $2350^\circ F$  for 1 hour at 4.5-ksi pressure was used for preparing flexural test specimens. The results are shown in Table XXXV.

TABLE XXXV  
FLEXURAL PROPERTIES OF  $Ni-Al_2O_3 \cdot 1/4TiO_2$  COMPOSITES

Condition	FYS, ksi	UFS, ksi	Deflection, in.	Apparent Porosity, %
As Pressed	40.0	62.0	0.017	0.1
Post Treated*	44.9	49.6	0.008	8.9
As Pressed	40.0	63.8	0.017	0.1
Post Treated*	40.5	44.8	0.008	8.0

\*69-hour cycle at  $2400^\circ F$  (Figure 23).

The as-pressed properties were significantly improved over those of the previous  $Ni-Al_2O_3$  composites; however, the post-treat cycle at  $2400^\circ F$  increased porosity and reduced strength. The  $TiO_2$  additions were attributed with improving the strength and reducing the porosity in the as-pressed specimens.

Additions of tungsten to the metal phase were evaluated as a means of further improving strength by solid solution and reducing the thermal expansion of nickel to produce a closer expansion match with  $Al_2O_3$ . Specimens of a  $Ni \cdot 20W-Al_2O_3 \cdot 1/4TiO_2$  composite were hot-pressed for 1 hour at  $2350^\circ F$  and 4.5-ksi pressure. The results are shown in Table XXXVI.

**TABLE XXXVI**  
**FLEXURAL PROPERTIES OF Ni · 20W-Al<sub>2</sub>O<sub>3</sub> · 1/4TiO<sub>2</sub> COMPOSITES**

Condition	FYS, ksi	UFS, ksi	Deflection, in.	Apparent Porosity, %
As Pressed	62.0	78.0	0.012	1.6
Post Treated*	47.1	55.6	0.009	5.6
As Pressed	55.5	74.3	0.018	0.6
Post Treated*	53.4	61.3	0.011	6.0
As Pressed	66.7	77.2	0.019	0.8
Post Treated*	54.0	65.6	0.011	5.8

\*69-hour cycle at 2400°F (Figure 23).

Flexural strengths that approached 80 ksi were reached with as-pressed specimens. Post-treating, however, again increased ceramic porosity and reduced strength.

Oxidation Resistance - The oxidation resistance of several preliminary compositions prepared previously was also evaluated. The oxidation tests were conducted on rectangular specimens, measuring 0.4 x 0.1 x 1.0 inch, at 2200°F in static air. The test results are given in Table XXXVII.

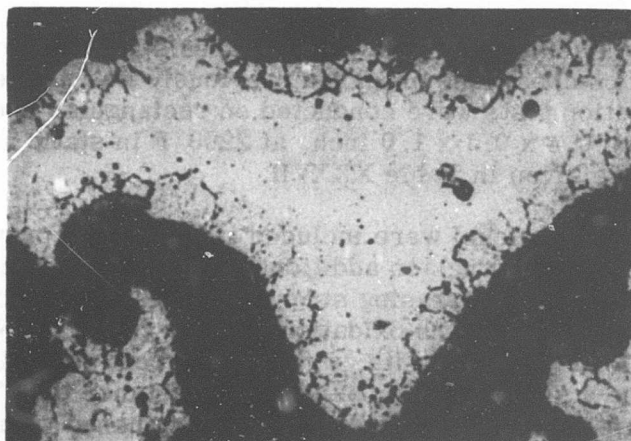
Samples of TD nickel were included in the test to provide a basis of comparison. Tungsten additions to the Ni-Al<sub>2</sub>O<sub>3</sub> composite were effective in increasing strength as previously noted, but appreciably reduced the oxidation resistance. The (Ni · 2ThO<sub>2</sub>)-Al<sub>2</sub>O<sub>3</sub> · 1/4TiO<sub>2</sub> composite, while 50-percent ceramic by volume, showed only slightly better oxidation resistance than TD nickel; i. e., high-purity nickel dispersion strengthened with ThO<sub>2</sub>.

On subsequent metallographic evaluation, it was apparent that subsurface oxidation of the metal was occurring as the result of porosity either in the ceramic phase or along the metal-ceramic interface.

TABLE XXXVII  
 OXIDATION RESISTANCE OF Ni-Al<sub>2</sub>O<sub>3</sub> COMPOSITES

Composite	Weight Gain by Oxidation at 2200°F, mg/cm <sup>2</sup>	
	24 hours	72 hours
(Ni · 2ThO <sub>2</sub> )-Al <sub>2</sub> O <sub>3</sub> · 1/4TiO <sub>2</sub>	14.0	27.8
Ni · 13Cr · 0.7ThO <sub>2</sub> -Al <sub>2</sub> O <sub>3</sub>	0.7	1.3
Ni · 20W-Al <sub>2</sub> O <sub>3</sub> · 1/4TiO <sub>2</sub>	31.9	63.3
TD Nickel	18.0	29.0

An example of subsurface metal oxidation is shown in Figure 40. The area shown in the micrograph was near the surface of a (Ni · 2ThO<sub>2</sub>)-Al<sub>2</sub>O<sub>3</sub> · 1/4TiO<sub>2</sub> composite after oxidation testing. Intergranular oxidation of the metal phase had occurred adjacent to the ceramic phase.



Unetched

1000X

Figure 40. Subsurface Oxidation in Metal Phase

The addition of chromium to the metal phase had a very pronounced improvement in oxidation resistance to the Ni-Al<sub>2</sub>O<sub>3</sub> system. Consequently, the addition of chromium to the nickel phase and the addition of sintering aids to the ceramic phase to improve strength were selected for further evaluation in the Ni-Al<sub>2</sub>O<sub>3</sub> system, as discussed in the next section.

### 3.3.2 Compositional Development

Based on the results of the initial studies, subsequent work on the Ni-Al<sub>2</sub>O<sub>3</sub> composite system was oriented toward the evaluation of compositions with chromium additions for oxidation resistance and sintering-aid additions for ceramic porosity reduction. The best composites and processes defined from this work were used for specimens in the metal-ceramic ratio study described in Section 3.3.3.

Chromium Additions - A Ni · 17Cr-Al<sub>2</sub>O<sub>3</sub> composite was selected for evaluating alternate means of introducing chromium into the metal phase and for evaluating processing variables related to the removal of the organic binder prior to hot-pressing.

The metal phase was prepared using elemental chromium powder (Electro Metallurgical Co. - electronic grade) and 80Ni - 20Cr alloy powder as the sources of chromium. In each case, type 255 carbonyl-nickel powder was used for the balance of the metal phase. Linde-A 0.3 micron Al<sub>2</sub>O<sub>3</sub> was used for the ceramic phase. Organic burnout cycles at 1100° F for 3 hours in either vacuum (200-300 microns) or hydrogen were used prior to hot-pressing. Flexural specimens were hot-pressed at 2350° F for 1 hour at 4.5-ksi pressure and post-treated at 2400° F using the 69-hour cycle described in Figure 23. Tests results are given in Table XXXVIII.

The data from the flexural and oxidation tests indicate that the best results were produced by using nickel-chromium alloy powder for the metal phase and conducting the organic burnout in vacuum.

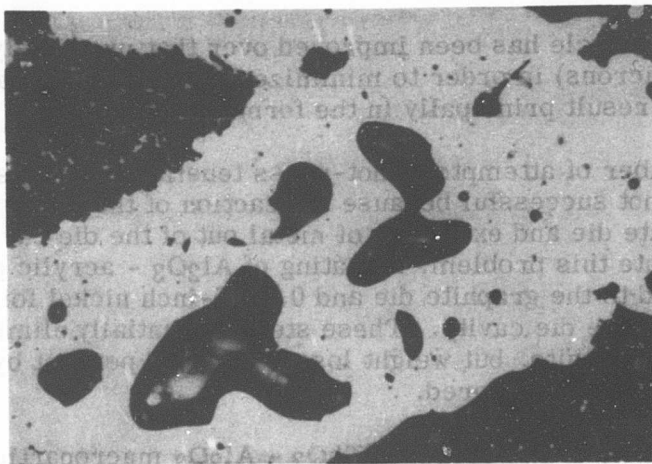
The large drop in properties noted for post-treated specimens made with elemental powders was believed to be the result of an excessive quantity of chromium oxide being formed during the organic decomposition cycle. Carbon analyses made on hot-pressed specimens fabricated with alloy powder showed a 0.28-percent and a 0.33-percent carbon content for the vacuum and

TABLE XXXVIII  
FLEXURAL PROPERTIES OF Ni · 17 Cr - Al<sub>2</sub>O<sub>3</sub> COMPOSITES

Chromium Source	Organic Burnout Atmosphere	Condition	UFS, ksi	Apparent Porosity, %	Weight Gain, 100 Hours at 2300°F mg/cm <sup>2</sup>
Alloy	Vacuum	As Pressed	58.7	0.3	3.8
Alloy	Vacuum	As Pressed	54.3	0.3	-
Alloy	Vacuum	Post Treated	65.2	3.4	-
Alloy	H <sub>2</sub>	As Pressed	58.6	0.4	4.2
Alloy	H <sub>2</sub>	As Pressed	60.9	0.3	-
Alloy	H <sub>2</sub>	Post Treated	54.5	7.2	-
Elemental	Vacuum	As Pressed	52.3	8.4	33.5
Elemental	Vacuum	As Pressed	54.9	10.3	-
Elemental	Vacuum	Post Treated	25.3	19.9	-
Elemental	H <sub>2</sub>	As Pressed	64.3	0.8	6.8
Elemental	H <sub>2</sub>	As Pressed	67.0	0.4	-
Elemental	H <sub>2</sub>	Post Treated	47.5	9.0	-

hydrogen organic decomposition cycles, respectively. Carbon contents this high are undesirable because they lower the melting point of the metal phase and could result in increased porosity by participating in gaseous reactions.

A metallographic evaluation of specimens from the Ni-Al<sub>2</sub>O<sub>3</sub> composite system showed a relatively large amount of nonmetallic material present in the nickel metal phase. The micrograph in Figure 41 shows inclusions that were found in a Ni · 13Cr · 0.7ThO<sub>2</sub> - Al<sub>2</sub>O<sub>3</sub> composite specimen. The transparent and globular nature suggests that the inclusions were molten during the hot-press cycle. Microprobe analysis of the inclusions showed that they were rich in silicon and aluminum contents, indicating the presence of SiO<sub>2</sub> and Al<sub>2</sub>O<sub>3</sub>. This contamination was attributed to the ball-milling operation performed to mix the acrylic binder with the metal and ceramic powders, and reflected wear that occurred on the porcelain container.



Unetched 500X  
Figure 41. Nonmetallic Inclusions in Metal Phase.

To prevent contamination during ball-milling, a polyethylene liner was installed in the container and was subsequently used for the preparation of all metal and ceramic phase paints. A thermal gravimetric analysis performed on the polyethylene material indicated that no residue resulted from its decomposition, so that any wear which occurred on the polyethylene liner would not result in contamination of the material.

A number of specimens of the Ni-Al<sub>2</sub>O<sub>3</sub> composite system also showed the presence of metallic particles in the ceramic phase similar to those shown in Figure 41. An accurate microprobe analysis was not possible because of the small size of the particles and the fact that they were contained in a nonconductive matrix. However, the presence of nickel in the ceramic phase was indicated, which would suggest that some mixing was occurring during preparation of the laminate sheet, or that metal was infiltrating the ceramic phase during hot-pressing. The effects of very small metal particles in the Al<sub>2</sub>O<sub>3</sub> phase were not known. However, massive infiltration of the ceramic phase by metal was subsequently shown to have an undesirable effect on thermal fatigue life.

Following the previous evaluation of Ni · 17Cr - Al<sub>2</sub>O<sub>3</sub> composites, as shown in Table XXXVIII, additional test specimens of this composition were prepared using alloy powder for the metal phase. Polyethylene-lined containers were used to prepare the metal and ceramic phase paints. The organic binder was decomposed in vacuum (0.1 micron) at 1100°F for 3 hours. The vacuum in the

burnout cycle has been improved over that previously used (200 to 300 microns) in order to minimize metal phase oxidation, which would result principally in the formation of  $\text{Cr}_2\text{O}_3$ .

A number of attempts to hot-press tensile bar blanks at  $2350^\circ\text{F}$  were not successful because of reaction of the metal with the graphite die and extrusion of metal out of the die cavity. To alleviate this problem, a coating of  $\text{Al}_2\text{O}_3$  - acrylic paint was applied to the graphite die and 0.0015-inch nickel foil liners were used in the die cavity. These steps essentially eliminated attack on the graphite, but weight losses up to 12 percent by extrusion were still encountered.

A quantity of  $\text{Ni} \cdot 17\text{Cr} \cdot 2\text{ThO}_2 - \text{Al}_2\text{O}_3$  macroparticles was prepared and hot-pressed using processing procedures similar to those described above. It was felt that the  $\text{ThO}_2$  addition to the metal phase would improve hot-pressing by retarding the tendency of the metal phase to extrude out of the die cavity. Some extrusion of metal did occur, however, during hot-pressing at  $2350^\circ\text{F}$ . The only significant factor that appeared relevant to the hot-pressing behavior of the above materials was the effort made to reduce  $\text{SiO}_2$  and  $\text{Cr}_2\text{O}_3$  contamination during preparation of the macroparticles. The presence of these contaminants could have the effect of acting as sintering aids for the ceramic phase. It was felt that improved sintering of the ceramic phase would reduce the metal phase extrusion being experienced during hot-pressing.

In an effort to verify the significance of oxide contamination in improving hot-pressing, the remaining macroparticles that had been prepared for the  $\text{Ni} \cdot 17\text{Cr} - \text{Al}_2\text{O}_3$  and  $\text{Ni} \cdot 17\text{Cr} \cdot 2\text{ThO}_2 - \text{Al}_2\text{O}_3$  composites were preheated in air at  $1000^\circ\text{F}$  for 5 minutes prior to hot-pressing. Specimens of these materials were hot-pressed without extrusion at  $2350^\circ\text{F}$  for 1 hour using a pressure of 4 ksi. However, elevated temperature tensile and thermal-fatigue properties of these specimens were relatively low, as shown in Table XXXIX.

As the data indicate, the  $\text{Ni} \cdot 17\text{Cr} \cdot 2\text{ThO}_2 - \text{Al}_2\text{O}_3$  composite, compared to the other composite, had very low resistance to thermal fatigue. Cracking occurred on the edge of the hot zone, and would be more correctly termed a thermal-shock failure. As previously described in Section 3.2.8, this type of cracking results from the inability of the material to accommodate local thermal strains. Metallographic evaluation of the  $\text{Ni} \cdot 17\text{Cr} \cdot 2\text{ThO}_2 - \text{Al}_2\text{O}_3$  specimens showed that the ceramic phase was heavily infiltrated

TABLE XXXIX  
ELEVATED TEMPERATURE PROPERTIES OF MACROLAMINATE  
COMPOSITES WITH CHROMIUM ADDITIONS

Composition	Test Temperature, °F	3 UTS, psi	Thermal 1 Fatigue No. Cycles to Failure	Apparent Porosity, %
Ni · 17Cr-Al <sub>2</sub> O <sub>3</sub>	1800°F	7,050	-	4.5
Ni · 17Cr-Al <sub>2</sub> O <sub>3</sub>	2200°F	630	-	8.8
Ni · 17Cr-Al <sub>2</sub> O <sub>3</sub>	-	-	375	5.8
Ni · 17Cr-Al <sub>2</sub> O <sub>3</sub>	-	-	222	5.8
Ni · 17Cr · 2ThO <sub>2</sub> -Al <sub>2</sub> O <sub>3</sub>	1800°F	6,800	-	3.9
Ni · 17Cr · 2ThO <sub>2</sub> -Al <sub>2</sub> O <sub>3</sub>	2200°F	700 2	-	-
Ni · 17Cr · 2ThO <sub>2</sub> -Al <sub>2</sub> O <sub>3</sub>	-	-	6	0.2
Ni · 17Cr · 2ThO <sub>2</sub> -Al <sub>2</sub> O <sub>3</sub>	-	-	20	0.2

1 300°- 2300°F cycle.      2 Failed in grip.      3 No yield point reached.

by metal, whereas the Ni · 17Cr-Al<sub>2</sub>O<sub>3</sub> composite showed a more normal laminate structure. Figure 42 shows that metal infiltration of the ceramic phase had resulted in almost complete mixing of the phases of the Ni · 17Cr · 2ThO<sub>2</sub>-Al<sub>2</sub>O<sub>3</sub> composite. The low thermal-fatigue properties were attributed to this mixing.

Sintering Aid - Concurrent with the previous evaluation of chromium additions, a second study was conducted to evaluate sintering aids for Al<sub>2</sub>O<sub>3</sub>. Jones (Reference 5) had reported that in addition to TiO<sub>2</sub>, oxides of manganese were found to be effective for sintering Al<sub>2</sub>O<sub>3</sub>. It also was reported that their behavior was influenced by the sintering atmosphere, with nitrogen being more effective than hydrogen.

In this study, additions of MnO<sub>2</sub>, Mn<sub>2</sub>O<sub>3</sub> and TiO<sub>2</sub> were made to the ceramic phase of Ni · Al<sub>2</sub>O<sub>3</sub> and Ni · 2ThO<sub>2</sub>-Al<sub>2</sub>O<sub>3</sub> composites. Mond type 255 nickel powder was used for the metal phase and



Figure 42. Metal Infiltration in a  
 $\text{Ni} \cdot 17\text{Cr} \cdot 2\text{ThO}_2\text{-Al}_2\text{O}_3$   
Composite.

Linde-A 0.3 micron  $\text{Al}_2\text{O}_3$  was used for the ceramic phase. Cabbot's P-25  $\text{TiO}_2$  and reagent grades  $\text{MnO}_2$  and  $\text{Mn}_2\text{O}_3$  were used for the additives. The P-25  $\text{TiO}_2$  had a very fine particle size (0.04 micron) which would tend to provide a better distribution of  $\text{TiO}_2$  in the 0.3 micron  $\text{Al}_2\text{O}_3$  than was obtained previously with the coarser reagent grade  $\text{TiO}_2$ . Polyethylene-lined containers were used for ball-milling operations.

Prior to hot-pressing, the organic binder was decomposed in vacuum at  $1100^\circ\text{F}$  for 3 hours. All specimens were hot-pressed at  $2350^\circ\text{F}$  for 1 hour using a pressure of 4.5 ksi. Following hot-pressing, 69-hour post-treatment cycles at  $2400^\circ\text{F}$  were conducted in either nitrogen or hydrogen. Flexural properties of these composites are shown in Table XL.

The  $(\text{Ni} \cdot 2\text{ThO}_2)\text{-Al}_2\text{O}_3 \cdot 0.25\text{TiO}_2$  composite showed the best overall strength, and on this basis the Cabbot's P-25  $\text{TiO}_2$  was selected for use in subsequent composite test specimens. In all but two instances, post-treating at  $2400^\circ\text{F}$  reduced flexural strength; in all instances, post-treating increased apparent porosity. As described in Section 3.2.8, improvements in flexural properties had been obtained with composites of the Ni-MgO system by using an  $1850^\circ\text{F}$  post-treat cycle. The purpose of the  $1850^\circ\text{F}$  post-treat cycle was to relieve internal stresses from hot-pressing and also to permit some outgassing of entrapped gases. In view of the

TABLE XL  
EFFECT OF SINTERING AIDS ON FLEXURAL PROPERTIES

Composition	Condition	UFS, ksi	Apparent Porosity, %	Wt. Gain Apparent by Oxi- dation, mg/cm <sup>2</sup> *
(Ni · 2ThO <sub>2</sub> )-Al <sub>2</sub> O <sub>3</sub> · 0.25TiO <sub>2</sub>	As Pressed	72.2	0.6	-
	Post-Treated-N <sub>2</sub>	67.4	6.8	37.3
	Post-Treated-H <sub>2</sub>	68.7	4.5	33.2
(Ni · 2ThO <sub>2</sub> )-Al <sub>2</sub> O <sub>3</sub> · 0.24MnO <sub>2</sub>	As Pressed	64.9	0.9	-
	Post-Treated-N <sub>2</sub>	48.8	5.6	-
	Post-Treated-H <sub>2</sub>	42.5	8.9	35.7
(Ni · 2ThO <sub>2</sub> )-Al <sub>2</sub> O <sub>3</sub> · 0.27Mn <sub>2</sub> O <sub>3</sub>	As Pressed	71.1	0.1	-
	Post-Treated-N <sub>2</sub>	53.2	5.8	32.6
	Post-Treated-H <sub>2</sub>	58.6	5.2	31.8
Ni-Al <sub>2</sub> O <sub>3</sub> · 0.25TiO <sub>2</sub>	As Pressed	50.9	0.3	-
	Post-Treated-N <sub>2</sub>	54.2	4.2	38.9
	Post-Treated-H <sub>2</sub>	69.8	3.2	38.1
Ni-Al <sub>2</sub> O <sub>3</sub> · 0.24MnO <sub>2</sub>	As Pressed	57.8	2.4	-
	Post-Treated-N <sub>2</sub>	37.3	9.7	44.8
	Post-Treated-H <sub>2</sub>	58.6	9.9	41.5
Ni-Al <sub>2</sub> O <sub>3</sub> · 0.27Mn <sub>2</sub> O <sub>3</sub>	As Pressed	56.6	1.9	-
	Post-Treated-N <sub>2</sub>	53.6	5.5	35.2
	Post-Treated-H <sub>2</sub>	51.8	3.3	33.1

\*100 hours at 2300°F

inability of the 2400°F post-treat cycle to effect further sintering and reduce porosity, subsequent post-treating was accomplished using the 1850°F post-treat cycle described in Figure 31.

Following the above flexural tests, several (Ni · 2ThO<sub>2</sub>) - Al<sub>2</sub>O<sub>3</sub> · 1/4TiO<sub>2</sub> specimens were hot-pressed for elevated temperature tensile tests and thermal-fatigue tests. The purpose of these tests was to provide comparison data for the metal-ceramic ratio tests which subsequently were conducted for the Ni · 17Cr-Al<sub>2</sub>O<sub>3</sub> · 1/4TiO<sub>2</sub> composite.

The specimens were prepared using Mond type 255 nickel powder for the metal phase, with ThO<sub>2</sub> added by decomposition of reagent grade thorium nitrate as described previously. Linde-A 0.3 micron Al<sub>2</sub>O<sub>3</sub> and Cabbot's P-25TiO<sub>2</sub> were used for the ceramic phase. The organic binder was decomposed in vacuum at 1100°F for 3 hours, and hot-pressing was accomplished at 2350°F for 1 hour, using a double-acting suspended die and a pressure of 4.5 ksi. The specimens were post-treated at 1850°F using the cycle described previously in Figure 31. Properties obtained on these specimens are given in Table XLI.

The tensile properties at 1800°F were the highest obtained for macrolaminate composites in this program. The relatively high apparent porosity of the tensile specimens reflects the larger volume of the hot-pressed tensile blanks; the smaller flexural test specimens generally showed less porosity. The thermal-fatigue specimens successfully withstood 500 cycles without any evidence of the cracking, erosion or bowing that was observed with the (Ni · 2ThO<sub>2</sub>) · 2TiN- (MgO · 5HfO<sub>2</sub>) thermal-fatigue specimens shown in Figure 36.

### 3.3.3 Metal-Ceramic Ratio Study

From the results of work conducted previously on the Ni-Al<sub>2</sub>O<sub>3</sub> system, a Ni · 17Cr-Al<sub>2</sub>O<sub>3</sub> · 1/4TiO<sub>2</sub> composite was selected for evaluation with various metal-ceramic ratios. As previously described in Section 3.2.8 for the Ni-MgO system, the metal-ceramic ratio study involved tensile, oxidation, and thermal-fatigue testing to evaluate the suitability of the material for nozzle vane application.

TABLE XLI  
ELEVATED TEMPERATURE PROPERTIES OF  
(Ni · 2ThO<sub>2</sub>)-Al<sub>2</sub>O<sub>3</sub> · 1/4TiO<sub>2</sub> COMPOSITES

Test Temperature, °F	UTS, psi	Thermal-Fatigue 300°-2300°F Cycle, No. Cycles to Failure	Apparent Porosity, %
1800°F	15,230	-	12.0
1800°F	15,790	-	11.7
1800°F	15,540	-	11.2
1800°F	18,860	-	9.7
1800°F	13,800	-	10.7
1800°F	10,800	-	12.7
1800°F	14,700	-	5.8
1800°F	10,500	-	8.1
2200°F	5,500	-	4.9
2200°F	5,100	-	9.6
-	-	500*	9.7
-	-	512*	5.3
-	-	512*	3.0

\*Test terminated - no failure.

The Ni · 17Cr metal phase used proportional amounts of 80Ni-20Cr alloy powder and Mond type 255 carbonyl-nickel powder. Linde-A 0.3 micron Al<sub>2</sub>O<sub>3</sub> with a 0.25-percent addition of Cabbot's P-25 TiO<sub>2</sub> was used for the ceramic phase. In both cases, mixing was accomplished by ball-milling in polyethylene-lined containers while preparing the acrylic-base paints. Laminate sheets with metal-ceramic ratios of 70:30, 50:50, and 30:70 were prepared using draw-knife techniques described in Section 3.2.7.

Prior to hot-pressing, the organic binder was decomposed by heating in vacuum at 1100°F for 3 hours. This was followed by heating in air at 1000°F for 5 minutes. Macroparticles were pre-pressed at room temperature in graphite dies with a pressure of 3 ksi. All specimens were hot-pressed using a double-acting suspended die at 2350°F for 1 hour with a maximum pressure of 4 ksi. The pressure was not applied until 10 minutes after reaching a temperature of 2350°F, to allow some consolidation of the ceramic phase and thereby reduce the tendency of the metal phase to infiltrate the ceramic phase. Following hot-pressing, the specimens were post-treated at 1850°F using the cycle previously described in Figure 31.

Flexural Tests - Room temperature flexural properties increased significantly with increasing metal content, as shown in Figure 43. The post-treat cycle at 1850°F was effective in improving the flexural strength of all composites.

Subsequent metallographic evaluation showed that the chromium additions resulted in increased porosity along the metal-ceramic interface.

Oxidation Tests - Static oxidation tests at 2300°F in air were conducted for 24- and 100-hour durations. The data, plotted in Figure 44, show that the composite with the lowest metal content had the highest weight gain resulting from oxidation. While these data show a different trend than that shown for the Ni-MgO system in Figure 33, further evaluation indicated that it was still the result of subsurface oxidation.

Metallographic evaluation of Ni · 17Cr-Al<sub>2</sub>O<sub>3</sub> · 1/4TiO<sub>2</sub> composites indicated that the ceramic phase of the 30-volume-percent metal composites was very porous by comparison with the composites with higher metal contents. It also was observed that there was relatively little metal infiltration in the ceramic phase of the 30-volume-percent metal composites.

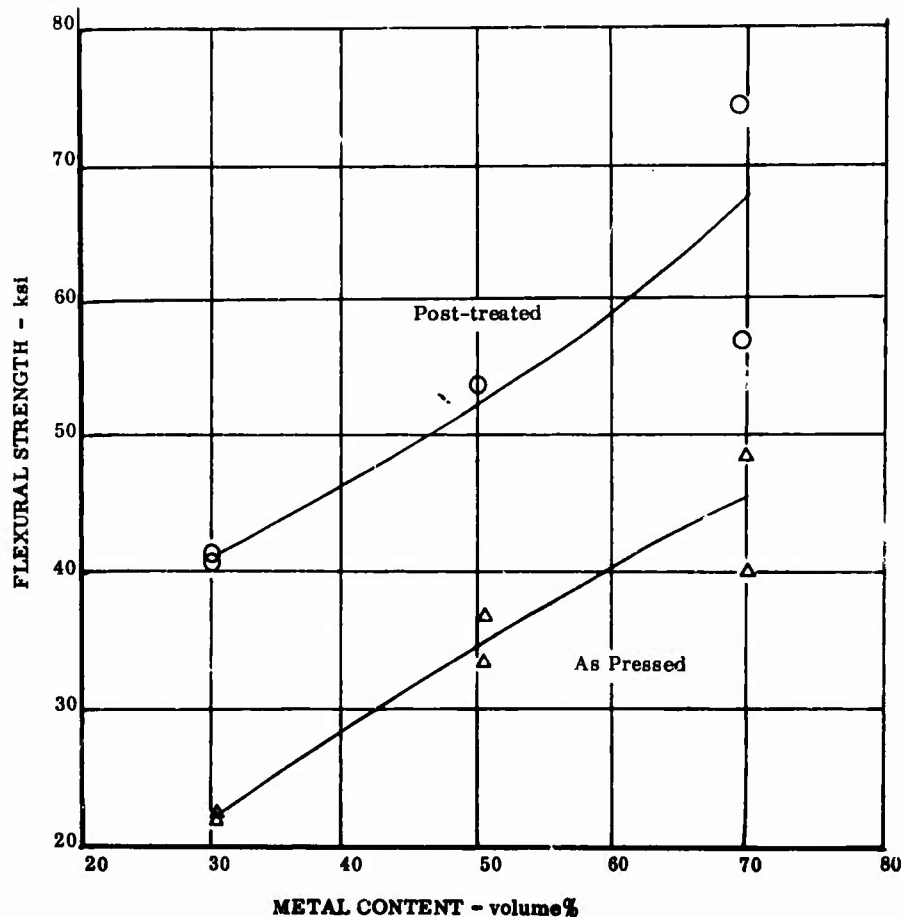


Figure 43. Flexural Strength Versus Metal Content for Ni · 17Cr-Al<sub>2</sub>O<sub>3</sub> · 1/4TiO<sub>2</sub> Composites.

These factors suggest that bridging between the ceramic platelets was occurring during hot-pressing. This bridging action could prevent a uniform application of pressure, and would explain the absence of metal infiltration of the ceramic phase. Porosity in the 50- and 30-volume-percent metal composites was observed predominantly along the metal-ceramic interface. Typical examples of porosity in composites with 30- and 70-volume-percent metal contents are shown in Figure 45. This interface porosity is attributed to the presence of the 17-percent chromium

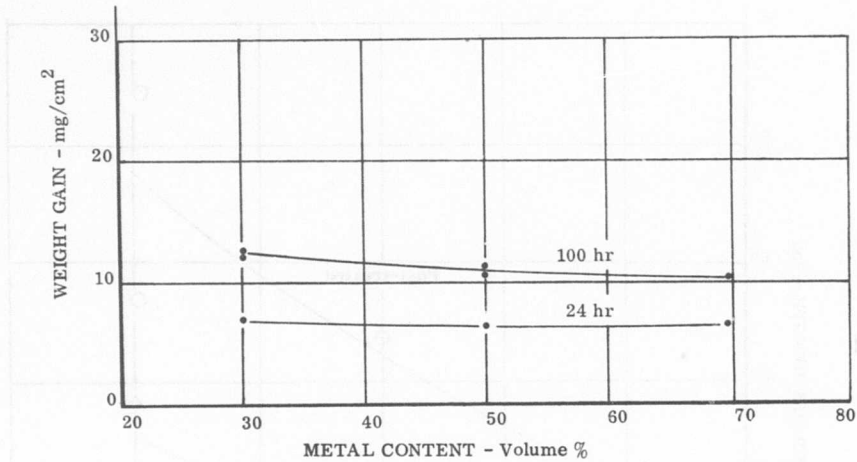
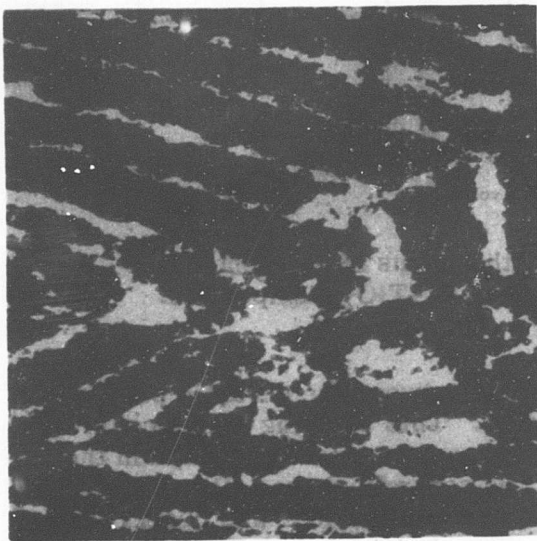
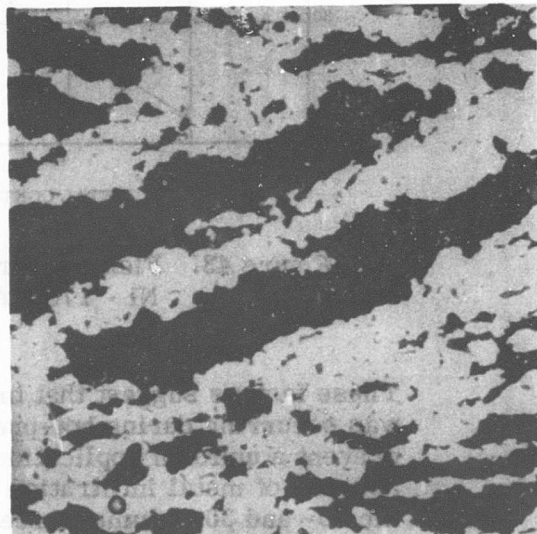


Figure 44. Oxidation Resistance at 2300°F Versus Metal Content for Ni · 17Cr-Al<sub>2</sub>O<sub>3</sub> · 1/4TiO<sub>2</sub> Composites.



Unetched 30 Volume % Metal 200X



Unetched 70 Volume % Metal 200X

Figure 45. Variations in Porosity in Ni · 17Cr-Al<sub>2</sub>O<sub>3</sub> · 1/4TiO<sub>2</sub> Composites.

addition to the metal phase. By comparison, no porosity is evident at the interface of the composite without chromium shown in Figure 46. This composite specimen had an apparent porosity of 5.3 percent and was thermal-fatigue-tested to 512 cycles without failure (See Table XLI).

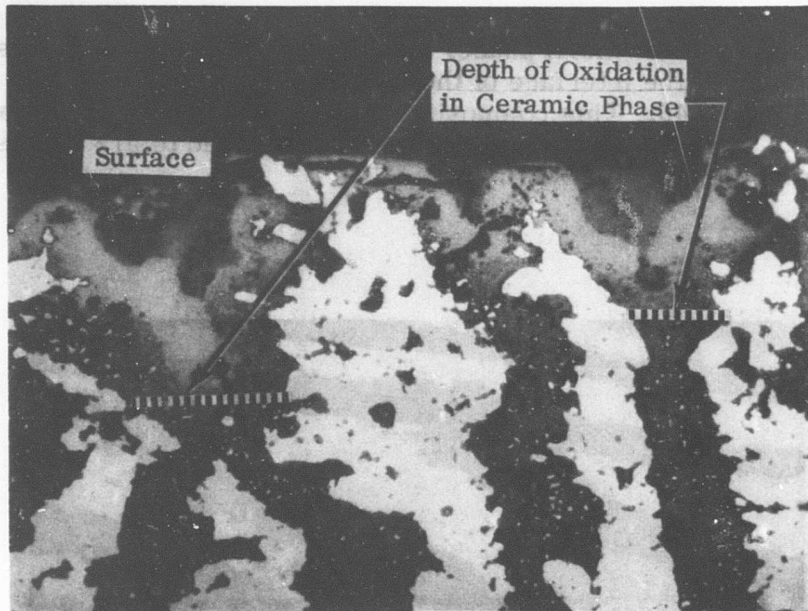


Unetched

400X

Figure 46. Microstructure of a  $(\text{Ni} \cdot 2\text{ThO}_2)$   
 $-\text{Al}_2\text{O}_3 \cdot 1/4\text{TiO}_2$  Composite.

Oxidation in the  $\text{Ni} \cdot 17\text{Cr}-\text{Al}_2\text{O}_3 \cdot 1/4\text{TiO}_2$  composites progressed in a slightly different manner for each of the metal-ceramic ratios. For the 70-volume-percent metal composite, metal particles that infiltrated the ceramic during hot-pressing were oxidized to a greater depth than the adjacent metal lamellae. The depth to which the small metal particles were oxidized in the ceramic phase is illustrated by arrows in Figure 47. Oxidation of the infiltrated metal particles increased the porosity of the ceramic phase, after which oxidation appeared to progress to the adjacent metal lamellae.



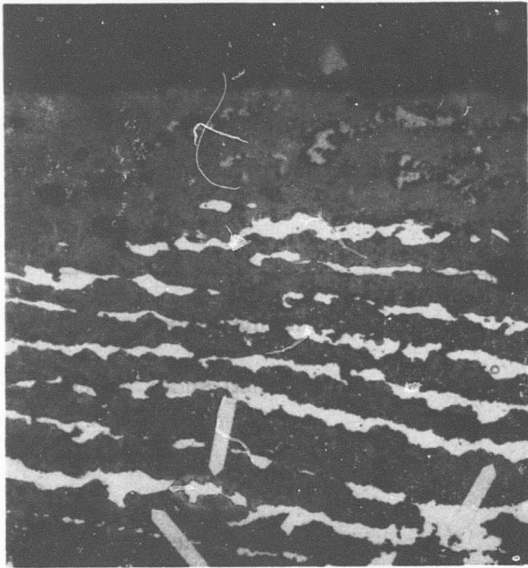
Unetched 400X

Figure 47. Oxidation in a 70-Volume-Percent Metal Composite After 100 Hours at 2300°F.

Evidence of oxidation by the diffusion of oxygen along metal-ceramic interfaces generally was not evident in the above example. In all samples evaluated, oxidation of the metal phase was characterized by a blue-green coloration of the  $\text{Al}_2\text{O}_3$  lamellae. This coloration was readily apparent under polarized light.

In the 50-volume-percent metal composites, evidence of oxidation by diffusion of oxygen along metal-ceramic interfaces was apparent in many areas. These samples tended to show more porosity along the metal-ceramic interfaces than the 70-volume-percent metal composites.

An example of subsurface oxidation that appeared to have occurred along metal-ceramic interfaces is shown in Figure 48. Arrows on bright field and polarized light micrographs of the same area indicate subsurface oxidation in a 50-volume-percent metal composite.



Bright Field



Polarized Light

Unetched

200X

Figure 48. Subsurface Oxidation in a 50-Volume-Percent Metal Composite After 100 Hours at 2300°F.

The overall oxidation resistance of the  $\text{Ni} \cdot 17\text{Cr}-\text{Al}_2\text{O}_3 \cdot 1/4\text{TiO}_2$  composites was improved over the oxidation resistance of the Ni-MgO system by a factor of about five. However, in view of the porosity that was evident in the  $\text{Al}_2\text{O}_3$  ceramic, it was apparent that the oxidation resistance potential of the  $\text{Ni} \cdot 17\text{Cr}-\text{Al}_2\text{O}_3 \cdot 1/4\text{TiO}_2$  composites was not realized.

Thermal-Fatigue Tests - Thermal-fatigue tests, using a 300° to 2300°F thermal cycle, were conducted using procedures previously described in Section 2.3. The number of cycles required to produce failure for the various metal-ceramic ratios is shown in Table XLII.

All of the specimens cracked before reaching the minimum number of 500 cycles established for this test. The specimens with low metal contents showed thermal-shock cracks on the edge of the hot zone similar to the results noted previously for the low-metal-content specimens of the Ni-MgO system (Table XXXI). The thermal-shock crack noted on the 50:50 metal-ceramic specimen

**TABLE XLII**  
**THERMAL-FATIGUE RESULTS OF**  
**Ni · 17Cr-Al<sub>2</sub>O<sub>3</sub> · 1/4TiO<sub>2</sub> COMPOSITES**

Metal Content, Volume %	Cycles to Failure	Remarks
30	4	Thermal-shock crack
30	4	Thermal-shock crack
50	166	-
50	6	Thermal-shock crack
70	182	1/32-inch bow
70	295	1/32-inch bow

was subsequently attributed to a tendency for this specimen to have mixed metal and ceramic phases. Metallographic evaluation of this specimen showed that there was some infiltration of the metal phase into the ceramic phase.

Tensile Tests - Tensile tests for the three metal-ceramic ratios of the Ni · 17Cr-Al<sub>2</sub>O<sub>3</sub> · 1/4TiO<sub>2</sub> composite were conducted at room temperature, 1800°, and 2200°F. A plot of the test results is given in Figure 49.

The 2200°F tensile data point for the 30-volume-percent metal composition was extrapolated from 1800°F and 2000°F data. The significant factor concerning the data in Figure 49 is that the metal-ceramic ratio had no effect on the tensile strength of the various specimens. In Figure 43, it was previously shown that the metal-ceramic ratio had a pronounced influence on room-temperature flexural strength. It can also be seen that the elevated temperature tensile strengths of these composites were only about one-half of those reported for the (Ni · 2ThO<sub>2</sub>)-Al<sub>2</sub>O<sub>3</sub> · 1/4TiO<sub>2</sub> composites in Table XLI. The low properties and the apparent lack of influence of the metal-ceramic ratio on overall strength are attributed primarily to the porosity that was prevalent at the metal-ceramic

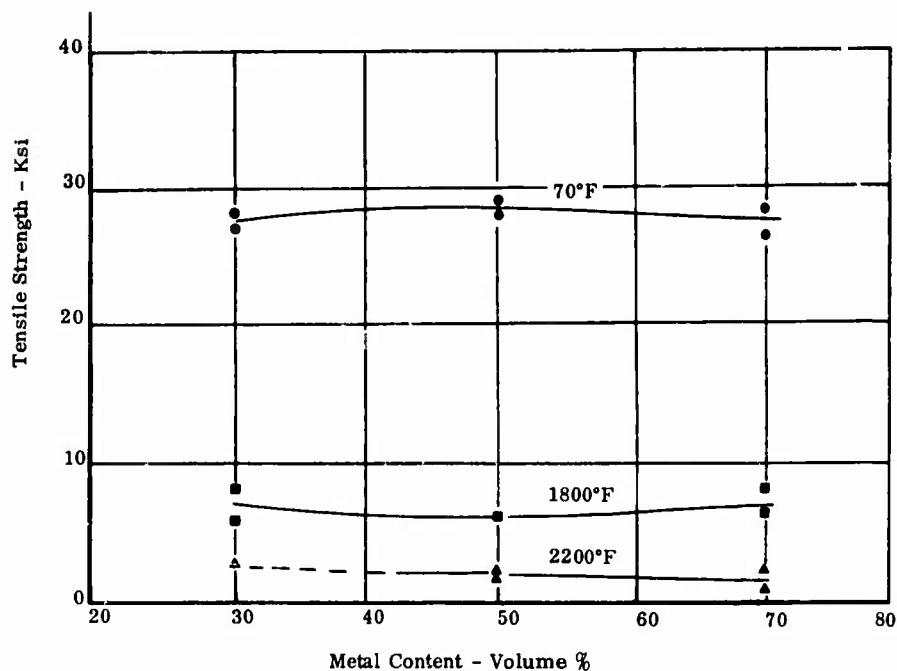


Figure 49. Tensile Strength Versus Metal Content for Ni · 17Cr-Al<sub>2</sub>O<sub>3</sub> · 1/4TiO<sub>2</sub> Composites.

interface of the Ni · 17Cr-Al<sub>2</sub>O<sub>3</sub> · 1/4TiO<sub>2</sub> composite specimens, as discussed previously. The difference between the tensile and flexural tests, with respect to the metal-ceramic ratio, can only be attributed to the influence of specimen size on hot-pressing. The larger cross-sectional area of the tensile specimen blanks, approximately four times that of the flexural test specimens, has the tendency to retain more porosity during hot-pressing.

Only three of the Ni · 17Cr-Al<sub>2</sub>O<sub>3</sub> · 1/4TiO<sub>2</sub> composites showed tensile yield points, and none of these showed tensile ductility of 1 percent or more. In contrast, several of the tensile tests for the Ni-MgO composite system, reported previously in Table XXXII, showed tensile yield points and tensile ductility in excess of 1 per-

A summary of the metal-ceramic ratio tensile and oxidation test data for the Ni · 17Cr-Al<sub>2</sub>O<sub>3</sub> · 1/4TiO<sub>2</sub> composites is given in Table XLIII.

**TABLE XLIII**  
**SUMMARY OF Ni · 17Cr - Al<sub>2</sub>O<sub>3</sub> · 1/4TiO<sub>2</sub> COMPOSITE TEST**  
**DATA FOR VARIOUS METAL-CERAMIC RATIOS**

Test Temperature, °F	0.2% YS, psi	UTS, psi	Elongation, %	Density, gm/cc	Apparent Porosity, %	Weight Gain Due to Oxidation, mg/cm <sup>2</sup>
<u>Metal Content - 30 Volume %</u>						
-	-	-	-	4.98	1.0	12.7
-	-	-	-	5.22	0.6	12.2
70	2	27,400	0	5.13	1.2	-
70	2	28,300	0	5.34	0.4	-
1800	2	6,000	0	4.99	5.0	-
1800	2	8,200	0	5.06	3.4	-
2000	2	6,400	0	5.21	1.0	-
2000	2	4,900	0	5.16	1.3	-
<u>Metal Content - 50 Volume %</u>						
-	-	-	-	5.87	3.5	10.9
-	-	-	-	5.97	0.6	11.8
70	2	29,400	0	5.91	1.3	-
70	2	28,100	0	5.80	1.8	-
1800	2	6,200	0	5.84	3.3	-
2200	2,200	2,300	0.5	5.83	2.9	-
2200	2,000	2,000	0.5	5.79	4.2	-

TABLE XLIII (Continued)

Test Temperature, °F	0.2 % YS, psi	UTS, psi	Elongation, %	Density, gm/cc	Apparent Porosity, %	Weight Gain Due to Oxidation, mg/cm <sup>2</sup>
-	-	-	-	6.38	1.8	10.7
70	2	27,000	0	6.31	1.6	-
70	2	28,300	0	6.28	2.2	-
1800	2	8,300	0	6.18	3.9	-
1800	6,500	6,500	0.2	6.28	2.9	-
2200	2	1,000	0	-	-	-
2200	2,400	2,500	0.5	6.26	4.3	-

Metal Content - 70 Volume %

1 Exposed 100 hours at 2300°F.

2 Yield point not reached.

### 3.3.4 Summary of Ni-Al<sub>2</sub>O<sub>3</sub> Macrolaminate Composite Results

The main objectives of the work associated with the Ni-Al<sub>2</sub>O<sub>3</sub> composite system were to improve the strength, density, and oxidation resistance of this composite and then to evaluate its suitability as a high-temperature nozzle vane material. The studies conducted involved developing a suitable hot-pressing procedure, and included evaluations of chromium additions to the metal phase and sintering-aid additions to the ceramic phase. Based on this work, a composition was selected and a process defined for the preparation of specimens with various metal-ceramic ratios. Evaluation of these specimens included tensile, thermal-fatigue, and oxidation tests, and was similar to the type of evaluation conducted for the Ni-MgO composite system.

$\text{Al}_2\text{O}_3$  was selected for the ceramic phase because it was stronger than  $\text{MgO}$  and it offered a potential for high strength at elevated temperatures. As  $\text{Al}_2\text{O}_3$  is somewhat less compatible with nickel than  $\text{MgO}$ , specific attention was given to developing techniques to consolidate the composite. Initial work with the  $\text{Ni-Al}_2\text{O}_3$  composites involved the evaluation of hot-pressing temperatures and pressures that were higher than those used for  $\text{Ni-MgO}$ . Because of the limitations of hot-press die material and the softness of the metal phase at high temperatures, hot-pressing temperatures and pressures were limited to about  $2350^\circ\text{F}$  and 4 to 4.5 ksi, respectively. The use of  $\text{TiO}_2$  as a sintering aid for the ceramic phase resulted in reduced porosity and improved flexural strength.

Although apparent porosities were still higher than desired (10 to 12 percent), a  $(\text{Ni} \cdot 2\text{ThO}_2)\text{-Al}_2\text{O}_3 \cdot 1/4\text{TiO}_2$  composite showed tensile strengths of almost 19,000 psi at  $1800^\circ\text{F}$  and 5,500 psi at  $2200^\circ\text{F}$ . These figures represent approximately a twofold improvement in properties obtained from similar tests for  $\text{Ni-MgO}$  type composites. Thermal-fatigue resistance of the above  $\text{Ni-Al}_2\text{O}_3$  composite also was considered to be good; specimens withstood 500 thermal cycles ( $300^\circ\text{-}2300^\circ\text{F}$ ) without failure. However, the oxidation resistance of the  $(\text{Ni} \cdot 2\text{ThO}_2)\text{-Al}_2\text{O}_3 \cdot 1/4\text{TiO}_2$  composite was not considered adequate, even though it showed a 30-percent improvement over  $\text{Ni-MgO}$ . Weight gain resulting from oxidation was about  $35 \text{ mg/cm}^2$  after 100 hours at  $2300^\circ\text{F}$ . The improvement in oxidation resistance of the  $\text{Ni-Al}_2\text{O}_3$  composite is attributed to the formation of a  $\text{NiAl}_2\text{O}_4$  spinel on the surface during oxidation. The spinel is considered to be more protective than the solid-solution  $\text{NiO-MgO}$  scale formed during oxidation of a  $\text{Ni-MgO}$  composite.

To improve oxidation resistance, an evaluation was conducted on a series of  $\text{Ni-Al}_2\text{O}_3$  composites with chromium additions.  $\text{Ni-Cr}$  alloy powder was preferred over elemental  $\text{Ni}$  and  $\text{Cr}$  powders for the metal phase. The use of a sintering aid, i. e., a  $\text{TiO}_2$  addition to the ceramic phase, was also found to be very beneficial in the fabrication of  $\text{Ni-Al}_2\text{O}_3$  composites containing chromium.

Based on these results, a  $\text{Ni} \cdot 17\text{Cr-Al}_2\text{O}_3 \cdot 1/4\text{TiO}_2$  composite was selected for evaluation with metal-ceramic ratios of 70:30, 50:50 and 30:70, respectively. Tensile, thermal-fatigue and oxidation tests were conducted on specimens with each of the metal-ceramic ratios. At both room and elevated temperatures, the tensile strength was observed to be essentially independent of the metal-ceramic ratio. The tensile properties measured were low, with ultimate strengths of only 8300 psi and 2500 psi obtained

at 1800° and 2200°F, respectively. These properties were only about one-half of those obtained for the  $(\text{Ni} \cdot 2\text{ThO}_2)\text{-Al}_2\text{O}_3 \cdot 1/4\text{TiO}_2$  composites tested previously. Weight gain resulting from oxidation at 2300°F in still air ranged from 10.7 to 12.7 mg/cm<sup>2</sup>, with the low metal content specimens showing the lowest oxidation resistance. It was apparent from metallographic evaluation that a significant amount of subsurface oxidation was occurring as a result of porosity in the ceramic phase or along the metal-ceramic interface, particularly in the 70:30 and 50:50 metal-ceramic ratio specimens. This porosity also was believed to be the primary cause of the low tensile properties. For the thermal-fatigue tests (300° to 2300°F cycle), none of the specimens demonstrated adequate resistance to severe thermal cycles. Specimens with low metal content failed by thermal shock after only a few cycles because of insufficient ductility. Failure in specimens with higher metal content was attributed to low mechanical properties. In one instance, a breakdown of the laminate structure, caused by metal infiltrating the ceramic phase, resulted in early thermal-fatigue failure.

By comparison with the Ni-MgO type composites, Ni-Al<sub>2</sub>C<sub>3</sub> was inherently more difficult to sinter and had higher porosity as a result. This is due to the fact that Al<sub>2</sub>O<sub>3</sub> requires a hot-pressing temperature of about 2500°F to achieve high density compacts. Despite this disadvantage, Ni-Al<sub>2</sub>O<sub>3</sub> showed potential in achieving suitable strength levels. Chromium additions, while significantly improving oxidation resistance, had the adverse effect of increasing porosity at the metal-ceramic interface and reducing strength. It is considered possible that differential diffusion rates between constituents (Kirkendall effect) were contributing to the porosity at the metal-ceramic interface.

Test results indicate that the fabricating techniques employed were not suitable to demonstrate the properties potentially available in these composites. Processing techniques that would permit the fabrication of composites with low levels of porosity and fine macrolaminate structure (thinner lamellae and smaller macroparticle size) should produce significant improvements in properties. To define processes capable of producing these improvements, more basic research is required to evaluate diffusion effects, high-temperature reactions between constituents, and more advanced consolidation techniques. Examples of the latter that are considered feasible are hot-isostatic pressing and high-temperature extrusion. However, the results of this program indicate that melting point and reactivity of the constituents at elevated temperatures would eventually place a practical temperature limitation of about 2300°F

on any Ni-Al<sub>2</sub>O<sub>3</sub> composites that have chromium additions. These considerations would prevent application of this type of material in a nozzle vane for a 2300°F turbine inlet temperature because temperature excursions to at least 2500°F might be encountered in engine operation.

Subsequent research on this material system was conducted by the Boeing Company, Aerospace Division, under another contract. The results of this work are discussed in a separate report (Reference 16).

### 3.4 DISPERSION-STRENGTHENED NICKEL-BASE ALLOYS

The objective of this portion of the program was to conduct research leading to the development of an oxidation-resistant, dispersion-strengthened alloy suitable for turbine blade application. As discussed in Section 2.0, the primary object of this research was to develop, using thermal decomposition techniques, methods of producing alloys with low levels of oxygen contamination. Elevated temperature tests and a metallographic evaluation subsequently were conducted to determine the ability of these processing techniques to produce a suitable material.

#### 3.4.1 Preparation of Alloy Powders

Alloy powders composed of 80-percent Ni - 20-percent Cr and 72-percent Ni - 18-percent Cr - 10-percent Mo were used for the preparation of alloys. The alloy powders with a nominal particle size of 9 microns were furnished by Acieries de Gennevilliers, Paris, France. In view of the fine particle size requirements for effective dispersion strengthening, a grinding study was initiated with the 80Ni - 20 Cr powder. The grinding was conducted in an attrition mill consisting of a water-cooled, stationary, stainless-steel tank and a spiked shaft rotating at 250 to 300 rpm. The charge consisted of the powder to be ground, stainless-steel balls, and isopropyl alcohol as a grinding media to prevent welding of the particles. Following grinding, the powder was dried in a vacuum oven at 200°F.

Vacuum-fusion oxygen analyses were conducted on powders comminuted by this process. The oxygen content was observed to increase rapidly as the powder particle size was reduced, with the oxygen level increasing by a factor of four as the powder was comminuted from a 9-micron size to a 0.5-micron size. In an effort to determine if drying at 200°F was contributing to

the oxygen pickup, a batch of 0.5-micron powder was dried at ambient conditions and was found to have an appreciably lower oxygen content, as shown in Table XLIV.

**TABLE XLIV  
OXYGEN CONTENT OF GROUND POWDER**

Particle Size (Microns)	%Oxygen
9 (As Received)	0.18
4.8	0.20 (Vacuum Oven Dried at 200°F)
2.3	0.27 (Vacuum Oven Dried at 200°F)
1.2	0.37 (Vacuum Oven Dried at 200°F)
0.5	0.80 (Vacuum Oven Dried at 200°F)
0.5	0.47 (Ambient Air Dried)

#### **3.4.2 Thermal Decomposition Studies**

To reduce the level of oxygen contamination associated with the thermal decomposition process, studies were conducted using two approaches. The first of these studies involved thermal decomposition of thorium nitrate, and the second was directed toward evaluating the substitution of thorium organic salts for the thorium nitrate as the source of ThO<sub>2</sub>.

**Thorium Nitrate Studies** - The thermal decomposition of thorium nitrate was studied to define more closely the nature of the process. An X-ray diffraction analysis was conducted on the residue from pure thorium nitrate that had been thermally decomposed in vacuum. The results indicated the presence of thorium nitrate at temperatures up to 300°F, the presence of an amorphous phase (assumed to be hydrated thorium hydroxide and ThO<sub>2</sub> nuclei) at temperatures of 300° to 660°F, and the presence of thoria at temperatures greater than 660°F. The particle size of the thoria, as measured by X-ray line-broadening techniques, was a maximum of 0.03 micron for

1-hour decomposition cycles in vacuum, argon, or hydrogen atmospheres at temperatures up to 1500° F.

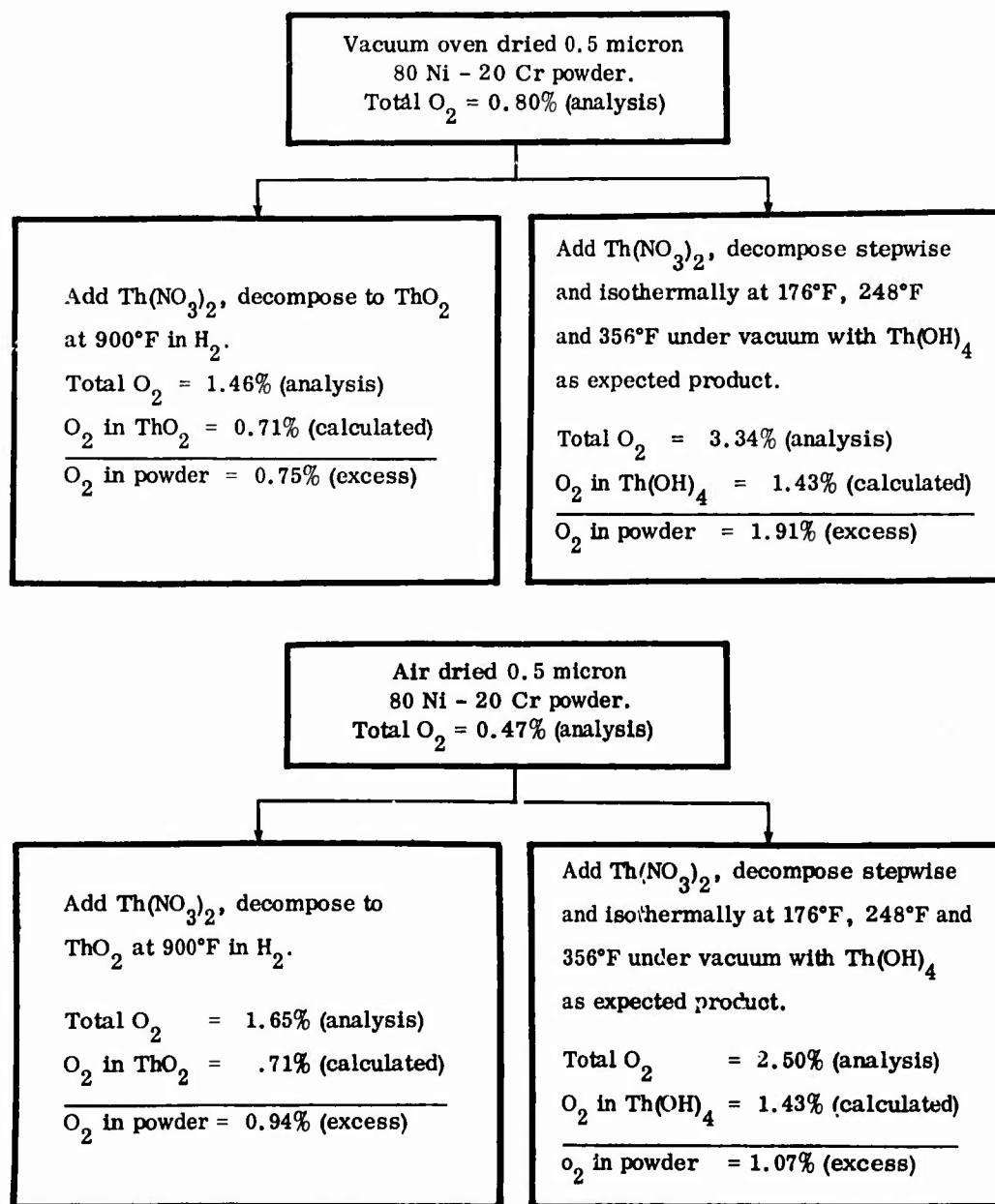
Since the thermodynamic rules of nucleation and growth processes indicate finer particle sizes with lower decomposition temperatures, the above observations indicated that a minimum temperature of 660° F would be necessary to produce ThO<sub>2</sub> of less than 0.03-micron particle size by the decomposition of thorium nitrate.

Thermal decomposition studies were next conducted using thorium nitrate and 80 Ni - 20 Cr alloy powder ground to a 0.5-micron particle size. A solution of isopropyl alcohol and thorium nitrate, in sufficient amounts to produce 5-volume-percent thoria on decomposition, was used to coat the alloy powder by mechanical mixing. Two thermal decomposition cycles were used and evaluated with respect to oxygen contamination produced during the cycle. The first cycle consisted of heating in hydrogen at 900° F for 1 hour, while the second was conducted in vacuum using a stepwise heating cycle. The latter cycle consisted of heating to 356° F in three 1-hour steps with intermediate isothermal steps at 176° and 248° F. Thorium hydroxide was the expected product of this cycle, and its conversion to ThO<sub>2</sub> would depend on a subsequent thermal cycle. Both cycles were conducted with oven-dried and air-dried powder as described previously.

Block diagrams depicting the processing cycles and the results of oxygen analyses are shown in Figure 50. While there appears to be some inconsistency in the oxygen analyses, the data generally indicated that the hydrogen decomposition cycle at 900° F was preferable to the vacuum stepwise cycle.

Thorium Organic Salt Studies - A group of thorium-organic compounds were evaluated to determine the possibility of their providing decomposition products that would be less oxidizing in nature than those of thorium nitrate. The compounds, without metal powder additions, were initially subjected to thermal decomposition cycles and then evaluated by X-ray diffraction techniques to determine if ThO<sub>2</sub> had been produced. The compounds evaluated and the results of X-ray diffraction analyses are as follows:

Thorium Acetylacetonate	ThO <sub>2</sub> not detected
Thorium Stearate	ThO <sub>2</sub> not detected
Thorium Hexoate	ThO <sub>2</sub> not detected
Thorium Acetate	ThO <sub>2</sub> not detected
Thorium Oxycarbonate Monohydrate	ThO <sub>2</sub> present



\*Available to form Cr<sub>2</sub>O<sub>3</sub>

Figure 50. Process Diagram and Results for Thermal Decomposition Studies.

With the exception of the oxycarbonate, all of the above compounds produced a carbonaceous residue. Thorium carbide was detected by X-ray diffraction in the residue of thorium acetate.

Based on the above results, subsequent work was conducted with thorium oxycarbonate to assess its potential for introducing ThO<sub>2</sub> into nickel-chromium alloys by thermal decomposition.

Following the thermal decomposition of thorium oxycarbonate for 1 hour in air, argon, hydrogen or carbon monoxide at temperatures of 1000° to 2200° F, the ThO<sub>2</sub> particle size was evaluated by X-ray line-broadening techniques. Table XLV summarizes these measurements.

TABLE XLV  
EFFECT OF TEMPERATURE AND ATMOSPHERE ON  
ThO<sub>2</sub> PARTICLE SIZE

Decomposition Temperature, °F	Particle Size, Microns			
	Air	Argon	Hydrogen	Carbon Monoxide
1000	< 0.01	< 0.01	< 0.01	< 0.01
1200	< 0.01	< 0.01	< 0.01	< 0.01
1400	< 0.01	0.01	< 0.01	< 0.01
1600	0.01	0.01	0.01	0.01
1800	0.02	0.02	0.05	0.02
2000	0.02	0.04	-	0.03
2200	0.02	0.06	-	0.05

Although the decomposition data indicated a fine ThO<sub>2</sub> particle size, a major drawback to consideration of the oxycarbonate was its nonsolubility in fluids compatible with the alloy powder. Coating of the metal powder using the oxycarbonate would be more difficult than when using thorium nitrate which is soluble in various alcohols. If decomposition of the oxycarbonate resulted in low oxygen contamination, this benefit could outweigh the solubility limitation.

Additional decomposition studies were conducted using thorium oxycarbonate and 1.0 micron air-dried 80 Ni - 20 Cr powder. Small quantities of the alloy powder were mechanically mixed with sufficient thorium oxycarbonate to produce 5.0-volume-percent ThO<sub>2</sub> and were thermally decomposed in atmospheres of carbon monoxide, hydrogen, and argon at 1600°F. The results of carbon and oxygen analyses made after decomposition are shown in Table XLVI.

TABLE XLVI  
CONTAMINATION LEVELS IN 80 Ni - 20 Cr - 5 ThO<sub>2</sub>  
PROCESSED POWDER

Atmosphere	Total Oxygen, %	Excess Oxygen, %*	Carbon, %
Hydrogen	1.7	0.99	0.06
Argon	2.6	1.89	0.15
Carbon Monoxide	1.0	0.29	2.10

\*Calculated by allowing 0.71% O<sub>2</sub> as ThO<sub>2</sub>

By comparison of the above data with the results in Figure 50, the level of oxygen contamination (excess oxygen) obtained for thorium oxycarbonate was slightly higher than that obtained for thorium nitrate when thermally decomposed in hydrogen. While the excess oxygen level was low for thorium oxycarbonate with the carbon monoxide atmosphere, the 2.1-percent carbon content was too high to be tolerated in a nickel-chromium alloy system because of the possible formation of unstable chromium carbides. In view of

these results, and the necessity of introducing the oxycarbonate by a mechanical mixing procedure rather than by a coating technique, thorium nitrate was selected as the source of ThO<sub>2</sub> for subsequent studies.

### 3.4.3 Selective Reduction Studies

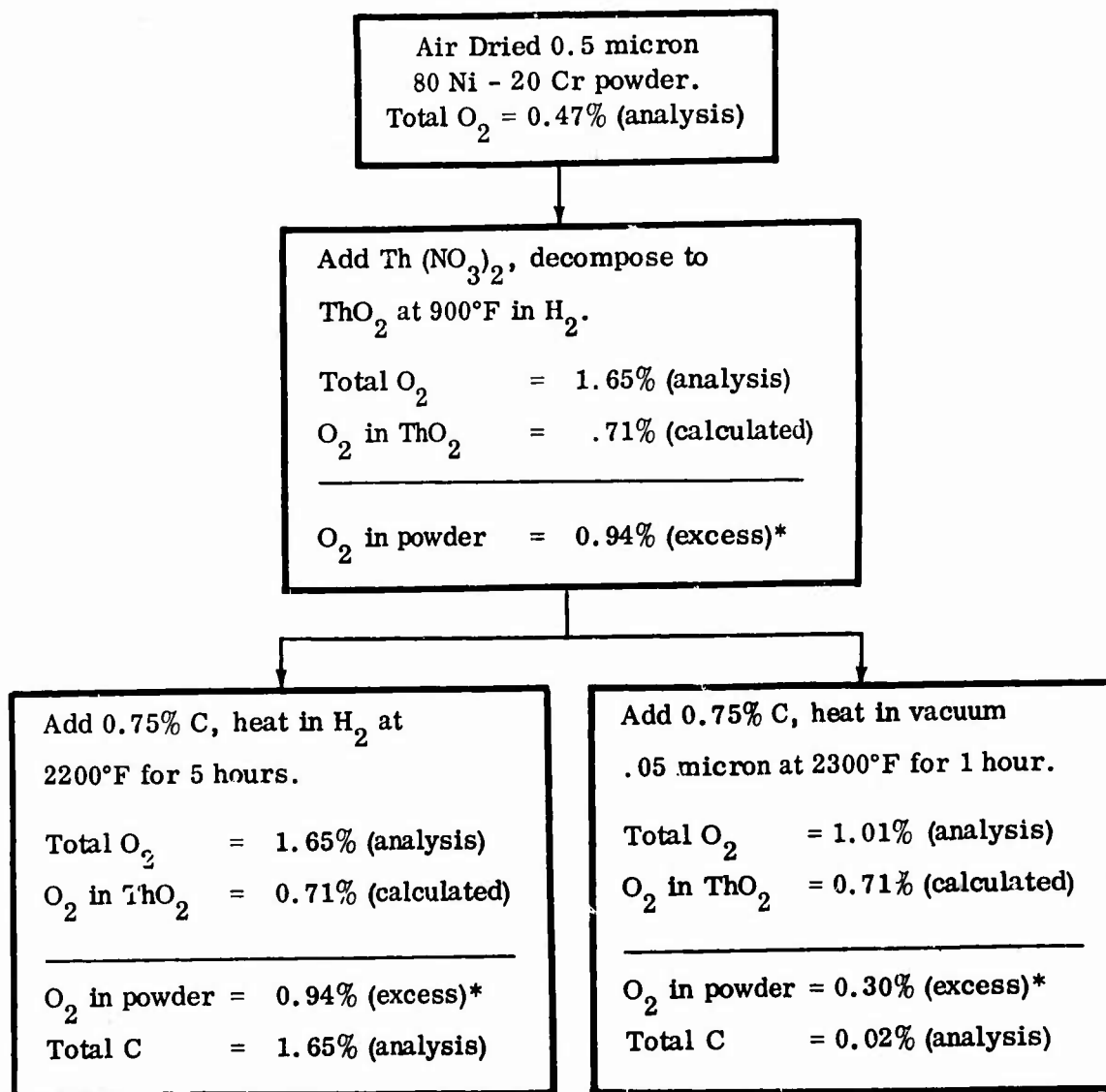
Alloy Powder Study - In an effort to lower the level of matrix oxygen contamination further, studies were initiated to evaluate selective oxygen-reduction techniques. A quantity of 80 Ni - 20 Cr alloy powder (0.5 micron) was mixed with sufficient thorium nitrate to produce 5.0-volume-percent ThO<sub>2</sub> and was thermally decomposed at 900°F in hydrogen. Carbon in the form of lampblack was added to the thermally decomposed powder by ball-milling. Small quantities of this powder mixture were then heated in hydrogen or vacuum to effect selective reduction of the matrix oxides. The procedure used and the results of oxygen and carbon analyses are shown in the block diagram in Figure 51. It is apparent from the data that the hydrogen-carbon cycle was not effective in removing the excess oxygen, while the vacuum-carbon cycle lowered the excess oxygen level from 0.94 percent to 0.30 percent.

Preliminary Extruded Alloy Study - Based on the above results, laboratory quantities of four alloys were prepared for extrusion primarily to evaluate further the effectiveness of the vacuum-carbon reduction cycle. The alloys prepared are described in Table XLVII.

TABLE XLVII  
PRELIMINARY EXTRUDED ALLOYS

Alloy No.	Composition
1	80 Ni - 20 Cr - 2.5* ThO <sub>2</sub> (1.0-Micron Alloy Powder)
2	80 Ni - 20 Cr - 5.0 ThO <sub>2</sub> (1.0-Micron Alloy Powder)
3	80 Ni - 20 Cr - 2.5 ThO <sub>2</sub> (2.5-Micron Alloy Powder)
4	80 Ni - 20 Cr - 5.0 ThO <sub>2</sub> (2.5-Micron Alloy Powder)

\*ThO<sub>2</sub> % by volume



\*Available to form  $\text{Cr}_2\text{O}_3$

Figure 51. Process Diagram and Results for Selective Reduction Studies.

Each of the alloys was processed by decomposing thorium nitrate in hydrogen at 900°F. Carbon black was then mechanically added in amounts equal to 20 percent in excess of that necessary to reduce the indicated chromium oxide content. The alloy mixtures were pressed into a mild steel extrusion can and then heated to 2300°F in a vacuum of at least 2 microns. A heating cycle time of 150 hours was dictated by the desire to hold a good vacuum, because heating was interrupted when outgassing was noted. Outgassing occurred primarily in the temperature range of 800° to 1800°F. The holding time at 2300°F was 1 hour, after which the extrusion can was cooled to room temperature under vacuum and sealed. Extrusion was conducted at 1800°F with a 22:1 reduction ratio and yielded, for further evaluation, bar stock approximately 40 inches long by 0.4 inch in diameter.

A carbon and oxygen history of each of the four alloys during the various stages of processing is presented in Figures 52 and 53. The oxygen analyses were conducted by vacuum fusion at 1900°F. Alloys 1 and 4 showed lower excess oxygen contents after extrusion than the other two alloys. This would indicate that an oxygen reduction by the vacuum-carbon treatment was realized only for alloys 1 and 4, and that this reduction still was accompanied by a relatively high (0.37 percent) residual carbon content.

Longitudinal sections of the extruded alloys were examined metallographically, and representative unetched microstructures at 100X are shown in Figure 54. It was noted that the ThO<sub>2</sub> particles were fairly well distributed in the matrix and that there was a general absence of stringers. To determine the effect of the vacuum-carbon cycle on the ThO<sub>2</sub>, an evaluation was conducted on second-phase particles prepared by electrolytic extraction in either phosphoric or phosphoric-sulfuric acid baths. X-ray diffraction analysis identified the second-phase particles from the four alloys as ThO<sub>2</sub> and Cr<sub>2</sub>O<sub>3</sub>. Electron microscopic examination of the particles indicated that they were in the 0.1-to-1.0-micron size range. This coarsening of the second phase probably was related to the long cycle time used for the vacuum-carbon reduction cycle and showed the need for an improved cycle.

Tensile tests at room temperature and 1800°F were conducted on the four alloys. In view of the coarsening that was observed metallographically for the second-phase particles, it was expected that the elevated temperature tensile properties would not be very high, as for example, by comparison with commercially available TD nickel. The data, given in Table XLVIII, show that this was the case.

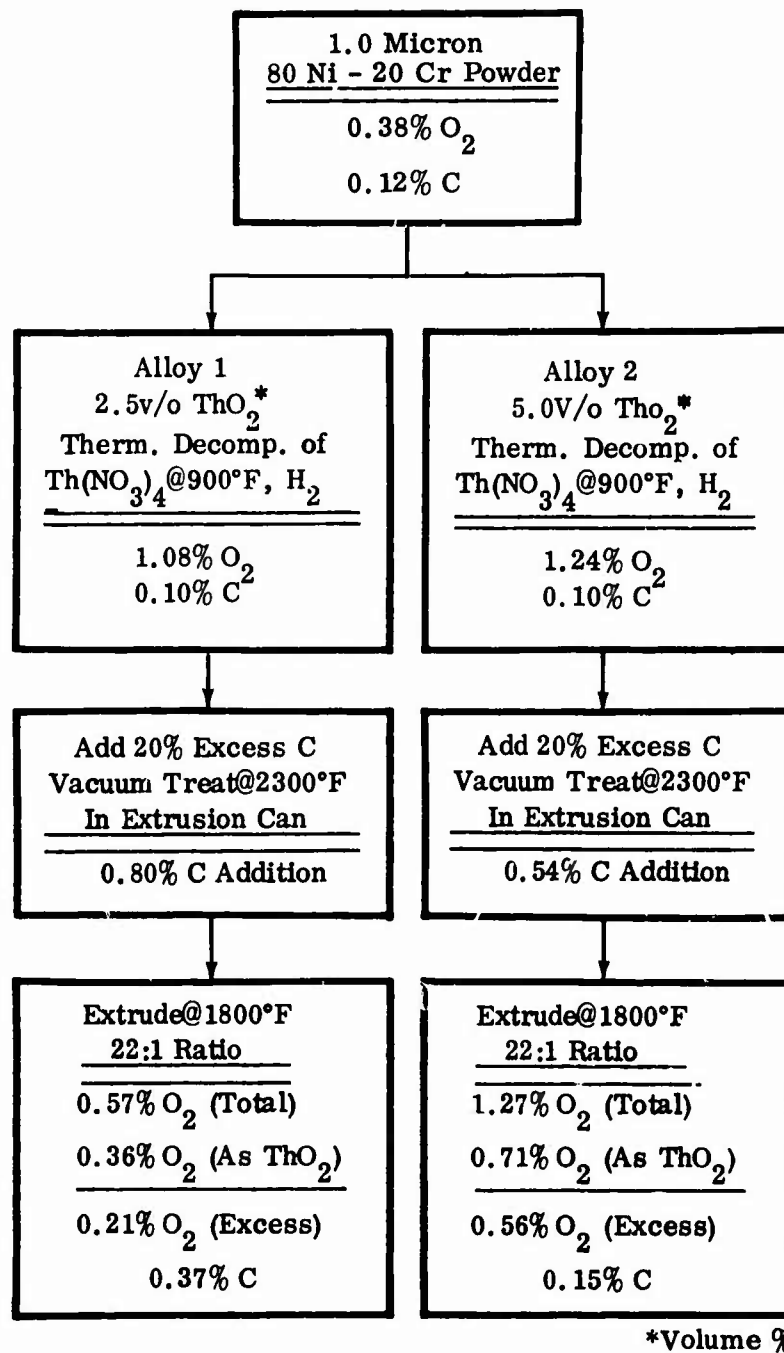
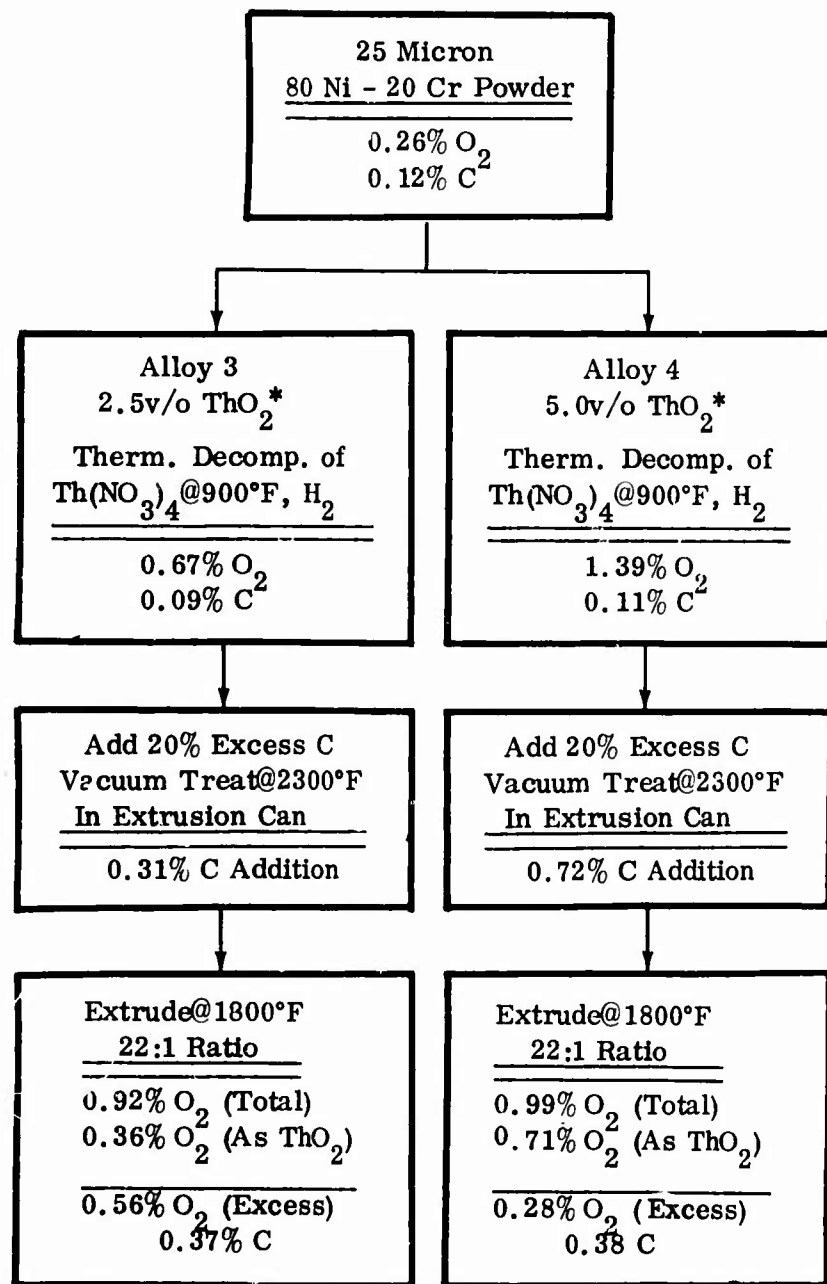
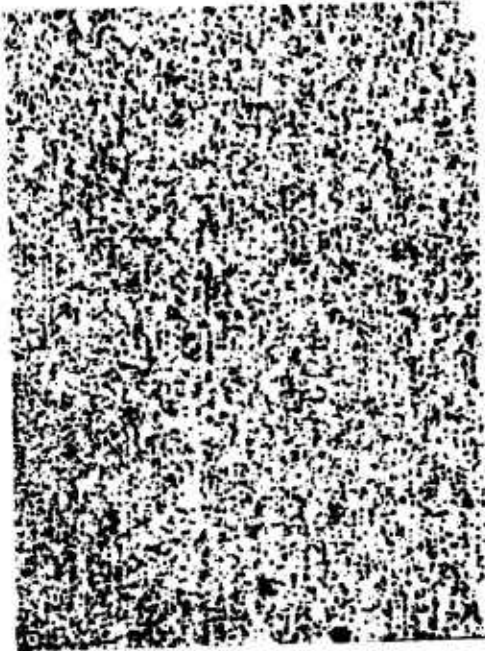


Figure 52. Process Diagram and Analysis Data for Extruded Alloys.



\*Volume %

Figure 53. Process Diagram and Analysis Data for Extruded Alloys.



Alloy Number 1



Alloy Number 2



Alloy Number 3



Alloy Number 4

---

Figure 54. As-Extruded Longitudinal Microstructures of Ni-Cr-ThO<sub>2</sub> Alloys. 100X. Unetched.

**TABLE XLVIII**  
**TENSILE PROPERTIES OF EXTRUDED ALLOYS**

Alloy	Temperature, °F	UTS, psi	Reduction		
			0.2% YS, psi	Elongation, %	of Area, %
1	R. T.	102,500	56,000	16	18
	1800	6,300	5,500	7	12
2	R. T.	97,200	58,800	14	15
	1800	5,000	4,200	7	5
3	R. T.	102,000	54,500	17	14
	1800	6,000	5,500	6	5
4	R. T.	91,900	60,600	7	11
	1800	4,500	4,000	-	5

**Vacuum-Carbon Cycle Studies** - A vacuum induction furnace facility, with an improved vacuum pumping capability, was set up in an effort to reduce the unusually long heating times experienced in the previous studies. To evaluate various time-temperature parameters, samples of 80 Ni - 20 Cr powder with 7.5-volume-percent ThO<sub>2</sub> added by thermal decomposition were given vacuum-carbon reduction treatments. The results of initial analyses, and analyses after cycles ranging from 2100° to 2375°F, are shown in Table XLIX.

With the exception of the samples treated at 2100°F, all of the data indicated that the total oxygen content was lowered by approximately two-and-one-half percentage points, with greater reduction indicated at higher temperatures or longer time. In addition, X-ray and electron microscopy investigations determined that the oxygen reduction was effected without a severe coarsening of the ThO<sub>2</sub> during the vacuum-carbon reduction treatment. Second-phase particles prepared by electrolytic extraction were found to be generally finer than 0.2 micron, which compares favorably with the 1.0-micron maximum particle size associated with the previously evaluated reduction cycle.

**TABLE XLIX**  
**RESULTS OF VACUUM-CARBON REDUCTION CYCLES**

Temperature, °F	Time, hr	Vacuum, Torr	Total O <sub>2</sub> , %	C, %
Initial Analysis	-	-	4.77	0.06*
2100	1	10 <sup>-5</sup>	2.59 4.32	0.76 0.74
2200	1	10 <sup>-4</sup>	2.57 2.16	0.70 0.73
2200	5	10 <sup>-5</sup>	2.16 2.16	0.24 0.25
2275	1	10 <sup>-5</sup>	2.26 2.26	0.45 0.49
2375	1	10 <sup>-5</sup>	2.50 2.03	0.29 0.32

\*2.71% carbon added prior to vacuum treatment

Extruded Alloy Study - A second group of extruded alloys was prepared using the thermal decomposition and selective reduction techniques developed from the previous studies. The compositions of the alloys are described in Table L.

**TABLE L**  
**COMPOSITION OF EXTRUDED ALLOYS**

Alloy	Composition *
5	80 Ni - 20 Cr - 2.5 ThO <sub>2</sub>
6	80 Ni - 20 Cr - 5.0 ThO <sub>2</sub>
7	72 Ni - 18 Cr - 10 Mo - 2.5 ThO <sub>2</sub>
8	72 Ni - 18 Cr - 10 Mo - 5.0 ThO <sub>2</sub>

\*ThO<sub>2</sub> % by volume

The alloy powder for alloys 5 and 6 had an average particle size of 0.84 micron, and the alloy powder for alloys 7 and 8 had an average particle size of 1.6 microns. The different grinding characteristics of the alloy containing molybdenum yielded a slightly coarser particle size. The processing parameters defined from previous studies and utilized in the preparation of approximately 3 pounds of each of the alloys are as follows:

1. Alloy powders were comminuted in a water-cooled, stainless-steel attrition mill, using isopropyl alcohol as the grinding medium. The powders were ambient-air-dried after grinding.
2. Thorium nitrate, dissolved in isopropyl alcohol, was mixed with the powder and thermally decomposed in hydrogen at 900° F.
3. A carbon addition equal to 120 percent of the stoichiometric amount required for complete reduction of excess oxygen was added to the metal-thoria powder after thermal decomposition. The carbon addition was based on an oxygen analysis of the powder.
4. The metal-thoria-carbon mixture, in the form of pellets, was heated in vacuum to 2375° F and held for a period of 3-1/2 hours at temperature.
5. A vacuum of  $2 \times 10^{-5}$  Torr was achieved during the heating cycle, with a minimum of  $1 \times 10^{-4}$  Torr maintained during outgassing.
6. The processed powder was sealed in mild steel containers and extruded at 1800° F with a reduction ratio of approximately 22:1.

In addition to the alloys and procedure described above, one alloy, identified as 5a, was processed without the vacuum-carbon reduction treatment to provide a comparison of the effect of chromium oxide on the high-temperature properties with the influence of the vacuum-carbon reduction treatment on the high-temperature properties.

Carbon and oxygen analyses were obtained for the alloy powders after comminution and for each of the alloys after thermal decomposition and extrusion. These data are given in Table LI.

TABLE LI  
OXYGEN AND CARBON ANALYSIS OF EXTRUDED ALLOYS

Alloy	Total Oxygen, %	Excess Oxygen, % <sup>1</sup>	Carbon, %
<b>a) As Ground</b>			
5	0.29	-	0.12
5a	0.29	-	0.12
6	0.29	-	0.12
7	0.20	-	0.06
8	0.20	-	0.06
<b>b) After Decomposition</b>			
5	0.93	0.57	0.09
5a	0.93	0.57	0.09
6	1.36	0.65	0.14
7	0.66	0.30	0.05
8	1.09	0.38	0.06
<b>c) After Extrusion</b>			
5	0.53	0.17	0.03
5a <sup>2</sup>	1.00	0.64	0.10
6	0.94	0.23	0.04
7	0.45	0.09	0.12
8	0.92	0.21	0.06

<sup>1</sup> Calculated by subtracting oxygen due to ThO<sub>2</sub> from analyzed oxygen value.

<sup>2</sup> Processed without vacuum-carbon reduction cycle.

Following extrusion, tensile specimens were machined from the nominal 0.4-inch-diameter bar stock, and tests were conducted at room temperature and 1800°F. These data are shown in Table LII.

TABLE LII  
PROPERTIES OF EXTRUDED ALLOYS

Alloy	Temperature, °F	UTS, psi	0.2% YS, psi	Reduction	
				Elongation, %	of Area, %
5	R. T.	116,700	83,300	11	14
	1800	8,000	7,500	5	5
5a*	R. T.	123,000	89,500	8	12
	1800	6,100	5,100	4	5
6	R. T.	116,500	82,500	9	10
	1800	7,200	6,500	9	10
7	R. T.	148,900	123,500	11	12
	1800	2,700	2,500	30	22
8	R. T.	151,500	131,600	5	9
	1800	2,900	2,600	20	18

\*Processed without vacuum-carbon reduction cycle.

The carbon and oxygen contents of the extruded alloys represent the lowest contamination levels that have been obtained for dispersion-strengthened nickel-chromium alloys processed in this program.

The mechanical properties of alloys 5 and 6 partially reflect the lower levels of contamination and show some improvement over those of similar alloys; i. e., alloys 1 and 2, tested previously and reported in Table XLVIII. A comparison of alloys 5 and 5a shows that while the level of oxygen contamination was reduced to about one-fourth of its original value through the vacuum-carbon reduction process, the mechanical properties at 1800°F showed only modest improvements. The reason for the low properties in this series of alloys is evident in the electron micrograph shown in Figure 55. The second-phase particles in this micrograph, the

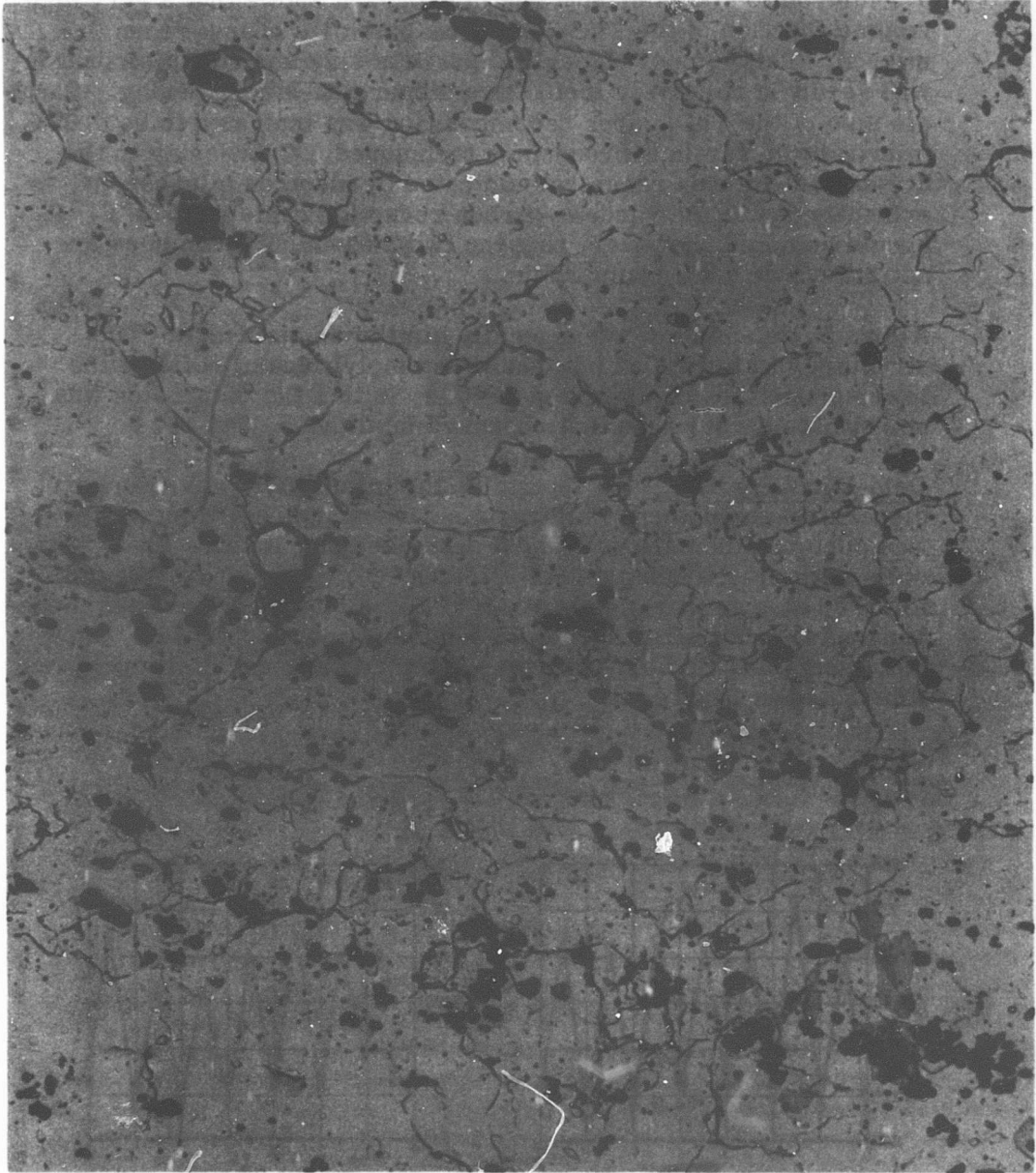


Figure 55. Electron Micrograph of Ni-Cr-ThO<sub>2</sub> Alloy  
(Alloy Number 5) After Extrusion.

majority of which are  $\text{ThO}_2$ , range from a size of slightly less than 0.1 micron to 1.0 micron. The micrograph shows that a very high volume fraction of the  $\text{ThO}_2$  exists as particles coarser than 0.5 micron. This type of dispersoid particle size and size distribution will result in relatively ineffective dispersion-strengthening. Particle size of the  $\text{ThO}_2$  after decomposition was indicated to be 0.03 micron by X-ray line-broadening techniques. Coarsening to the 0.1-to-1.0-micron range, as indicated by electron microscopy, is evidently due to the vacuum-carbon reduction cycle at  $2375^\circ\text{F}$ . It should be noted, however, that the two measuring techniques are not always directly comparable.

Alloys 5, 5a, and 6 were generally similar in structure. The structure of alloys 7 and 8 (containing molybdenum) reflects the lower properties measured at  $1800^\circ\text{F}$ , in that the dispersion was somewhat coarser than that observed in alloys 5, 5a, and 6.

**Cold-Work Studies** - To determine the influence of cold-work on dispersion-strengthened alloys, a series of cold-working cycles was performed on alloys 1 and 3 described previously. Each of the cold-work cycles consisted of a 15-percent reduction by swaging followed by a 1-hour anneal at  $1800^\circ\text{F}$  in air. Microhardness measurements, made after each cold-work and anneal operation, show that essentially no cold-work was retained after each full cycle, as illustrated in Figure 56.

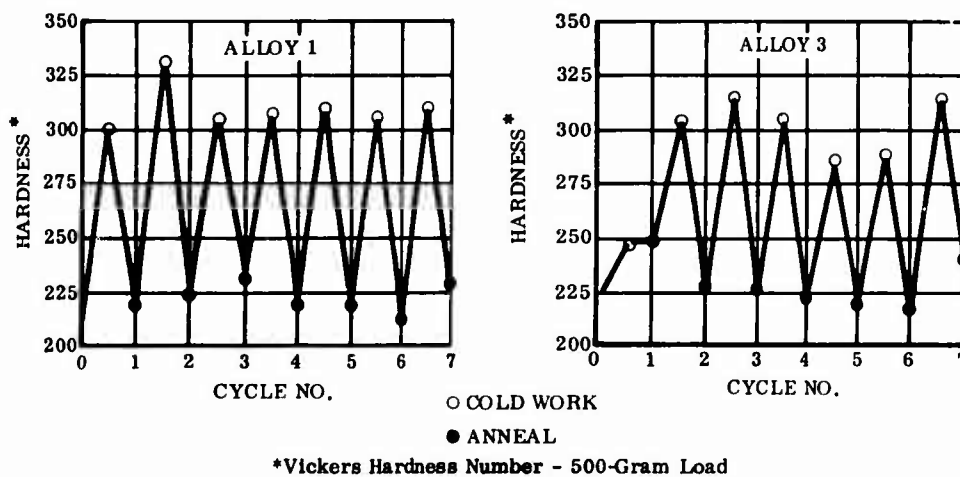


Figure 56. Effect of Cold-Work and Anneal Cycles on Hardness.

Tensile tests at 1800°F also were conducted on the cold-worked bar stock after various cycles. As shown in Table LIII, slight reductions in elevated temperature properties occurred as a result of the cold-working operations. The half-cycle points in Table LIII represent the alloy after swaging and the full-cycle points after the anneal.

**TABLE LIII**  
**TENSILE PROPERTIES AT 1800°F ON COLD-WORKED ALLOYS**

<u>Alloy</u>	<u>Cycle</u>	<u>UTS psi</u>	<u>Elongation %</u>
1	0	6,300	7
1	5-1/2	4,600	-
1	6	4,000	9
1	6-1/2	4,400	9
1	7	4,400	13
3	0	6,000	6
3	5-1/2	4,000	9
3	6	4,500	8
3	6-1/2	4,400	12
3	7	4,500	14

It is felt that the lack of improvement in the high-temperature properties as a result of the cold-swaging and anneal treatments is related to the coarse dispersion and high chromium oxide content of the two alloys.

#### 3.4.4 Summary of Dispersion-Strengthened Alloy Results

The objective of the dispersion-strengthened alloy study was to improve the strength and oxidation resistance of dispersion-strengthened nickel through alloy additions, and determine the suitability of this material for turbine bucket application.

The studies on dispersion-strengthened Ni-Cr-ThO<sub>2</sub> alloys were concerned primarily with improving the elevated temperature properties of this material system by reducing the level of oxygen contamination that is associated with processing the Ni-Cr alloy powders.

It was found that oxygen contents increased rapidly as Ni-Cr powders were comminuted to finer particle sizes. A reduction in oxygen pickup was obtained by ambient-air-drying the powders after comminution instead of by vacuum-oven-drying at 200°F. However, an oxygen content of about 0.5 percent was still associated with 0.5-micron Ni-Cr powder.

Studies conducted on the thermal decomposition cycles achieved only slight decreases in the amount of oxygen contamination associated with the operation. Several thorium organic compounds did not produce ThO<sub>2</sub> on decomposition. Although thorium oxycarbonate did yield ThO<sub>2</sub> on decomposition, it did not provide an advantage over thorium nitrate in terms of decreasing the level of oxygen contamination introduced during thermal decomposition. Based on these results, thorium nitrate was selected as the source of ThO<sub>2</sub>. Ni-Cr-ThO<sub>2</sub> powders were subsequently prepared in which the oxygen contamination levels were held within the range of 0.5 to 0.6 percent after thermal decomposition. Earlier in the program, excess oxygen contents of 0.7 to 0.9 percent had been measured.

To effect further decreases in oxygen contamination, treatments to reduce selectively base-metal oxides were evaluated. A vacuum-carbon reduction cycle at 2375°F for 3-1/2 hours was able to decrease the level of oxygen contamination to approximately one-third of its original value. However, this reduction cycle apparently resulted in some ThO<sub>2</sub> particle coarsening. Consequently, elevated temperature mechanical properties of the extruded material were lower than anticipated. An 1800°F ultimate tensile strength of 8000 psi was obtained on a Ni-Cr-ThO<sub>2</sub> alloy after extrusion. A majority of the ThO<sub>2</sub> particles were observed to be 0.5 micron or larger in size.

Successive cold-working cycles, each consisting of a 15-percent reduction by swaging followed by a 1-hour anneal at 1800°F, were performed on two preliminary extruded alloys. Increases in hardness because of working subsequently were lost during the 1800°F anneal cycle. Failure to retain the hardness produced by cold-working was attributed to an ineffective dispersoid distribution caused by a coarse ThO<sub>2</sub> particle size.

## SECTION 4.0 - CONCLUSIONS

Conclusions reached as a result of the work conducted in this program for the macrolaminate composites and the dispersion-strengthened nickel-base alloys are as follows:

### 4.1 Ni-Al<sub>2</sub>O<sub>3</sub> MACROLAMINATE COMPOSITES

- 1) Ni-Al<sub>2</sub>O<sub>3</sub> composites showed the best thermal-fatigue characteristics and strength at elevated temperatures, and were considered to have the best potential of the composites evaluated for nozzle vane application. Strength levels were double those of the Ni-MgO system, despite high porosity.
- 2) Major additions of chromium to the metal phase were found to improve oxidation resistance; however, chromium had the adverse effect of reducing both strength and resistance to thermal fatigue. The loss of properties was attributed to the presence of excessive chromium oxide and to diffusion reactions between the metal and ceramic phases.
- 3) It is estimated that this material system would be limited to an average metal temperature of 2100°F. This limitation is based on the assumption that chromium additions will be required to obtain the necessary oxidation resistance, and, as a result, the limiting factors will become the melting point of the metal phase and the diffusion reactions between the metal and ceramic phases at elevated temperatures.
- 4) Further work to improve fabrication techniques, particularly with respect to reducing porosity, would be necessary to determine the full potential of the Ni-Al<sub>2</sub>O<sub>3</sub> composite.

### 4.2 Ni-MgO MACROLAMINATE COMPOSITES

- 1) Hot-pressing techniques were developed which produced composites with low levels of porosity. Because the processing techniques were the same as those used for the Ni-Al<sub>2</sub>O<sub>3</sub> composites, low porosity was attributed to the compatibility of the metal and ceramic phases.
- 2) The use of dispersed oxide particles in the metal and ceramic phases and the use of titanium nitride to improve the metal-ceramic bond were found to be effective in increasing the strength of this material.

- 3) Elevated temperature properties were independent of the metal-ceramic ratios investigated; however, room-temperature strength increased with increasing metal content.
- 4) Oxidation resistance, thermal-fatigue properties, and elevated-temperature strengths were judged insufficient to consider application of this material in a gas turbine nozzle vane application.

#### 4.3 Mo-HfO<sub>2</sub> MACROLAMINATE COMPOSITES

- 1) Composites of this material can be fabricated to low levels of porosity using warm-pressing and vacuum-sintering techniques.
- 2) Modifying the ceramic phase with oxide additives and applying protective coatings on the surface of composites produced significant improvement in oxidation resistance of this material. These improvements, however, were insufficient to consider application of this material in a gas turbine nozzle vane application.

#### 4.4 DISPERSION-STRENGTHENED ALLOYS

- 1) Thermal decomposition cycles in hydrogen, using thorium nitrate as the source of ThO<sub>2</sub>, were found to be the most effective means of introducing the dispersoid. However, some oxygen contamination of the metal powders during the thermal decomposition process could not be avoided completely.
- 2) Several Thorium organic compounds were found to be unsuitable for thermal decomposition techniques because most did not yield ThO<sub>2</sub> on decomposition. Thorium oxycarbonate did yield ThO<sub>2</sub> on decomposition, but produced no advantage over thorium nitrate on the basis of oxygen contamination.
- 3) Selective reduction treatments, using a vacuum-carbon reduction cycle, reduced oxygen contamination levels to about one-third of their original values.
- 4) Mechanical properties of material produced, using the modified processing techniques, were lower than anticipated because of an apparent coarsening of the dispersoid during processing.
- 5) Further work is required to define a process that would produce a small dispersoid particle size (less than 0.1 micron) in a suitable alloy matrix.

#### 4.5 COMPARATIVE PROPERTIES

Table LIV gives a comparison between the target properties and selected test data for the various material systems and represents the best values obtained.

**TABLE LIV  
COMPARISON OF TARGET AND BEST TEST PROPERTIES**

a) Short-Time Tensile Strength

Material System	Temperature, °F	Ultimate Tensile Strength, psi		0.2% Yield Strength, psi	
		Goal	Actual	Goal	Actual
Ni-MgO	70	40,000	36,700	36,000	
	1800	27,500	11,300	23,500	
	2200	18,000	4,000	14,000	3,900
Ni-Al <sub>2</sub> O <sub>3</sub>	70	40,000	29,400	36,000	
	1800	27,500	18,860	23,500	
	2200	18,000	5,500	14,000	
Dispersion-Strengthened Alloy	70	120,000	102,500	95,000	56,000
	1800	45,000	6,300	40,000	5,500

b) Oxidation Resistance

Material System	Exposure	Weight Change After Exposure, mg/cm <sup>2</sup>	
		Goal	Actual
Mo-HfO <sub>2</sub>	24 Hours at 1200°F	± 2.0	- 16.0
	24 Hours at 1800°F	± 2.0	-278.0
	24 Hours at 2500°F	± 2.0	-143.0
Ni-MgO	100 Hours at 2300°F	± 2.0	+ 45.6
Ni-Al <sub>2</sub> O <sub>3</sub>	100 Hours at 2300°F	± 2.0	+ 10.9

TABLE LIV (Continued)

c) Thermal-Fatigue Resistance

Material System	Temperature Range	Number Cycles Without Failure	
		Goal	Actual
Ni-MgO <span style="border: 1px solid black; padding: 0 2px;">2</span>	300° F - 2300° F	500	490
Ni-Al <sub>2</sub> O <sub>3</sub> <span style="border: 1px solid black; padding: 0 2px;">5</span>	300° F - 2300° F	500	512+

- 1 No yield point reached
- 2 Test material: (Ni · 2ThO<sub>2</sub>) · 2TiN - (MgO · 5HfO<sub>2</sub>), metal content - 50 volume %
- 3 Test material: Same as 2 except metal content - 30 volume %
- 4 Test material: Ni · 17 Cr - Al<sub>2</sub>O<sub>3</sub> · 1/4 TiO<sub>2</sub>, metal content - 50 volume %
- 5 Test material: (Ni · 2ThO<sub>2</sub>) - Al<sub>2</sub>O<sub>3</sub> · 1/4 TiO<sub>2</sub>, metal content - 50 volume %
- 6 Test material: Mo - (HfO<sub>2</sub> · 4.3 CeO<sub>2</sub> · 4.5 SrO<sub>2</sub> · 10 Cr<sub>2</sub>O<sub>3</sub>), metal content - 50 volume %

Because oxidation resistance of the Mo-HfO<sub>2</sub> material system did not show promise after the preliminary 24-hour tests, further work on this system was deleted from the program.

## BIBLIOGRAPHY

- 1) Vasilos, T., and Spriggs, R.M., 'Mechanical Properties of Pure, Dense Aluminum Oxide as a Function of Temperature and Grain Size', Journal of the American Ceramic Society, Vol. 47, No. 7, 1964, pg. 323.
- 2) Vasilos, T., et al., 'Microstructure Studies of Polycrystalline Refractory Oxides', Summary Report, U.S. Navy Bureau of Weapons Contract NOw 64-0217-d, March 31, 1965.
- 3) Vasilos, T., Mitchell, J.B., and Spriggs, R.M., 'Mechanical Properties of Pure Dense Magnesium Oxide as a Function of Temperature and Grain Size', Journal of the American Ceramic Society, Vol. 47, No. 12, 1964, pg. 608.
- 4) Sterry, W.M., 'Ductile, Anti-Friction Ceramic Composites', Ceramic Industry, Vol. 84, No. 3, March 1965, pg. 54.
- 5) Jones, J.T., Maitra, P.K., and Cutler, I.B., 'Role of Structural Defects in the Sintering of Alumina and Magnesia', Journal of the American Ceramic Society, Vol. 41, No. 9, pg. 353.
- 6) Murphy, R., and Grant, N.J., 'Properties of Nickel-Thoria Alloys Prepared by Thermal Decomposition of Thorium Nitrate', Powder Metallurgy, No. 10, 1962, pg. 1.
- 7) Tracey, V.A., and Worn, D.K., Ibid, 'Some Observations on the Cold-Drawing and Annealing Behavior of Nickel Containing a Dispersed Phase of Thoria''.
- 8) Stuart, R.E., and Starr, C.D., 'New Design Data on TD Nickel', Materials in Design Engineering, August 1963.
- 9) Curtis, E.E., et al, 'Some Properties of Hafnium Oxide, Hafnium Silicate, Calcium Hafnate and Hafnium Carbide', Journal of the American Ceramic Society, Vol. 37, 1954, pg. 458.
- 10) Ohnystry, Basil and Rose, 'Thermal Expansion Measurements on Thoria and Hafnia to 4500°F', Journal of the American Ceramic Society, Vol. 47, 1964, pg. 398.
- 11) Tinklepaugh, J.R., and Crandall, W.B., Cermets, Reinhold Publishing Co., New York, 1960.

BIBLIOGRAPHY (Continued)

- 12) Economos, G., and Kingery, W.D., 'Metal-Ceramic Interactions: II Metal-Oxide Interfacial Reactions at Elevated Temperatures', Journal of the American Ceramic Society, Vol. 38, No. 12, pg. 403.
- 13) Hower, L.D., Jr., Londeree, J.W., Jr., and Ueltz, H.F.G., 'High Temperature Bodies Derived from Mixtures of MgO-TiN-NiO', Journal of the American Ceramic Society, Vol. 34, No. 10, pg. 309.
- 14) Sutton, W.H., 'Investigation of Bonding in Oxide Fiber (Whisker) Reinforced Metal', Report No. ARMA CR-63-O1/5, Fifth Quarterly Technical Report, U.S. Army, 1963.
- 15) Brammar, I.S., and Dawe, D.W., 'Metallography of Dispersion Hardened Alloys and Its Relation to Creep Resistance,' ASD-TDR-63-343, 1963.
- 16) Simpson, F.H., 'Macrolaminate Particle Composite Material Development', Summary Report, U.S. Navy Bureau of Weapons Contract NOW 65-0403-d, July 1966.

Unclassified

Security Classification

DOCUMENT CONTROL DATA - R&D		
<i>(Security classification of title, body of abstract and indexing annotation must be entered when the overall report is classified)</i>		
1. ORIGINATING ACTIVITY (Corporate author) The Boeing Company, Turbine Division P. O. Box 3955 Seattle, Washington 98124		2a. REPORT SECURITY CLASSIFICATION Unclassified
		2b. GROUP
3. REPORT TITLE Small Gas Turbine Engine Component Technology, High-Temperature Turbine Materials Research		
4. DESCRIPTIVE NOTES (Type of report and inclusive dates) Final		
5. AUTHOR(S) (Last name, first name, initial) Acurio, John Fiedler, Lou J. Simpson, Fred H.		
6. REPORT DATE December 1966	7a. TOTAL NO. OF PAGES 166	7b. NO. OF REFS 16
8a. CONTRACT OR GRANT NO. DA 44-177-AMC-173(T)	9a. ORIGINATOR'S REPORT NUMBER(S) USAAVLABS Technical Report 66-88	
b. PROJECT NO. Task 1M121401D14413	9b. OTHER REPORT NO(S) (Any other numbers that may be assigned this report) D4-3298	
c.		
d.		
10. AVAILABILITY/LIMITATION NOTICES Distribution of this document is unlimited.		
11. SUPPLEMENTARY NOTES	12. SPONSORING MILITARY ACTIVITY U. S. Army Aviation Materiel Laboratories Fort Eustis, Virginia	
13. ABSTRACT <p>The report describes research conducted on two new material systems (macrolaminate metal-ceramic composites and dispersion-strengthened nickel base alloys) to determine their potential for future use, without special cooling, in the turbine section of an advanced small gas turbine engine, operating at a turbine inlet temperature of 2300°F. Although the research showed that the targeted high-temperature material properties could not be achieved with the macrolaminate composites or the dispersion-strengthened alloys, it was felt that these types of materials could be developed to increase turbine inlet temperatures to about 2100°F. However, it was recognized that this gain would not be sufficient in view of improvements being made with other new material systems.</p> <p>This report covers activities on this research program from May 1, 1964, to August 31, 1965.</p>		

DD FORM 1 JAN 64 1473

Unclassified

Security Classification

14. KEY WORDS	LINK A		LINK B		LINK C	
	ROLE	WT	ROLE	WT	ROLE	WT
Macrolaminate Composite Material Dispersion-Strengthened Material Turbine Blade Nozzle Vane Superalloy Ceramic Crystal Lamellae Powder Formulation Micron						

INSTRUCTIONS

1. **ORIGINATING ACTIVITY:** Enter the name and address of the contractor, subcontractor, grantee, Department of Defense activity or other organization (*corporate author*) issuing the report.

2a. **REPORT SECURITY CLASSIFICATION:** Enter the overall security classification of the report. Indicate whether "Restricted Data" is included. Marking is to be in accordance with appropriate security regulations.

2b. **GROUP:** Automatic downgrading is specified in DoD Directive 5200.10 and Armed Forces Industrial Manual. Enter the group number. Also, when applicable, show that optional markings have been used for Group 3 and Group 4 as authorized.

3. **REPORT TITLE:** Enter the complete report title in all capital letters. Titles in all cases should be unclassified. If a meaningful title cannot be selected without classification, show title classification in all capitals in parenthesis immediately following the title.

4. **DESCRIPTIVE NOTES:** If appropriate, enter the type of report, e.g., interim, progress, summary, annual, or final. Give the inclusive dates when a specific reporting period is covered.

5. **AUTHOR(S):** Enter the name(s) of author(s) as shown on or in the report. Enter last name, first name, middle initial. If military, show rank and branch of service. The name of the principal author is an absolute minimum requirement.

6. **REPORT DATE:** Enter the date of the report as day, month, year, or month, year. If more than one date appears on the report, use date of publication.

7a. **TOTAL NUMBER OF PAGES:** The total page count should follow normal pagination procedures, i.e., enter the number of pages containing information.

7b. **NUMBER OF REFERENCES:** Enter the total number of references cited in the report.

8a. **CONTRACT OR GRANT NUMBER:** If appropriate, enter the applicable number of the contract or grant under which the report was written.

8b, 8c, & 8d. **PROJECT NUMBER:** Enter the appropriate military department identification, such as project number, subproject number, system numbers, task number, etc.

9a. **ORIGINATOR'S REPORT NUMBER(S):** Enter the official report number by which the document will be identified and controlled by the originating activity. This number must be unique to this report.

9b. **OTHER REPORT NUMBER(S):** If the report has been assigned any other report numbers (*either by the originator or by the sponsor*), also enter this number(s).

10. **AVAILABILITY/LIMITATION NOTICES:** Enter any limitations on further dissemination of the report, other than those imposed by security classification, using standard statements such as:

- (1) "Qualified requesters may obtain copies of this report from DDC."
- (2) "Foreign announcement and dissemination of this report by DDC is not authorized."
- (3) "U. S. Government agencies may obtain copies of this report directly from DDC. Other qualified DDC users shall request through \_\_\_\_\_."
- (4) "U. S. military agencies may obtain copies of this report directly from DDC. Other qualified users shall request through \_\_\_\_\_."
- (5) "All distribution of this report is controlled. Qualified DDC users shall request through \_\_\_\_\_."

If the report has been furnished to the Office of Technical Services, Department of Commerce, for sale to the public, indicate this fact and enter the price, if known.

11. **SUPPLEMENTARY NOTES:** Use for additional explanatory notes.

12. **SPONSORING MILITARY ACTIVITY:** Enter the name of the departmental project office or laboratory sponsoring (*paying for*) the research and development. Include address.

13. **ABSTRACT:** Enter an abstract giving a brief and factual summary of the document indicative of the report, even though it may also appear elsewhere in the body of the technical report. If additional space is required, a continuation sheet shall be attached.

It is highly desirable that the abstract of classified reports be unclassified. Each paragraph of the abstract shall end with an indication of the military security classification of the information in the paragraph, represented as (TS), (S), (C), or (U).

There is no limitation on the length of the abstract. However, the suggested length is from 150 to 225 words.

14. **KEY WORDS:** Key words are technically meaningful terms or short phrases that characterize a report and may be used as index entries for cataloging the report. Key words must be selected so that no security classification is required. Identifiers, such as equipment model designation, trade name, military project code name, geographic location, may be used as key words but will be followed by an indication of technical context. The assignment of links, rules, and weights is optional.